University of Alberta

Hormone Metabolism and Action in Developing Pea Fruit

by

Courtney David Nadeau

A thesis submitted to the Faculty of Graduate Studies and Research
in partial fulfillment of the requirements for the degree of

Master of Science

Department of Agriculture, Food, and Nutritional Sciences

Fall 2009
Edmonton, Alberta

Examining Committee

Jocelyn Ozga, Agriculture, Food, and Nutritional Sciences

Enrico Scarpella, Biological Sciences

Allen Good, Biological Sciences

Abstract

The developmental programs of maturing seed and fruit in pea (*Pisum sativum* L.) are tightly controlled by the interactions of several phytohormones, including gibberellins (GAs), auxins, and abscisic acid (ABA). To more fully understand these hormone networks and their roles in controlling development, transcription profiles of GA metabolism genes and metabolite profiles of key GAs, auxins, and ABA were determined in developing seeds, and histological studies were employed to correlate physiology and hormone metabolism. Data suggest that bioactive GA stimulates several aspects of seed growth, and ABA appears to promote bioactive GA_1 synthesis in rapidly growing seed coats, and inhibit GA biosynthesis in the embryo axes of maturing embryos. Two putative auxin receptor genes were cloned, and their transcription profiles examined in developing seed and pericarp tissues. Pericarp *PsAFB6A* transcription was responsive to auxin and seed signals, indicating a potential role for the modulation of auxin sensitivity in fruit development.

Acknowledgements

I would like to thank the numerous people who have supported me during my graduate research. Firstly, I would like to thank my family and friends for their continual and unconditional support throughout the duration of my studies. I would like to thank my supervisor, Dr. J. Ozga, for her guidance and suggestions. My supervisory committee, consisting of Drs. A. Good and E. Scarpella, has provided invaluable critiques and ensured that my research proceeded in appropriate directions. I would like to thank a number of individuals for their technical advice, including Dr. D. Reinecke and Randy Mandryk. I would like to thank my collaborators at the University of Calgary, Drs. Leonid Kurepin and Richard Pharis for their work on hormone quantitation, Lisa Ostafichuk and Cheryl Nargang at the MBSU for their assistance, and Szidonia Botar, Bruce Alexander and the other technical staff in AFNS who helped keep my plants alive long enough to perform experiments on. I am also very appreciative of NSERC, the University of Alberta FGSR, and the Government of Alberta for financial support which made this research possible.

Contents

List of Tables

List of Figures

List of Abbreviations

Abbreviation	Definition
4-Cl-IAA	4-chloroindole-3-acetic acid
4-Et-IAA	4-ethylindole-3-acetic acid
4-Me-IAA	4-methylindole-3-acetic acid
ABA	abscisic acid
ARE	auxin responsive element
ARF	auxin responsive factor
ATP	adenosine triphosphate
BSTFA	N,O,-bis(trimethylsilyl)trifluoroacetamide
cDNA	complementary DNA
CODEHOP	consensus degenerate hybrid oligonucleotide primer
CPP	*ent*-copalyl diphosphate
DAA	days after anthesis
DEPC	diethylpyrocarbonate
DNA	deoxyribonucleic acid
DTT	dithiothreotol
EDTA	ethylenediaminetetraacetic acid
EtOH	ethanol
FAM	6-carboxyfluorescein
GA	gibberellic acid
GC-MS	gas chromatography-mass spectrometry

Abbreviation	Definition
gDw	grams dry weight
gFw	grams fresh weight
GGDP	geranyl geranyl diphosphate
HOAc	acetic acid
HPLC	high performance liquid chromatography
HSL	hormone sensitive lipase
IAA	indole-3-acetic acid
IBA	indole-3-butyric acid
IPDP	isopentenyl diphosphate
LB	Luria-Bertani broth
LiCl	lithium chloride
LRR	leucine rich repeat
MeOH	methanol
MGB	minor groove binding
$MgCl_2$	magnesium chloride
mRNA	messenger ribonucleic acid
NaCl	sodium chloride
PCR	polymerase chain reaction
PIPES	piperazine-N,N′-bis(2-ethanesulfonic acid)
qRT-PCR	quantitative real-time reverse transcriptase polymerase chain reaction
RACE	random amplification of cDNA ends

Abbreviation	Definition
RLM-RACE	RNA ligase mediated random amplification of cDNA ends
RNA	ribonucleic acid
rRNA	ribosomal ribonucleic acid
RTA	relative transcript abundance
SE	standard error of the mean
SEM	scanning electron microscopy
SIM	selected ion monitoring
SP	split pod
SPNS	split pod no seeds
STS	silver thiosulfate
TAMRA	tetramethylrhodamine
TMCS	trimethylchlorosilane
TRIS	tris(hydroxymethyl)aminomethane
tRNA	transfer ribonucleic acid
UTR	untranslated region

Chapter 1

Introduction

1.1 Motivation

Recent research in plant physiology has demonstrated that the sequence and timing of events essential to normal development is tightly regulated by a variety of mechanisms, many of which involve one or more phytohormones. Moreover, the biosynthesis, transport, and perception mechanisms of these hormones are often closely linked, creating a highly complex regulatory network. As a biochemically well-characterized and commercially important plant, the use of *Pisum sativum* as a model species provides opportunities to examine in depth the interactions between GA biosynthesis, auxin perception, ethylene production and sensitivity, and ABA within the developmental context of seed maturation, fruit development, and the transition from unfertilized ovary to pollinated fruit.

1.2 Thesis Outline

This thesis is organized as follows:

- Chapter 2 reviews literature on the GA biosynthesis and signal transduction pathways, with a particular focus on the similarities and differences between pea and other model organisms. Aspects of GA metabolism in pea fruit and seed development are discussed. This chapter presents growth and histological data

describing seed development in pea, metabolite profiling of ABA and major GAs, and the transcript profiling of GA biosynthesis and catabolism genes. It discusses the regulation of GA metabolism by ABA, and the relations between these phytohormones and the development of the seed.

- Chapter 3 reviews literature on mechanisms of auxin signal transduction and the role of auxins in pea fruit and seed development. It presents data describing the cloning and transcription profiling of two putative auxin receptor genes in the tissues of the fruit and seed, the influences of auxins and GAs on transcript accumulation of these two genes, the localization of endogenous auxins in pea seeds, and the role of seeds in regulating expression of these receptors in the pericarp. This chapter discusses the regulation of the isolated auxin receptors and their putative roles in the hormone network supporting fruit development.

- Chapter 4 summarizes the research presented in this thesis, provides overall conclusions of this work, and discusses directions for future research.

- Chapter 5 contains several appendices. This chapter includes results of metabolite profiling experiments presented on a dry weight and per seed basis, describes the spatial and temporal localization of GA biosynthesis and catabolism gene transcripts within the fruit, contains putative protein sequences and structural domains of the auxin receptors isolated in this work, and describes protocols used in PCR amplification of the putative auxin receptor gene *PsAFB6A*.

Chapter 2

Regulation of Gibberellin Biosynthesis

2.1 Background

2.1.1 Introduction

Gibberellins (GAs) are a class of hormones first isolated from the fungus *Gibberella fujikuroi* (Yabuta and Sumiki, 1938). At the time of writing, 136 structurally distinct GAs have been isolated from a variety of plant and fungal sources (MacMillan *et al*., 2009). *In vivo*, these hormones control a wide variety of developmental processes including seed germination (Ayele *et al*., 2006), stem elongation (Cosgrove and Sovonick-Dunford, 1989), and fruit and seed development (Ozga *et al*., 2002, 2009).

GAs are a structurally diverse class of diterpenoid acids containing two five-carbon and two six-carbon rings. Additionally, some GAs also possess a lactone ring formed from carbons 19 and 20 (and skeleton carbons 4 and 10), while other GAs can also have either stable (GA_6) or transient (16α,17-epoxy GA_4) epoxide moieties (MacMillan *et al*., 1962). Many GAs consist of the same *ent*-gibberellane structure and differ from one another primarily through the position(s) of one or more hydroxyl groups. In particular, hydroxylation at carbons 2 and 3 has particular biological significance. Hydroxylation at carbon 3 can produce biologically active GAs from non-active precursors, whereas hydroxylation at carbon 2 typically deactivates biologically active GAs or precludes precursor GAs from conversion to bioactive GAs. Major bioactive

GAs include GA_1, GA_3, and GA_4, depending on the organism and tissue (all these GAs have hydroxyl groups at carbon 3). Each of these biologically active GAs, and in most cases their precursors as well, has a corresponding 2-hydroxylated version. Hydroxylation at carbon 2 can inactivate biologically active GAs, such as conversion of bioactive GA_1 to biologically inactive GA_8, or can remove GAs from the substrate pool, such as conversion of GA_{20} to GA_{29}.

2.1.2 Gibberellin Biosynthesis

Gibberellin biosynthesis can be divided into three major stages. The first stage of GA biosynthesis consists of the reactions which convert isopentenyl diphosphate (IPDP) to the 20-carbon linear precursor geranyl geranyl diphosphate (GGDP) and the cyclization of GGDP to *ent*-kaurene in a multi-step, ATP-dependant series of reactions. The second stage of GA biosynthesis is the conversion of *ent*-kaurene to GA_{12}-aldehyde, a ubiquitous precursor GA, by the actions of multiple cytochrome P450 mono-oxygenases. The third stage of GA biosynthesis involves the conversion of GA_{12} through a number of oxidation events catalyzed by multiple cytosolic 2-oxoglutarate dependent di-oxygenases to a wide variety of structurally unique GAs.

First stage of GA biosynthesis: IPDP to ent-kaurene

The linear 20-carbon precursor GGDP is common to a number of terpenoid synthesis pathways in addition to the GA pathway, and can be formed via two pathways: the methylerythritol phosphate pathway and the mevalonate pathway. Both pathways generate the IPDP and dimethylallyl diphosphate necessary to produce GGDP, but the

methylerythritol phosphate pathway occurs in the plastid while the mevalonate pathway is cytosolic (Bick and Lange, 2003). While there is some exchange between these two pathways, most likely via IPDP uptake (Soler *et al*., 1993), studies with ^{13}C-labeled intermediates specific to each pathway in combination with various knockout lines in *Arabidopsis* have demonstrated that the majority of the precursor IPDP for the GGDP used in GA biosynthesis are derived from the plastid-specific methylerythritol phosphate pathway (Kasahara *et al.*, 2002). This is not surprising, as the mRNAs of several genes required for GA biosynthesis also localize to the plastid (Sun and Kamiya, 1997).

Once GGDP is produced from IPDP generated through the plastid-specific methylerythritol phosphate pathway, two terpene synthase enzymes catalyze the formation of the 4 primary rings, the first committed steps in GA biosynthesis. The first of these enzymes is *ent*-copalyl diphosphate synthase, which catalyzes the formation of the bonds between carbons 4 and 5, and carbons 9 and 10 in the mature GA molecule (Figure 2.1). The second terpene synthase in the GA biosynthesis pathway is *ent*-kaurene synthase (Sun and Kamiya, 1994), which acts on *ent*-copalyl diphosphate to produce *ent*-kaurene in an ATP-dependant manner. Both *ent*-copalyl diphosphate synthase (Sun and Kamiya, 1997) and *ent*-kaurene synthase (Aach *et al*., 1997) localize to the plastid, supporting other data indicating that the early stages of GA biosynthesis occur in the plastid.

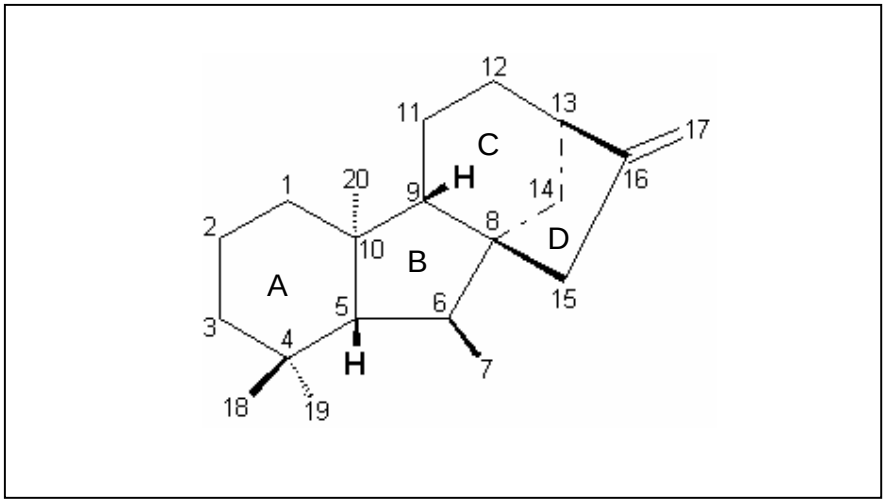

Figure 2.1: ent-Gibberellane (general GA) structure with carbons numbered. Structural features of some key GAs in *Pisum* include the formation of carboxylic acids or a lactone ring between carbons 19 and 20 and the hydroxylation of carbons 13, 2, and 3.

Second stage of GA biosynthesis: ent-kaurene to GA_{12}-aldehyde

The next steps in GA biosynthesis involve the sequential oxidation of *ent*-kaurene at carbon 19 by *ent*-kaurene oxidase, the rearrangement of ring B into a 5-carbon ring structure, and oxidation of carbon-7 by *ent*-kaurenoic acid oxidase (Figure 2.1). Both *ent*-kaurene oxidase and *ent*-kaurenoic acid oxidase are cytochrome P450 mono-oxygenases encoded by the CYP701A and CYP88A genes, respectively, in Arabidopsis (Nelson *et al.*, 2004). *ent*-Kaurene oxidase catalyzes three sequential oxidation reactions at carbon 19, first to an alcohol, then to an aldehyde and finally to a carboxylic acid (*ent*-kaurenol, *ent*-kaurenal, and *ent*-kaurenoic acid, respectively). In *Pisum*, these reactions are catalyzed by the PSKO1 protein (Davidson *et al*., 2004), encoded by the *LH* gene (*PsKO1* in more modern nomenclature), a member of the same subfamily of cytochrome P450 enzymes as the *Arabidopsis* enzymes. *ent*-Kaurenoic acid oxidase then catalyzes the oxidation of *ent*-kaurenoic acid at carbon 7, which is at this point still part of a 6

membered ring, to produce *ent*-7α-hydroxykaurenoic acid. GA_{12}-aldehyde synthase then converts *ent*-7α-hydroxykaurenoic acid to GA_{12}-aldehyde. One or more GA 7-oxidases then catalyze the oxidation of GA_{12}-aldehyde at carbon 7 to a carboxylic acid, producing GA_{12}, a precursor to bioactive GAs in many systems.

While the production of *ent*-kaurene occurs within the plastid, the later stage oxidations and other modifications of GA_{12} occur in the cytosol. Transport of GA precursors to the cytosol is promoted by changes in hydrophobicity in the molecules themselves. Import assays utilizing radio-labelled *ent*-kaurene oxidase show that this enzyme localizes to the outer layer of the chloroplastic membrane (Helliwell *et al*., 2001). While *ent*-kaurene is produced within the plastid, it is highly hydrophobic, and transport across the chloroplastic membrane is likely facilitated by this feature. Once *ent*-kaurene oxidase accepts *ent*-kaurene, it catalyzes three sequential oxidations at carbon 19, first to an alcohol, then to an aldehyde, and finally to a carboxylic acid. Each of these intermediates is more hydrophilic than the last, suggesting an obvious mechanism for release from the outer chloroplastic membrane. Fusion constructs containing the N-terminal targeting sequence of two *Arabidopsis ent*-kaurenoic acid oxidases and green fluorescent protein (GFP) indicate that this enzyme localizes to the endoplasmic reticulum, and is entirely absent from the plastid (Helliwell *et al.,* 2001). After release from the chloroplastid membrane via the actions of *ent*-kaurene oxidase, the now more hydrophilic GA precursor *ent*-kaurenoic acid is cytosolic and can interact with *ent*-kaurenoic acid oxidase for conversion to *ent*-7α-hydroxykaurenoic acid. The last stage of GA biosynthesis, catalyzed by multiple 2-oxoglutarate-dependent dioxygenases, is carried out in the cytosol.

Third stage of GA biosynthesis: GA_{12}-aldehyde to other GAs

The reactions in the last stage of GA biosynthesis are catalyzed by a number of cytosolic 2-oxoglutarate dependent di-oxygenases (Thomas *et al.*, 1999). GA biosynthesis in this stage can be divided into the early 13- and non-13-hydroxylation pathways (Figure 2.2). The non-13-hydroxylation pathway is the primary pathway in some species, including *Arabidopsis* (Talon *et al*., 1990*)*. In this pathway a GA 20-oxidase acts on GA_{12} to produce the lactone ring through a series of oxidations at carbon 20. A number of stable intermediates are formed during this process, including GA_{15} and GA_{24} (both lacking the lactone ring) before the final production of GA_9, the ultimate product of GA 20-oxidase in this pathway. Alternatively, GA_{12} can be converted to GA_{110}, irreversibly removing precursors of bioactive GA through β-hydroxylation at carbon 2 (Owen *et al*., 1998). GA_9 has two fates in this pathway; it is either catabolized in a similar manner as GA_{12} through 2β-hydroxylation to produce GA_{51}, or it can be converted to bioactive GA_4 through the actions of a GA 3β-hydroxylase. A further level of regulation is the deactivation of bioactive GA_4 through 2β-hydroxylation, producing GA_{34}.

The early 13-hydroxylation pathway, responsible for the production of the majority of bioactive GA in pea, is characterized by the initial hydroxylation of GA_{12} at carbon 13, and the retention of this group in all subsequent metabolites. The enzymes responsible for this reaction have not been isolated, but they may play an important regulatory role acting as gate-keepers, controlling levels of precursor available to the 13-hydroxylation pathway. The early 13-hydroxylation pathway is nearly identical to the non-13-hydroxylation pathway, with the only exception being the presence of the

hydroxyl group at carbon 13 in all GAs from GA_{53} onwards (Figure 2.2). GA 13-oxidase is presumed to act directly on GA_{12} in a single reaction to produce GA_{53}, the 13-hydroxylated equivalent to GA_{12} and initial precursor in this pathway. Enzymes capable of hydroxylating GA_{12} at carbon 13 have not been identified at this time, although one recombinant GA 3-oxidase is capable of 13-hydroxylating GAs *in vitro*, though this activity (as well as several others) is very weak and likely non-existent or an insignificant factor in GA flux *in vivo* (Appleford *et al*., 2006).

GA_{53} can either be irreversibly removed from the bioactive GA precursor pool by GA 2-oxidase (producing GA_{97}) or converted to GA_{20} via GA_{44} and GA_{19} by the multifunctional GA 20-oxidase. Like GA_9 in the non-13-hydroxylation pathway, GA_{20} is the biologically inactive precursor that is converted to bioactive GA by GA 3β-hydroxylase, in this case producing GA_1. GA_{20} can also be irreversibly removed from the bioactive GA precursor pool by GA 2-oxidases producing GA_{29}. Finally, bioactive GA_1 can be inactivated by GA 2-oxidases, yielding GA_8.

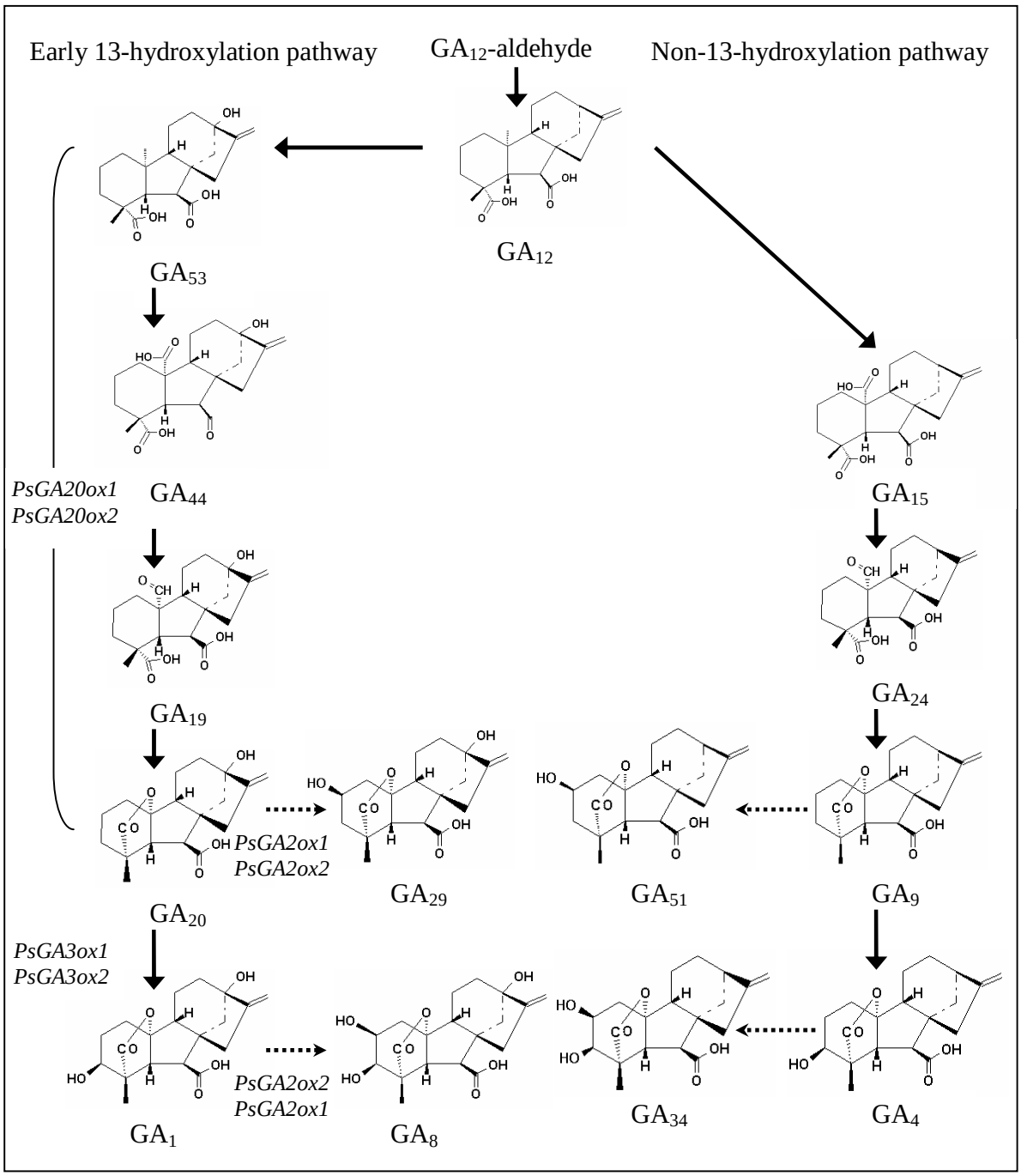

Figure 2.2: The third stage of GA biosynthesis: the non-13-hydroxylation and early-13-hydroxylation GA biosynthesis pathways. GA biosynthetic reactions are indicated by solid arrows; GA catabolic reactions are indicated with dashed arrows. Genes encoding for enzymes involved in this pathway in *Pisum* are indicated in italics.

2.1.3 Deactivation

GA biosynthesis is regulated at a number of sites in the pathway. The most thoroughly characterized mode of bioactive GA deactivation or the removal of precursors for bioactive GA production is through 2β-hydroxylation by GA 2-oxidases. There are three sub-families of GA 2-oxidase genes (classes I, II, and III; Lee and Zeevaart, 2005), and the various members have differences in substrate specificity and affinity, developmental roles, and expression patterns. GA 2β-hydroxylation is assumed to be non-reversible, and composes a primary mechanism in many systems by which bioactive GA levels are regulated.

In the non-13-hydroxylation pathway, another cytochrome P450 mono-oxygenase (in the same enzyme family as *ent*-kaurene oxidase that catalyzes the sequential conversion of ent-kaurene to *ent*-7α-hydroxykaurenoic acid) is capable of deactivating a number of bioactive GAs (or removing precursors of bioactive GAs) through another mechanism. The enzyme, CYP714D1 in rice (Nelson *et al*., 2004) is capable of generating an epoxide from the double bond present between carbons 16 and 17 (Figure 2.1). While the double bond between carbons 16 and 17 is present in most GAs, thise enzyme is specific to non-13-hydroxylated GAs, and cannot deactivate 13-hydroxylated forms (Zhu *et al*., 2006). Subsequent to epoxidization, the 16α,17-epoxy GA can be spontaneously hydrated to produce a 16,17-dihydro-16α,17-dihydroxy GA, an inactive GA catabolite.

In addition to 2β-hydroxylation and epoxidation at carbons 16 and 17, GAs can also be methylated by GA methyltransferases (Varbanova *et al*., 2007). These reactions are catalyzed by at least two members of the SABATH family of methyltransferases in

Arabidopsis, which methylate a number of GAs in both the non-13-hydroxylation and early-13-hydroxylation pathways at carbon 7 (Figure 2.1). In *Arabidopsis*, as well as several other angiosperms, the methyl esters produced from this reaction are not biologically active, but in other species, GA methylation may be an important step in the production of bioactive GAs. The role of GA methylation in development has not been extensively researched, and the implications of GA methylation in many species are as of yet unknown.

GAs can also be deactivated through glycosylation. GAs can be converted to O-linked glycosides at a number of hydroxyl groups, producing GA-O-glucosyl ethers, or through the carbon 7 carboxylic acid, yielding glucosyl-esters (reviewed in Schneider and Schliemann, 1994). In addition to deactivation through glycosylation, GA-glucose conjugates can be hydrolysed to yield the parent GA (Schneider *et al*., 1992). This mechanism allows the alteration of the profile of bioactive and precursor GAs with the later possibility of restoration, whereas 2-β-oxidation irreversibly removes GAs from the metabolite pool, although the degree to which GA glycosylation affects GA profiles in pea has not been determined.

2.1.4 Gibberellin Signal Perception

GA receptors

The first GA receptor was isolated from the *gid1* rice mutant (Ueguchi-Tanaka *et al*., 2005). These plants are dwarfed and sterile, as GAs are required for general plant growth as well as fruit and seed development. Several recessive, loss of function alleles

were isolated, and bioactive GA levels were much higher in these lines than in wildtype, indicating that while GA response was severely decreased, GA biosynthesis was not, and therefore the *gid1* gene is likely involved in GA signal perception. The *GID1* gene and its homologues in other species contain two hormone-sensitive lipase (HSL) motifs and have sequence similarity to bacterial HSL genes, but have no lipase activity due to mutations in an essential catalytic histidine residue. Fusions between GID1 and green fluorescent protein localize to the cytoplasm and nucleus. Kinetics studies with various GAs and analogues have demonstrated that GID1 (and its homologues) bind specifically to bioactive GAs, and not their inactive precursors (Ueguchi-Tanaka *et al*., 2005). While rice possesses just one GID1 homologue, there are three genes present with overlapping activities in *Arabidopsis*. Because of this functional redundancy, single loss of function mutants in Arabidopsis display largely wild-type features, but triple and some double mutants display severe dwarfing and delayed or no flowering (Griffiths *et al*., 2006).

While the soluble *GID1* family of receptors is clearly important in both rice and *Arabidopsis*, there is evidence that another receptor or group of receptors may be significant in other systems. In barley, the innermost layer of the seed coat, the aleurone layer, is an important tissue for seed germination and the mobilization of starch reserves (Chrispeels and Varner, 1967). In a mature barley seed, the endosperm consists of a dense mixture of starches. At germination, the embryo produces a pulse of bioactive GA_3, which travels to the aleurone layer of the seed coat stimulating α-amylase gene expression and enzyme activity to hydrolyze endosperm starch into the sugars necessary for growth of the embryo. Because of this strong GA response and the ease of measuring starch and sugar content, aleurone cells have been a preferred system of study for GA

effects (Gilroy and Jones, 1994). In experiments using protoplasts isolated from barley aleurone cells, α-amylase production and starch catabolism were observed when biologically active GA_3 was applied to the exterior of cells. However, when GA_3 was directly injected into the protoplasts, no GA response was observed. Controls for microinjection demonstrated that the protoplasts were still responsive to external GA application, precluding the possibility that microinjection damaged the protoplasts, and radio-labelling indicated that the injected GA_3 remained in the protoplasts for at least 24 hours, contradicting the possibility that injected GAs simply diffused out of the protoplasts (Gilroy and Jones, 1994). Taken together, these data suggest that, at least in the aleurone layer of barley seed coat, a second method of GA signal perception may be present, and that this method likely involves a plasma membrane-bound receptor.

GA signal transduction

Besides the GA receptors, another group of central players in GA signal transduction are the DELLA proteins. DELLA proteins are a subfamily of the GRAS family of transcriptional repressors, and localize to the nucleus (Silverstone *et al.*, 1998). The DELLA proteins are composed of two domains: an N-terminal regulatory DELLA domain and a larger C-terminal GRAS domain. The C-terminal GRAS domain is a transcriptional regulator, and contains the nuclear localization signal for the protein as well as two leucine-rich repeats required for contacts with the SCF (Skp1, Cullin, F-box) E3 ubiquitin ligase complex (Dill *et al.*, 2004). SCF is a large complex that targets a wide variety of proteins and transcriptional regulators for degradation via the 26s proteasome, and is involved in other hormone signalling pathways, including the auxin

pathway (Gray *et al*., 1999). The N-terminal DELLA domain is capable of making protein-protein contacts with the GID1 GA receptor (which is necessary for the induction of GA response; Willige *et al*., 2007). This domain is named after a conserved sequence (DELLA), but also contains a second conserved VHYNP sequence, and a large serine and threonine rich tract, the exact sequence of which varies between homologues. The DELLA and VHYNP domains are necessary for GA receptor binding.

When GID1 binds the appropriate active GA, conformational changes occur in the GID1-GA complex which permit protein-protein contacts between the GID1 receptor and the DELLA protein. The new structure produced by GID1-DELLA binding in turn makes protein-protein contacts with the SCF complex possible. Once bound to the SCF complex, ubiquitin is transferred by the SCF machinery to the DELLA protein, which is shuttled to the 26s proteasome and degraded (Figure 2.3), allowing expression of whichever gene it was previously repressing (Fu *et al*., 2002).

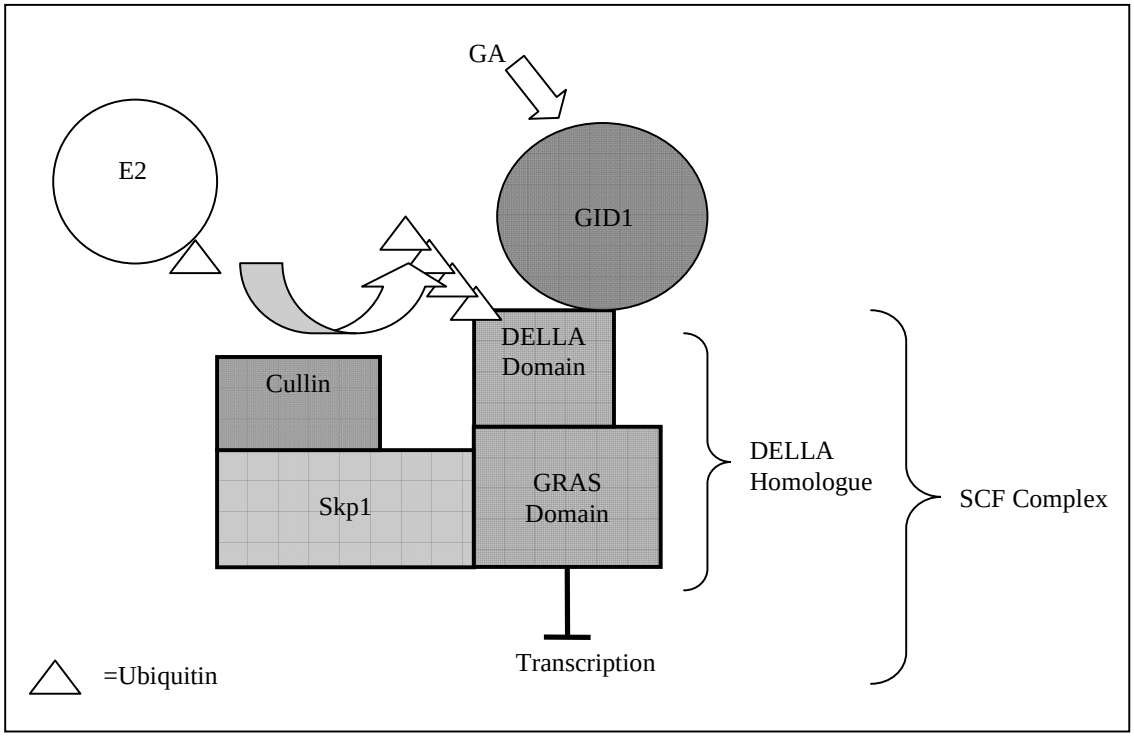

Figure 2.3: Schematic of SCF complex detailing interactions with key components of the GA signalling pathway. Upon GID1-GA binding and interactions with the N-terminal DELLA domain, the DELLA protein is targeted for ubiquitin-mediated degradation, relieving transcription repression of GA-responsive genes.

2.1.5 Gibberellins in *Pisum sativum* L.

Bioactive GA levels are determined primarily through regulation at the third stage of the GA biosynthesis pathway, the sequential oxidation of GA_{12} to other inactive GAs or to bioactive GAs. Overexpression of either or both terpene synthase genes (*AtCPS* and *AtKPS*) of the second stage of GA biosynthesis does not have an appreciable effect on the later GA metabolite profile, bioactive GA levels, or overall plant morphology in *Arabidopsis* (Fleet *et al*., 2003). While the second stage GA biosynthesis enzymes (*ent*-kaurene to GA_{12}-aldehyde) are present as single-copy genes or very small families in

plants, the various enzymatic steps of the last stage of GA biosynthesis (GA_{12} to bioactive GA) are catalyzed by larger gene families, partially explaining the wide structural diversity in GAs as well as offering opportunities for differential regulation of the pathway to fulfill the multitude of physiological roles involving GAs.

In the model legume *Pisum sativum* L., the early-13-hydroxylation pathway is responsible for the production of the primary bioactive GA, GA_1 (Kamiya and Graebe, 1983). GA_{12}, the precursor to all GAs and the branching point of the early-13-hydroxylation and non-hydroxylation pathways, is oxidized at carbon 13 by a yet unknown GA 13-oxidase.

The next three steps in the pathway are two sequential oxidations at carbon 20 followed by the loss of C20 at the aldehyde level with the formation of a lactone ring (Figure 2.2). These reactions are catalyzed by the multifunctional enzyme products of two known genes, *PsGA20ox1* (Garcia-Martinez *et al*., 1997) and *PsGA20ox2* (Lester *et al*., 1996). These reactions produce the immediate precursor of bioactive GA_1, GA_{20}. GA_{20} can be oxidized at carbon 3 by GA 3β-hydroxylases coded by *PsGA3ox1* (Lester *et al*., 1997) and recently cloned *PsGA3ox2* genes, to produce bioactive GA_1 (Weston *et al*., 2008). Both GA_1 and its immediate (biologically inactive) precursor, GA_{20}, are substrates for multiple GA 2-oxidases. In pea, two GA 2-oxidase genes named *PsGA2ox1* and *PsGA2ox2* have been cloned (Lester *et al.*, 1999). Using the most recently described nomenclature, which divides the GA 2-oxidase genes into three groups based on protein sequence homology (Lee and Zeevaart, 2005), the *PsGA2ox1* gene is a member of the class I group of GA 2-oxidases while *PsGA2ox2* is a member of the class II group. At the time of writing, no known class III GA 2-oxidases have been identified

in *Pisum*. The enzymes encoding these genes catalyze the hydroxylation of carbon 2 of both GA_1 and GA_{20}, producing the inactive metabolites GA_8 and GA_{29}, respectively (Martin *et al*., 1999). The *E. coli* heterologous expression products of both GA 2-oxidases are capable of catalyzing this reaction on either substrate, and while the class I enzyme *PsGA2ox1* has an approximately equal substrate affinity for both GA_{20} and GA_1, the class II enzyme *PsGA2ox2* has a much higher affinity for bioactive GA_1 (Lester *et al*., 1999).

The differential regulation of the various *PsGA20ox*, *PsGA3ox*, and *PsGA2ox* genes during pea seed development is evident from transcript profiling experiments (Ozga *et al*., 2009). In whole seeds, *PsGA20ox1* transcript abundance was high early on in development (2 to 5 DAA), while *PsGA20ox2* transcript abundance was high later (8 to 12 DAA). Steady-state transcript levels of *PsGA3ox1* were low shortly after fertilization but increased later (2 to 4 DAA), and the whole seed mRNA abundance of both *PsGA3ox* genes increased as the embryo gained mass (8 to 12 DAA). From fertilization to 10 DAA, transcript abundance of both *PsGA2ox* genes was minimal in the seeds, suggesting that GA catabolism was not a highly active process at this time. However, between 10 and 12 DAA, whole seed *PsGA2ox1* transcript abundance markedly increased, as did that of *PsGA2ox2* between 14 and 20 DAA (Ozga *et al*., 2009).

During seed development, other phytohormones including auxins and abscisic acid (ABA) function alongside or interact with gibberellins in a complex regulatory network. Early assays of hormone activity in pea demonstrated an increase in extractable ABA activity within the embryo during later stages of development (16 to 24 DAA; cv.

Alaska; Eeuwens and Schwabe, 1976). Wang *et al*. (1987) measured seed coat and embryo ABA content in pea seeds across development via GC-MS with the use of deuterated internal standards.

Their work described a biphasic distribution of ABA in the developing seed, with an initial smaller increase in ABA abundance in the rapidly growing seed coat followed by a much larger increase later in development in the maturing embryo, similar to that observed by Eeuwens and Schwabe (1976).

In *Arabidopsis* (Karssen *et al*., 1983) and *Nicotiana* (Frey *et al*., 2004) seeds, the transfer of maternally (seed coat) derived ABA plays a key role in promoting embryo development. This event triggers the further biosynthesis of ABA by the embryonic tissues, which in turn serves to further embryo growth. The consecutive peaks in ABA abundance in the seed coat and embryo (Wang et al., 1987) suggest a similar scenario in pea. Since GAs have well-documented roles as promoters of plant growth and development, it is possible that the effects of ABA on seed growth are mediated at least partially by GAs. Specifically, the initial production of ABA in the seed coat raises the possibility that, in addition to serving an important role in embryo maturation, ABA serves as a controller of seed coat development and morphology.

2.1.6 Goals

This study will use a variety of tools to examine the roles of phytohormones in legume seed development, specifically in *Pisum sativum*. To gain a better understanding of GA pathway flux through early seed development, the transcription profiles of key GA biosynthesis and catabolism genes will be investigated in the various tissues of the seed

via qRT-PCR, and the metabolite profiles of key GAs will be determined through GC-MS. To correlate endogenous hormone levels with physiological development, the morphology of the seed coat and embryo will be investigated with light microscopy. The possible roles of ABA in the regulation of GA biosynthesis at both the metabolite and gene transcript levels will be examined through the profiling of endogenous ABA and through hormone application studies.

2.2 Methods

2.2.1 Plant Material

Seeds of *Pisum sativum* L. I_3 (Alaska-type) were planted at an approximate depth of 2.5 cm in 3-L plastic pots (3 seeds per pot) in Sunshine #4 potting mix (Sun Gro Horticulture, Vancouver, Canada). Plants were grown in a climate-controlled growth chamber with a 16 h-light/8 h-dark photoperiod (19°C/17°C) with an average photon flux density of 383.5 $\mu E/m^2s$ (measured with a LI-188 photometer, Li-Cor Biosciences, Lincoln, Nebraska). Flowers were tagged at anthesis and seeds were harvested at selected stages as identified by date of anthesis and, where appropriate, pericarp length and width. Seeds were harvested directly onto ice and, if required, dissected immediately, then stored at -80°C. Seeds were harvested whole or dissected into seed coat, endosperm and embryo at 8, 10, and 12 days after anthesis (DAA). At 14, 16, 18, and 20 DAA, seeds were dissected into seed coat and embryo or seed coat, cotyledons, and embryo axis. When harvested, endosperm was removed from the seeds using a micropipette and immediately frozen on dry ice. Endosperm samples were centrifuged

briefly before RNA or metabolite extraction to remove any contaminating vegetative tissue. Seed coats and embryos at 8, 10, 12, and 14 DAA were transferred to microfuge tubes or 20 mL scintillation vials on ice containing distilled water and further washed three times with distilled water to remove any remaining endosperm prior to freezing at -80^{o}C.

2.2.2 ABA treatments

(+)-ABA was applied to seeds using a split-pericarp technique (Ozga *et al*., 1992). For ABA application to 10 DAA seeds, an incision was made down the middle of the dorsal suture of 10 DAA pericarps. The two halves of the pericarp were held apart with forceps, and two 1.5 µL aliquots of 100 µM ABA in aqueous 0.1% w/v Tween 80 were applied to the surface of each seed. Seeds from the control pericarps received two 1.5 µL aliquots of aqueous 0.1% w/v Tween 80. The inclusion of a detergent in this solution decreases surface tension on the droplet, increasing the area of the seed-droplet interface and allowing for more efficient absorption of ABA into the seed. Occasionally the most distal or proximal seeds in the pod were much smaller than the others, likely due to either late fertilization or recent spontaneous abortion, which were invariably identified by their lack of endosperm. In these cases, seeds were not treated but were instead removed with forceps to eliminate the unnecessary use of nutrients by these seeds and reduce variability due to staging discrepancies between these late-fertilized seeds and normal ones. Pericarps were fastened horizontally to bamboo stake scaffolding erected in the growth chamber to prevent droplets of the applied solutions from rolling off the seeds and contacting the endocarp. To prevent desiccation, treated pericarps were fastened closed

with tape and enclosed in plastic. Pericarps remained attached to the plant throughout the experiment. Seeds were harvested 6 h after ABA treatment for RNA extraction and 48 after ABA treatment for hormone extraction (to allow for changes in hormone profiles).

For ABA application to 16 DAA seeds, a modified application method was developed since 16 DAA seeds are in direct contact with the inner walls of the pericarp, making it infeasible to apply a solution to the outer surface of the seed coat without at the same time applying it to the inner walls of the pericarp. To treat seeds at 16 DAA, pods were split along the dorsal pericarp suture, the exposed part of each seed (opposite from attachment to the pericarp) was punctured once with a 10 gauge needle, and a section of seed coat and cotyledon approximately 2.5 mm in length was removed. A 3 µL solution of 100 µM ABA in aqueous 0.1% w/v Tween 80 was injected directly into the cavity of each seed within the pericarp. A control solution (aqueous 0.1% w/v Tween 80) was injected into the cavity of each seed in the control pericarps. Pericarps were taped shut and covered with plastic to maintain humidity, and remained attached to the plant throughout the experiment. Seeds were harvested 48 hours after ABA treatment for RNA and hormone extraction (to allow ABA applied to the cotyledons to move to both the embryo axis and the seed coat and to allow for changes in hormone profiles).

2.2.3 RNA Isolation and Processing

Tissues were ground in liquid N_2 and subsamples of 20 to 300 mg Fw were removed for total RNA isolation using a guanidinium thiocyanate-phenol-chloroform extraction (Ozga *et al*., 2003). After extraction with either TRIzol (Invitrogen) or TRI reagent (Ambion) and centrifugation at 4°C in a benchtop centrifuge to remove cellular

debris, a phase separation using chloroform (0.2 mL mL^{-1} Tri reagent) was performed and the organic phase discarded. RNA was precipitated from the aqueous phase with isopropanol (0.25 mL mL^{-1} Tri reagent) and a high salt solution (1.2 M sodium citrate and 0.8 M NaCl) to remove polysaccharides. The RNA pellet was resuspended and RNA was precipitated with 8 M aqueous LiCl. The RNA pellet was again resuspended and a final precipitation with 3 M sodium acetate (pH=5.2, final concentration=96.77mM) and 100% ethanol (final concentration=64.5% v/v) was performed. The RNA was pelleted and washed twice with 70% aqueous ethanol then resuspended and treated with DNAse (DNA-free kit; Ambion). DEPC-treated water was utilized throughout this procedure to reduce RNAse contamination. RNA concentration was quantified by measuring A_{260}, and RNA purity was estimated with A_{260}/ A_{280} and A_{260}/A_{230} ratios. RNA samples were diluted to 25 ng μL^{-1} and aliquoted to 96-well plates in a sterile laminar flowhood to reduce contamination.

2.2.4 qRT-PCR

Transcript quantification was performed on a model 7700 sequence detector (Applied Biosystems) except for most of the ABA treatment experiments (16 DAA injection assay seed coat samples, 10 DAA split-pericarp assay seed coat, embryo, whole seed samples, and all *PsGA3ox2* quantification), for which a StepOnePlus system (Applied Biosystems) was used. Reverse transcription and quantification of *PsGA3ox1*, *PsGA3ox2*, *PsGA2ox1*, *PsGA2ox2*, *PsGA20ox1*, and *PsGA20ox2* was performed using TaqMan One-Step RT-PCR Master Mix (Applied Biosystems; final concentration 1x) and 200 ng of DNAse treated total RNA (final concentration 8 ng μL^{-1}) in duplicate in a

final volume of 25 µL per well. The final concentration of forward and reverse primers was 300 nM each, and the final concentration of probe was 100 nM. Reverse transcription was carried out for 30 minutes at 48°C. DNA polymerase antibody was denatured at 95°C for 10 minutes. Quantification was carried out for 40 cycles of the following program: denaturation at 95°C for 15 seconds, primer annealing and extension at 60°C for 1 minute. Probes were labelled at the 5`end with FAM (6-carboxyfluorescein) and at the 3`end with the MGB quencher (Applied Biosystems).

As an additional loading control, 18s rRNA was quantified on 3 ng of DNAse treated total RNA generated from a single dilution of the original 8 ng μL^{-1} stocks (final concentration 120 pg μL^{-1}) using the same master mix, primer and probe concentrations, and thermocycling conditions. Given the wide variety of tissues and large developmental time-spans used in this study, many commonly used control genes (including actin and ubiquitin) are not expressed at consistent levels, and are thus are not suitable. A mixture of primers containing 3` hydroxyl and C_6NH_2 chain terminators in a 1:9 ratio was used to quantify 18s transcript levels. The addition of competitive primers allows a larger amount of template to be used while maintaining an acceptable reaction profile, effectively decreasing the variation which would be introduced during the serial dilution of RNA samples. The 18s probe was labelled at the 5`end with VIC and at the 3` end with the TAMRA quencher (Applied Biosystems). RNA templates and reaction components were aliquoted to 96-well plates in a sterile laminar flow hood, and all tools and the hood itself were washed regularly with RNAse Zap (Ambion) to reduce RNAse contamination. The coefficient of variation of 18s rRNA expression data was calculated

for each plate, and any samples with exceptionally high or low Ct values were removed from further analysis.

Probes and primers used in this study are described below (Table 2.1). Probes and primers for *PsGA3ox1* and 18s rRNA were designed by Ozga *et al.* (2003). Probes and primers for *PsGA2ox1*, *PsGA2ox2*, *PsGA20ox1*, and *PsGA20ox2* were designed by Ayele *et al.* (2006). Probes and primers for *PsGA3ox2* were designed by Ozga *et al.* (2009).

Transcript levels were calculated using the ΔCt method (Livak and Schmittgen, 2001) using the following formula, where X is an arbitrary value equal to or greater than the highest assayed Ct value and E is the reaction efficiency for the amplicon in question:

$$\text{Transcript abundance} = (1+E)^{(X-Ct)}$$

Reaction efficiency was calculated by diluting a single RNA sample over several log concentrations (typically from 400-500 ng/reaction to 0.05-0.08 ng/reaction), and running qRT-PCR as previously described. Data were plotted on a semi-log graph of Ct and log(input RNA), and a linear regression was calculated (Pfaffl, 2006). Assuming the r^2 value was sufficiently high, the slope of this equation was then used to calculate reaction efficiency (E; as a percentage) with the following formula:

$$\text{Efficiency} = (10^{[-1/\text{slope}]}-1)*100$$

Table 2.1: Primer and Probe Sequences for qRT-PCR Assays.

Gene		Sequence	Amplicon length
PsGA3ox1	Forward	5'-TTC GAG AAC TCT GGC CTC AAG	87 bp
	Reverse	5'-ATG TTC CTG CTA ACT TTT TCA TGG TT	
	Probe	5'-ACA ATA TCA CAG AAT CTG GT	
PsGA3ox2	Forward	5'-ATC ATG GGG TCA CCG TCT AA	104 bp
	Reverse	5'-GCT AGT GTC TTC ATT TGC TTT TGA	
	Probe	5'-CCT AAT GAC TAC GAA TAT T	
PsGA20ox1	Forward	5'-GCA TTC CAT TAG GCC AAA TTT C	104 bp
	Reverse	5'-CCA CTG CCC TAT GTA AAC AAC TCT T	
	Probe	5'-CCT TCA TGG CTC TTT C	
PsGA20ox2	Forward	5'-AAT ACA TCT TCT CTA CCG TTG CAA AT	88 bp
	Reverse	5'-TTG GCG GTG TTA AAC AAG GTT	
	Probe	5'-ACA TAC CCT CAG AGT TC	
PsGA2ox1	Forward	5'-TTC CTC CTG ATC ATA GCT CCT TCT	73 bp
	Reverse	5'-TTG AAC CTC CCA TTA GTC ATA ACC T	
	Probe	5'-GAG AAT CAC CAA CAT T	
PsGA2ox2	Forward	5'-AAC ACA ACA AAG CCT AGA ATG TCA A	83 bp
	Reverse	5'-ACC ATC TTC GAT AAC GGG CTT AT	
	Probe	5'-TGT ATT TTG CAG CAC CAC C	
18s rRNA	Forward	5'-ACG TCC CTG CCC TTT GTA CA	62 bp
	Reverse	5'-CAC TTC ACC GGA CCA TTC AAT	
	Probe	5'-ACC GCC CGT CGC TCC TAC CG	

2.2.5 Hormone Extraction

Hormone extraction and quantification was performed by Dr. Leon Kurepin at the department of Biological Sciences at the University of Calgary. Plant tissues were harvested and dissected at the University of Alberta as described previously, and frozen

tissues were subsequently freeze-dried (Virtis Freezemobile 6, Gardiner NY). Liquid endosperm samples were centrifuged briefly after harvesting to remove any contaminating cellular materials, and then were frozen on dry ice and maintained frozen until extraction.

Solid tissues were ground with liquid N_2 and washed sea sand. Ground tissue and liquid endosperm samples were extracted with 80% aqueous MeOH (v/v). Internal standards were added to the solvent as follows: 200 ng of [$^2H_6$] ABA (a gift from Drs. L. Rivier and M. Saugy, University of Lausanne, Switzerland) and 20-40 ng each of [$^2H_2$] GA_1, GA_3, GA_4, GA_8, GA_9, GA_{20} and GA_{29} (deuterated GAs were obtained from Prof. L.N. Mander, Research School of Chemistry, Australian National University, Canberra, Australia). The 80% MeOH extract was then filtered through a #2 Whatman filter (55 mm, Whatman International Ltd, Maidstone, England) and purified with a C_{18} preparative column (C_{18}-PC) consisting of a syringe barrel filled with 3g of C_{18} (Waters Ltd) preparative reversed-phase material (Koshioka *et al.*, 1983). The 80% MeOH eluate from this column was dried *in vacuo* at 35°C.

2.2.6 High-Performance Liquid Chromatography

The dried sample was dissolved in 1 mL of 10% MeOH with 1% acetic acid and injected into the HPLC using the method described by Koshioka *et al.* (1983). The HPLC apparatus (Waters Ltd) consisted of two pumps (model M-45), an automated gradient controller (model 680), and a Rheodyne injector (model 7125). The solvent reservoir for pump A was filled with 10% MeOH in 1% acetic acid [H_2O:MeOH:acetic acid=89:10:1, (v/v)], while pump B was 100% MeOH. A reversed phase C_{18} Radial-

PAK μ-Bondapak column (8 mm x10 cm) was used with a manually implemented 10–73% gradient program at a flow rate of 2 mL min^{-1}, i.e. 0–10 min (pump A, 100%; pump B, 0%), 10–50 min (pump A, 30%; pump B, 70%), 50–80 min (pump A, 0%; pump B, 100%), 80–90 min (pump A, 100%; pump B, 0%).

The HPLC fractions (4 mL) were dried *in vacuo* at 35ºC. Fractions from the C_{18} HPLC which were expected (based on retention times, minutes 9 to 32) to contain IAA, 4-Cl-IAA, ABA, GA_1, GA_3, GA_8, GA_{20} and GA_{29} were transferred with 100% MeOH to 2 mL glass vials and dried *in vacuo*. Later fractions (minutes 33 to 44, GA_4 and GA_9) from the C_{18} HPLC were grouped with 100% MeOH and dried *in vacuo*, then subjected to Nucleosil $N(CH_3)_2$ HPLC (nucleosil, 5μm, 5/16" OD× 4.6 mm ID) which was isocratically eluted with 0.1% HOAc in MeOH at 1.2 mL min^{-1} (Jacobsen *et al*. 2002). Three minute fractions from $N(CH_3)_2$ HPLC were taken to dryness *in vacuo*. Subsequently, fractions containing GA_4 and GA_9 (minutes 16 to 42) were transferred with 100% MeOH to 2 mL glass vials and dried *in vacuo*.

2.2.7 Gas Chromatography and Mass Spectrometry

Samples were methylated by ethereal CH_2N_2 for 20 min and then trimethylsilylated with N,O,-bis(trimethylsilyl)trifluoroacetamide (BSTFA) and 1% trimethylchlorosilane (TMCS) (Hedden, 1987; Gaskin and MacMillian, 1991). The identification and quantification of plant hormones was carried out using a gas chromatograph connected to a mass spectrometer (GC-MS) using the selected ion monitoring (SIM) mode. The derivatized sample was injected into a capillary column installed in an Agilent 6890 GC with a capillary direct interface to an Agilent 5973 mass

selective detector. The dimensions of the capillary column were 0.25 μm film thickness, 0.25 mm internal diameter, 30 m DB-1701 (model J&W122-0732, J&W Scientific, Inc). The GC temperature program was: 1 min at 60 °C, followed by an increase to 240 °C at a rate of 25 °C min^{-1} and an increase at 5 °C min^{-1} to 280 °C where it remained constant for 15 min before returning to 60 °C. The interface temperature was maintained at 280 °C. The dwell time was 100 ms and data was processed using HP G1034C MS ChemStation Software.

Comparisons of both GC-retention times of the GAs and [$^2H_2$]-GAs and of the relative intensities of molecular ion (M^+) pairs were used to identify endogenous GAs. Relative intensities of at least two other characteristic m/z ion pairs for each endogenous GA and its deuterated standard were also compared. The same approach was taken for identification of ABA utilizing [$^2H_6$] ABA as the internal standard. All stable isotope-labeled internal standards were added at the extraction stage with appropriate purification and chromatography being accomplished (see above) prior to GC-MS-SIM. Quantification was accomplished by reference to the stable isotope-labeled internal standard using equations for isotope dilution analysis, adapted by DW Pearce (Jacobsen *et al.*, 2002) from Gaskin and MacMillan (1991).

2.2.8 Histology

Seed coat tissues for histology studies were obtained by making two parallel cuts from the top to bottom (attachment site of the funiculus and pericarp) of the seed approximately 0.5 to 1 mm apart as indicated in Figure 2.4. Embryo samples were obtained from the regions directly underneath these sections, and excess material from

the inside of the cotyledons was trimmed to promote efficient fixation and resin infiltration. The final dimensions of the seed coat samples were 0.5 to 1 mm wide by 5 to 6 mm long (thickness of the entire seed coat). Final dimensions of embryo samples were 0.5 to 1 mm wide, 5 to 6 mm long, and 2 to 3 mm thick. Sections were taken from both right and left halves of the seed, and embryo samples were obtained from regions away from the cotyledon-cotyledon interface (Figure 2.4).

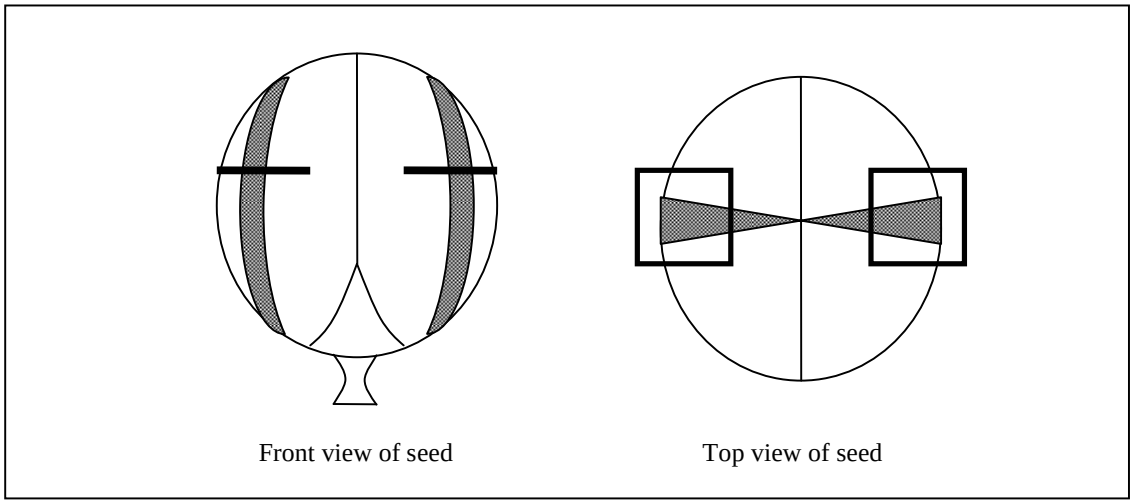

Figure 2.4: Schematic indicating orientation of sections used for histology experiments. Shaded regions indicate the region of tissue dissected and fixed, while the thick bars and boxes indicate the plane of sectioning visible in the micrographs.

Samples were fixed in 0.2% gluteraldehyde (v/v), 3% paraformaldehyde (v/v), 2 mM $CaCl_2$, 10 mM sucrose, and 25 mM PIPES (piperazine-N,N′-bis(2-ethanesulfonic acid)) at pH 7. Fixation was carried out overnight under vacuum to increase infiltration, then at atmospheric pressure for 2 days. Prior to embedding, tissues were washed three times for 10 minute intervals with 25 mM PIPES, then dehydrated usin a graded ethanol series of 30%, 50%, and 70% aqueous EtOH (v/v) for 15 minutes each. The 70%

aqueous ethanol was replaced, and tissues were stored for several days. Further dehydration was then carried out with 80%, 96%, and 100% EtOH (twice) at 15 minute intervals, then with 50% ethanol 50% propylene oxide (v/v), then 100% propylene oxide before embedding. Tissues were embedded in Spurr's epoxy resin (the hard resin protocol; Spurr, 1969) and cured at 70°C for 4 hours, then 60°C for 3 days.

Blocks were trimmed with blades and fine-toothed saws to a maximum surface area of approximately 2 mm^2. Seed coat samples were sliced to 1 µm-thick and cotyledon samples to 2 µm-thick sections with a Reichert Jung Ultracut E ultramicrotome using glass knives made by hand with an LKB Broma Knifemaker II. Sections were transferred from the water-filled collection boat to glass slides, stretched briefly with a JBS heat pen, and dried on a 60°C slide warmer. Slides were stained with 0.05% toluidine blue (w/v) in water for 3 minutes at room temperature and then were briefly washed with distilled water to remove excess stain. After drying at room temperature, slides were observed under a Zeiss Primostar light microscope and micrographs were taken with a Photometrics CoolSNAP CF camera. Image editing was performed with Adobe Photoshop. All scale bars were generated by calibration to a stage micrometer, not using field of view calculations. Cell area was estimated by manually tracing cells from each tissue type and stage using MetaMorph software (v 7.0r4, Molecular Devices). The average subsample size for cell area calculations was 98 cells per layer and time point, examined in two biological replicates

2.3 Results

2.3.1 Seed Development in *Pisum sativum* L.

Seed coat growth (Figure 2.5) and fresh weight (Figure 2.6A) markedly increased between 8 and 12 DAA, followed by more gradual fresh weight increase from 12 to 20 DAA. As the rate of seed coat growth (in fresh weight) decreased, the embryo began to expand rapidly and increased in both fresh weight (Figure 2.6B) and volume (Figure 2.5). By 14 to 16 DAA, the embryo composed the majority of the seed tissue by fresh weight (Figure 2.6A). From 12 to 20 DAA, increases in total seed fresh weight were driven primarily by embryo growth, while seed coat fresh weight increased minimally. Between 8 and 12 DAA, endosperm volume increased markedly, reaching maximum volume at 12 DAA, before being rapidly absorbed by the developing embryo between 12 and 14 DAA (Figures 2.5 and 2.6B).

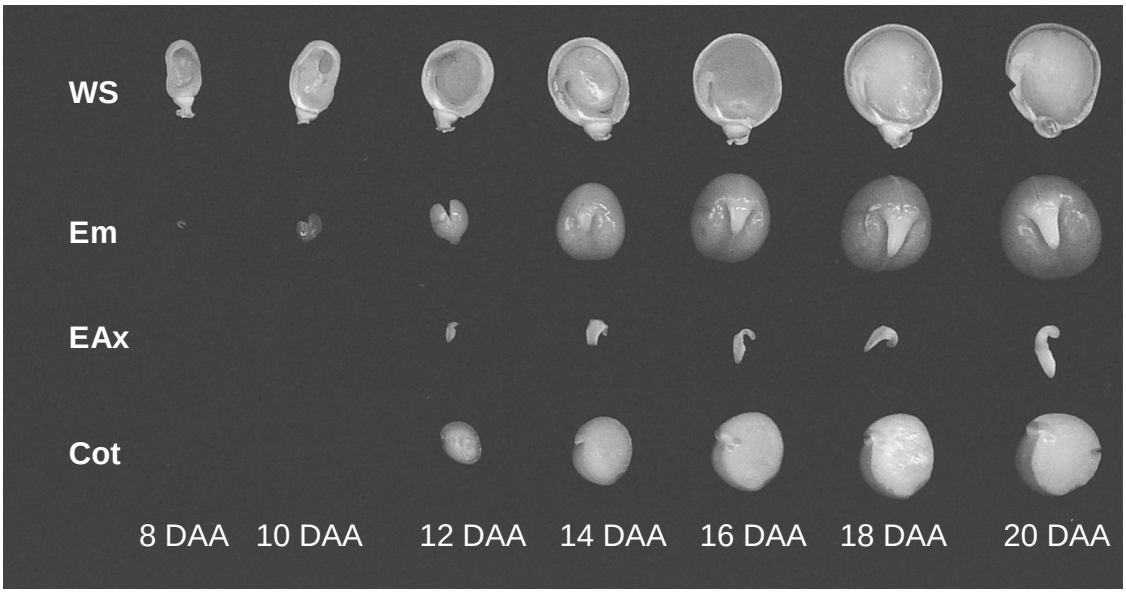

Figure 2.5: Representative pea seed tissues over development. Bisected whole seeds (WS) and embryos (Em) from 8 to 20 DAA, and embryo axes (EAx) and cotyledons (Cot) from 12 to 20 DAA.

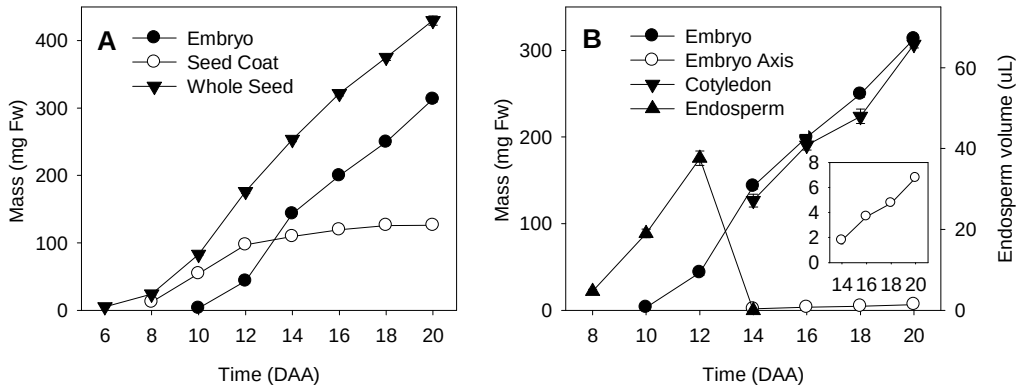

Figure 2.6: Development of seed tissues. (A) Whole seed, embryo, and seed coat fresh weight between 6 and 20 DAA. (B) Embryo, embryo axis (inset), and cotyledon fresh weight and endosperm volume (per seed) between 8 and 20 DAA. Data are expressed as means ± standard error. In some cases, standard error bars are not visible as they are obscured by symbols. Sample size varies by timepoint, n=53 to 228 for whole seed (except at 8 DAA, where n=8), n=43 to 106 for embryo, n=32 to 110 for seed coat (except at 8 DAA, where n=11), n=22 to 109 for embryo axis (except at 14 DAA, where n=8), n=21 to 107 for cotyledon (except at 14 DAA, where n=9), and n=10 to 28 for endosperm.

The seed coat of pea consists of several discernable layers. Outermost lies an epidermis consisting of several layers of thick-walled cells, subtended by a single layer of hypodermal cells (Figure 2.7A,B). The formation of macrosclereids in the seed coat epidermis and the differentiation of the seed coat hypodermis into hourglass-shaped cells were both observed as the seed developed from 10 to 20 DAA (Figure 2.7A,B). A layer of chlorenchyma cells subtend the hypodermis, and this layer decreased in area slightly from 10 to 16 DAA, but increased somewhat between 16 and 18 DAA (Figure 2.8A). Underneath the chlorenchyma cells are the ground parenchyma cells, larger cells with fewer chloroplasts than the chlorenchyma cells that increased in size gradually from 10 to 16 DAA (Figure 2.8A). Symplastic unloading of phloem nutrients ultimately destined for

the embryo occurs into the ground parenchyma cells (Patrick and Offler, 1995). The innermost layer of the seed coat is several layers thick of branched parenchyma cells, which are likely involved in apoplastic conversion of phloem-derived sucrose to glucose and fructose in the endospermal cavity (Weber *et al*., 1997). Seed coat thickness in the sampling area was relatively constant between 10 and 14 DAA (Figure 2.7B), during which time most of the increases in seed coat fresh weight occur. Between 14 and 16 DAA, the branched parenchyma rapidly increased to its maximum thickness (Figure 2.7B). In contrast to the rapid increase in branched parenchyma cell area between 14 and 16 DAA, By 16 DAA, the developing embryo has increased greatly in size (Figure 2.6B) and has contacted the inner surface of the seed coat (Figure 2.5). From 16 to 20 DAA, seed coat development was characterized by the compression of the branch parenchyma followed by the ground parenchyma by the expanding embryo (Figure 2.7B).

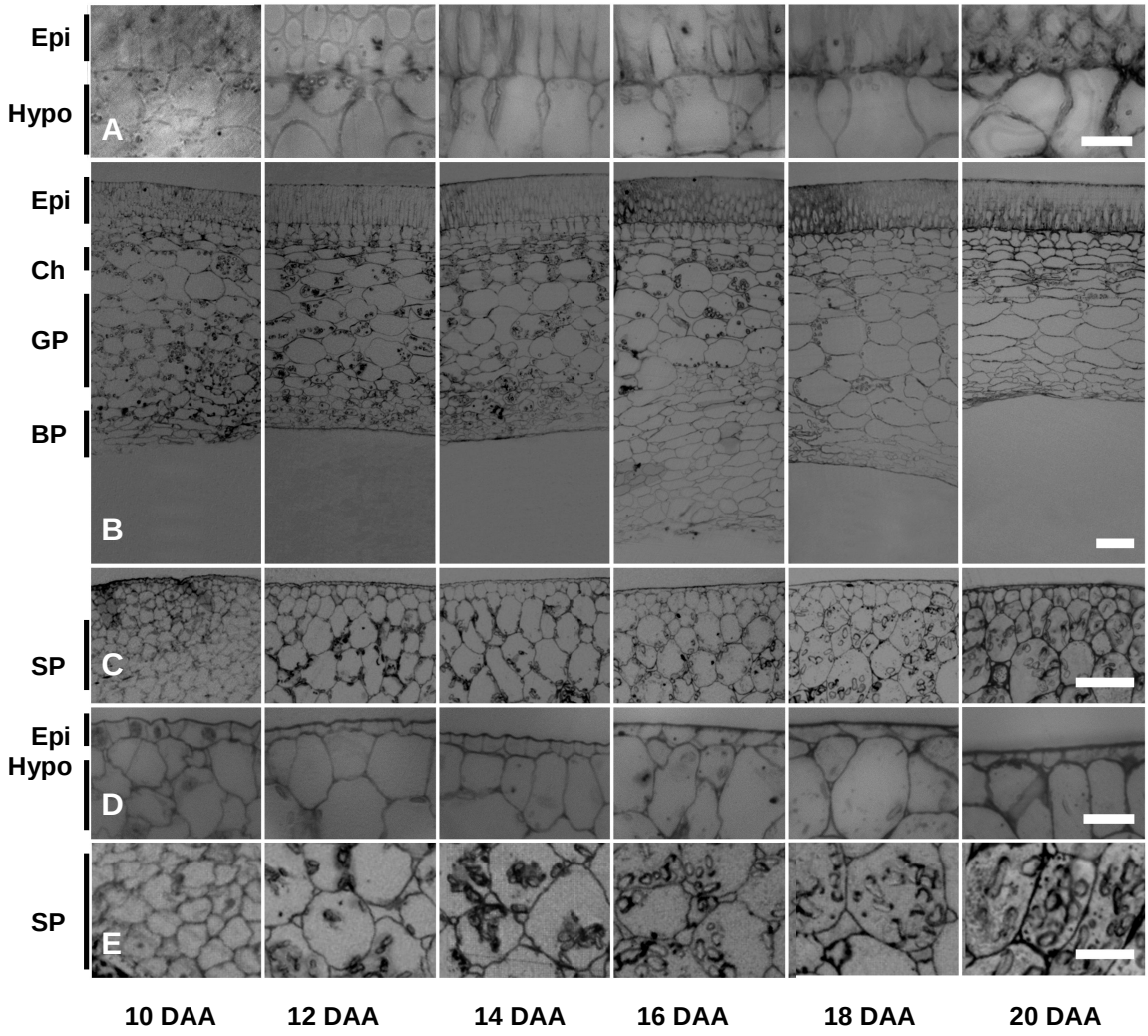

Figure 2.7: Morphology of seed coat (A and B) and cotyledon (C, D, and E) throughout development. Left to right: 10, 12, 14, 16, 18, and 20 DAA. Magnification bars are 100 µm (B and C), 20 µm (A and D), and 50 µm (E). Images of 10, 14, and 18 DAA seed coat and 10, 12, 16, and 20 DAA cotyledons are representative of 2 independent samples. Images of 12 and 16 DAA seed coat and 14 and 18 DAA cotyledons are representative of 3 independent samples. Image of 20 DAA seed coat is representative of 4 independent samples. Epi=epidermis, Ch=chlorenchyma, GP=ground parenchyma, BP=branch parenchyma, SP=storage parenchyma, Hypo=hypodermis.

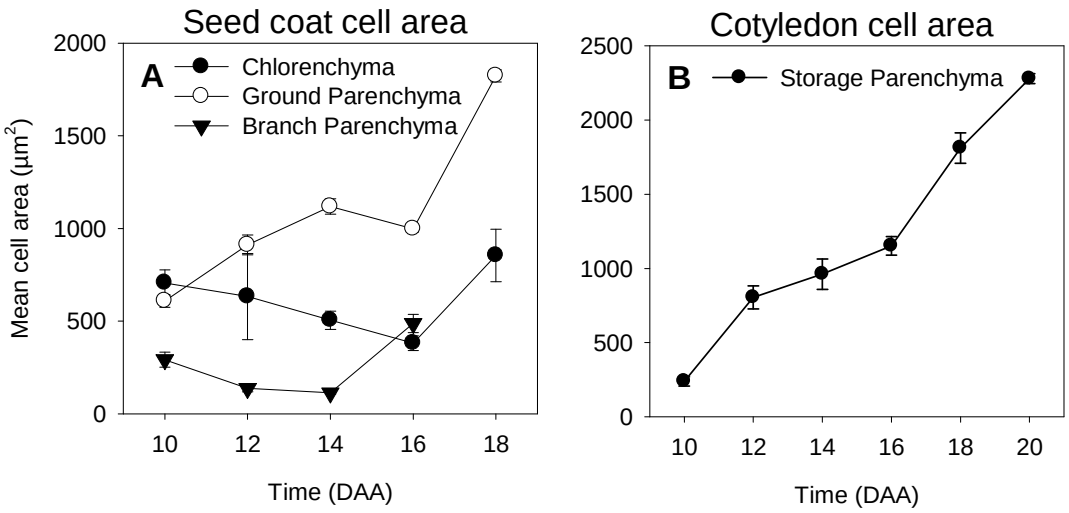

Figure 2.8: Average cross-sectional area of seed coat (A) and embryo (B) cells between 10 and 20 DAA. Subsamples (average size of subsample=98.2 cells) were obtained from two biological replicates, and data are presented as means of biological replicates ± standard error. In some cases, error bars are concealed by data-points. Embryo expansion crushes the branch parenchyma after 16 DAA, and the ground parenchyma and chlorenchyma after 18 DAA, so data at these times are not presented.

In the cotyledons, rapid expansion in storage parenchyma cell size occurred between 10 and 12 DAA (Figures 2.7C and 2.8B), coincident with increases in embryo fresh weight (Figure 2.6B). Additionally, the cells of the cotyledon epidermis were rapidly dividing at this time, as a larger proportion of cells with condensed nuclei (in prophase or metaphase) were visible at 10 DAA in comparison to later stages (Figure 2.7D). The appearance of a morphologically distinct cell layer subtending the epidermis of the cotyledons (the hypodermis) was observed by 12 DAA (Figure 2.7C). Between 12 and 14 DAA, embryo growth increased rapidly (Figure 2.6B) as the embryo reabsorbed the endosperm and filled the seed cavity (Figures 2.6B and 2.5). However, cotyledon storage parenchyma cell enlargement continued at a slower rate during this period (12 to

16 DAA, followed by a second phase of rapid cell enlargement from 16 to 20 DAA (Figure 2.8B).

2.3.2 qRT-PCR Reaction Efficiency

qRT-PCR reaction efficiency for each amplicon was calculated (Table 2.2) in order to allow more accurate comparison of transcript levels between samples, as the assumption of 100% reaction efficiency in the calculations for relative transcript abundance may inflate differences in gene expression if actual reaction efficiency is less than 100%. In most cases, calculated regressions explained the majority of the variation in Ct value ($r^2 \geq 0.990$), and most reactions proceeded with relatively high efficiency (E $\geq$0.94).

Table 2.2 Reaction efficiency of GA pathway qRT-PCR Assays

Amplicon	**Efficiency**	**r^2**
PsGA3ox1	94.8%	0.999
PsGA3ox2	100.0%	0.973
PsGA20ox1	94.5%	0.997
PsGA20ox2	88.2%	0.997
PsGA2ox1	84.9%	0.984
PsGA2ox2	96.4%	0.999

2.3.3 Expression of Gibberellin 3β-hydroxylases

The enzyme products of the *PsGA3ox1* and *PsGA3ox1* genes are responsible for the conversion of GA_{20} to bioactive GA_1. Levels of *PsGA3ox1* transcript in the earlier stages of development (8 to 10 DAA) were low in the seed coat, but began to increase at

10 DAA to eventually peak at 14 DAA, then decrease (Figure 2.9A). Whole seed *PsGA3ox1* levels primarily reflect those of the seed coat from 12 to 16 DAA, as the *PsGA3ox1* expression was several orders of magnitude less in the embryo and endosperm (when present, Figure 2.9B) during this period. *PsGA3ox1* transcript abundance was also developmentally regulated in the embryo and endosperm. Between 10 and 12 DAA, when the endosperm was at or near maximum volume (Figure 2.6B), *PsGA3ox1* levels in the endosperm increased sharply (Figure 2.9B). Embryo *PsGA3ox1* mRNA levels increased from 8 to 10 DAA, then subsequently decreased through 16 DAA and remained low to 20 DAA (Figure 2.9B). Within the embryo, *PsGA3ox1* transcript abundance was high in the embryo axis at 14 DAA (the earliest point in time at which embryo axis could be reliably obtained) compared to the cotyledons (Figure 2.9B). Subsequently, embryo axis *PsGA3ox1* transcript levels decreased but still were at higher levels than that in the cotyledons until 20 DAA. *PsGA3ox2* transcript was most abundant in the embryo earlier in development (Figure 2.9C), and like *PsGA3ox1* between 14 and 20 DAA, it was mainly expressed in the embryo axis (Figure 2.9D).

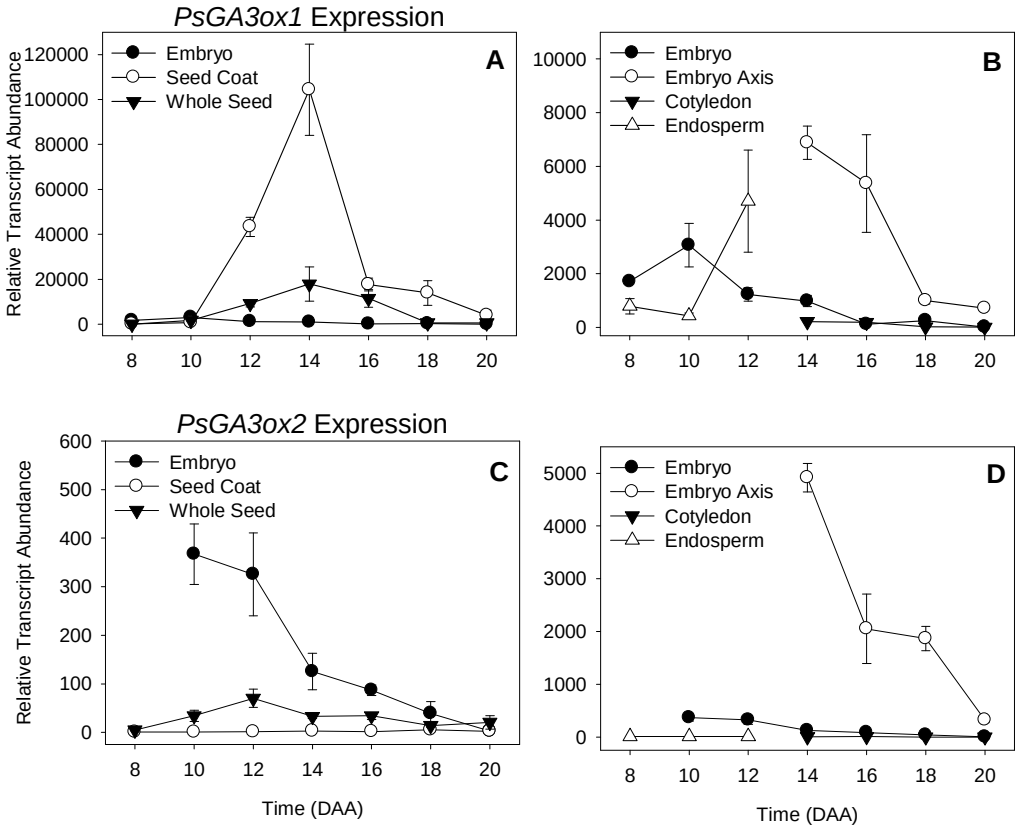

Figure 2.9: Expression of *PsGA3ox1* and *PsGA3ox2* genes (enzyme products of which are responsible for the conversion of GA_{20} to bioactive GA_1) in seed tissues from 8 to 20 DAA. Data are expressed as mean ± standard error, n=2 to 5 independent samples, except for 8 DAA embryo (n=1) and 14 DAA seed coat (n=6). Error bars are present at each point, but may be obscured by symbols if standard error is too small. All samples are normalized to the same scale, allowing direct comparison between tissues within the same gene.

2.3.4 Expression of Gibberellin 20-oxidases

Both *PsGA20ox1* and *PsGA20ox2* code for enzymes responsible for catalyzing the reactions that convert GA_{53} to GA_{20}. *PsGA20ox1* transcript abundance in both the seed coat (Figure 2.10A) and endosperm (Figure 2.10B) increased markedly between 8 and 10 DAA, followed by a peak in embryo *PsGA20ox1* transcript abundance at 12 DAA (Figure 2.10A). From 14 to 20 DAA, *PsGA20ox1* transcript abundance decreased to minimal levels in all seed tissues.

PsGA20ox2 is mainly expressed in the embryo from 8 to 20 DAA, as seed coat *PsGA20ox2* transcript abundance is minimal during this developmental period (Figure 2.10C). Furthermore, the majority of the embryo-derived *PsGA20ox2* mRNA is present in the cotyledons, while embryo axis levels are low (Figure 2.10D), as observed in 14 to 20 DAA seeds. Low but increasing levels of *PsGA20ox2* mRNA were also detected in the endosperm from 8-12 DAA (Figure 2.10D).

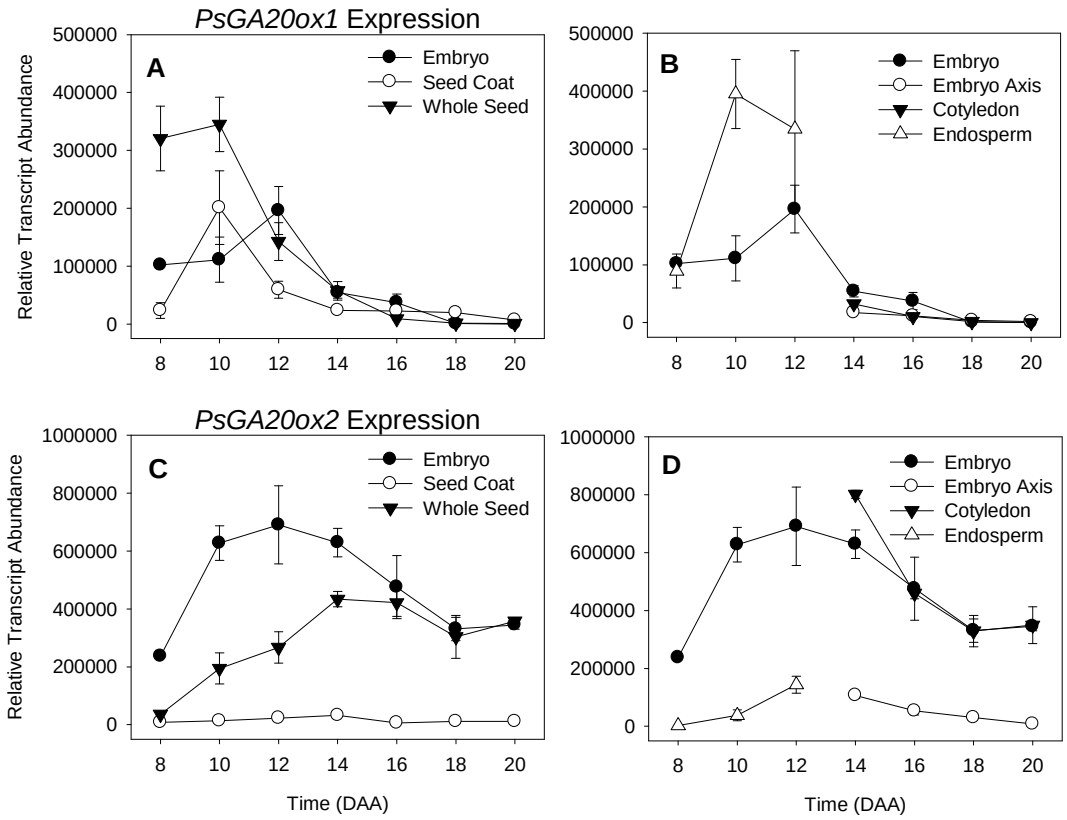

Figure 2.10: Expression of *PsGA20ox1* and *PsGA20ox2* genes (enzyme products responsible for catalyzing the reactions that convert GA_{53} to GA_{20}) in seed tissues from 8 to 20 DAA. Data are expressed as mean ± standard error, n=2 to 5 independent samples, except for 8 DAA embryo (n=1) and 14 DAA seed coat (n=6). Error bars are present at each point, but may be obscured by symbols if standard error is too small. All samples are normalized to the same scale, allowing comparison between tissues within the same gene.

2.3.5 Expression of Gibberellin 2-oxidases

Both *PsGA2ox1* and *PsGA2ox2* code for enzymes capable of catalyzing the reactions that convert GA_{20} to GA_{29} and GA_1 to GA_8, but while *PsGA2ox1* is responsible for both reactions, *PsGA2ox2* codes for the enzyme responsible primarily for the inactivation of bioactive GA_1 to GA_8. The transcript abundance of the catabolic gene *PsGA2ox1* increased steadily over seed coat development (from 8 to 20 DAA) reaching very high levels by later stages (Figure 2.11A). In contrast, *PsGA2ox1* mRNA levels were minimal in the developing embryo. *PsGA2ox1* transcript abundance also dramatically increased in the endosperm between 10 to 12 DAA (Figure 2.11B).

In contrast to *PsGA2ox1*, *PsGA2ox2* was expressed only minimally in the seed coat from 8 to 20 DAA (Figure 2.11C). Embryo *PsGA2ox2* transcript levels were low until 16 DAA, at which point they began to increase until 20 DAA. The increase in embryo *PsGA2ox2* transcript abundance between 18 and 20 DAA was mainly due to a dramatic increase in *PsGA2ox2* expression in the embryo axis, as cotyledon expression was substantially lower (Figure 2.11D).

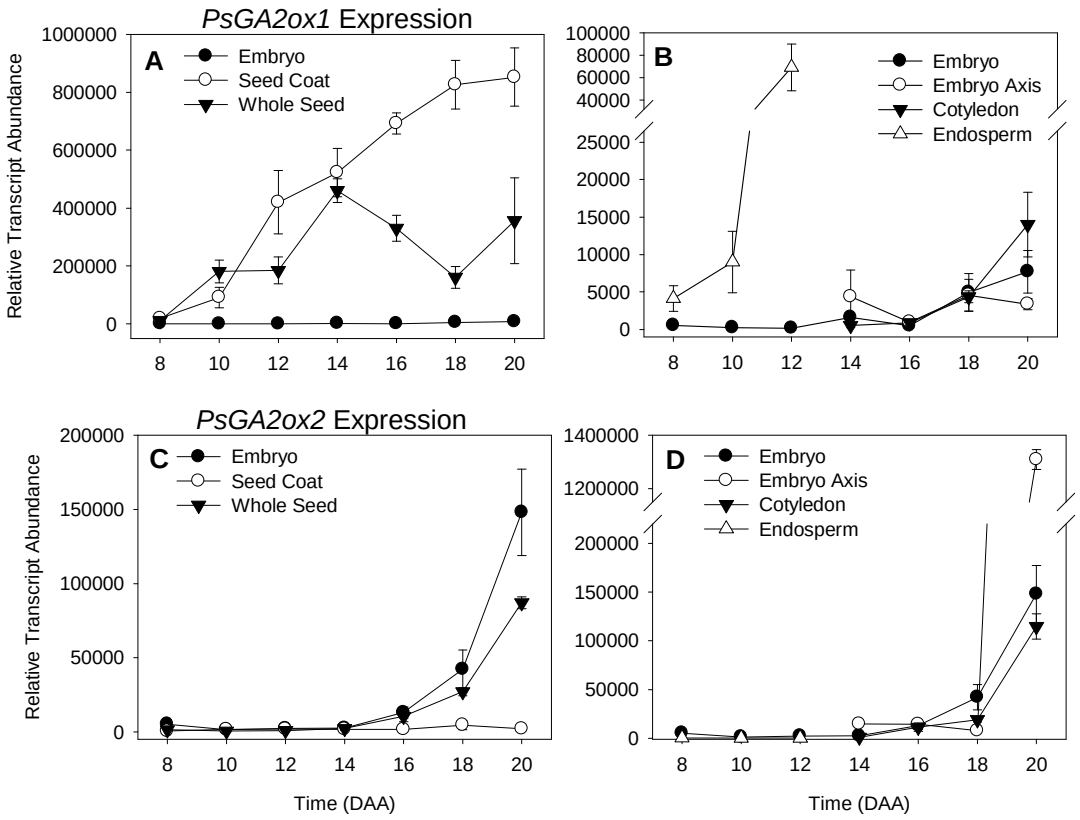

Figure 2.11: Expression of *PsGA2ox1* and *PsGA2ox2* genes (code for enzymes responsible for the inactivation of GA_1 to GA_8 and GA_{20} to GA_{29}) in seed tissues from 8 to 20 DAA. Data are expressed as mean ± standard error, n=2 to 5 independent samples, except for 8 DAA embryo (n=1) and 14 DAA seed coat (n=6). Error bars are present at each point, but may be obscured by symbols if standard error is too small. All samples are normalized to the same scale, allowing direct comparison between tissues within the same gene.

2.3.6 Non 13-Hydroxylated Gibberellins

While the early 13-hydroxylated branch of the GA biosynthesis pathway generally produces the major bioactive GAs and their precursors in *Pisum*, the report of another branch of the pathway capable of producing the equivalent non-13-hydroxylated GAs in pea seed tissues (Rodrigo *et al*., 1997) makes it necessary to determine levels of some of these metabolites in seeds as well.

GA_4, the non-13-hydroxylated equivalent to GA_1 which is a bioactive GA in some organisms, was not detected in any of the seed tissues at any stages in this study, although the deuterated internal standard [^{2}H]-GA_4 added at tissue homogenization was recovered. While GA_4 was not detected, its immediate precursor GA_9, the non-13-hydroxylated version of GA_{20}, was detected within an order of magnitude of GA_{20} levels in some seed tissues. GA_9 was most abundant in the embryo, with a small amount detected in the endosperm at 12 DAA and little to none found in the seed coat (Figure 2.12A,B,C). Within the embryo, GA_9 was predominantly found earlier in development, and decreased to low levels by 18 DAA (Figure 2.12A,B), at which point levels were 2.5-fold greater in the embryo axis than in the cotyledons (Figure 2.12B).

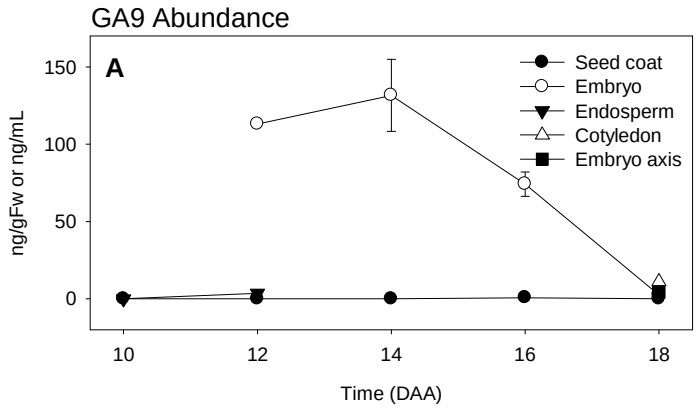

B	10 DAA	12 DAA	14 DAA	16 DAA	18 DAA
Embryo	-	113.74	131.27 ±21.23	73.90 ± 5.13	2.68 ± 0.81
Seed Coat	n.d.	n.d.	n.d.	0.79 ± 0.17	n.d.
Cotyledon	-	-	-	-	4.49
Embryo Axis	-	-	-	-	11.09 ± 0.36

C	10 DAA	12 DAA	14 DAA	16 DAA	18 DAA
Endosperm	n.d.	3.58 ± 0.06	-	-	-

Figure 2.12: GA_9 abundance in seed tissues from 10 to 18 DAA. GA_9 is the non-13 hydroxylated version of GA_{20}, and can be activated in that pathway to bioactive GA_4. Results are represented as mean of two independent samples ± standard error (n.d.= endogenous not detected, but internal standard recovered) except for 12 DAA embryo and 20 DAA embryo axis, n=1. No GA_4 was detected in any of the samples. For utility, data are represented graphically in ng gfw^{-1} or ng mL^{-1} for liquid endosperm (A), and in tabular form as ng gfw^{-1} (B), and ng mL^{-1} (C).

2.3.7 13-Hydroxylated Gibberellins

In addition to GA_1, another bioactive 13-hydroxylated GA in some organisms is GA_3, which is also produced from GA_{20} and differs from GA_1 only by the presence of a double bond between carbons 1 and 2. Because this GA could also play important roles in development, GA_3 levels were measured across development, but no GA_3 was detected in any samples in this study, although the deuterated internal standard [^{2}H]-GA_3 added at tissue homogenization was recovered in the samples (data not shown).

In the embryo, levels of bioactive GA_1 and its immediate catabolite GA_8 were highest at 10 DAA, then decreased to low or non-detectable levels by 18 DAA (Figure 2.13C,D; Table 2.3A). GA_{20} levels were relatively high in the embryo from 10 to 18 DAA, with the highest level observed at 16 DAA (Figure 2.13A; Table 2.3A). GA_{29} levels were lower in the embryo at 10 to 12 DAA, increased from 12 to 14 DAA, and then the elevated levels were maintained to 18 DAA (Figure 2.13B; Table 2.3A).

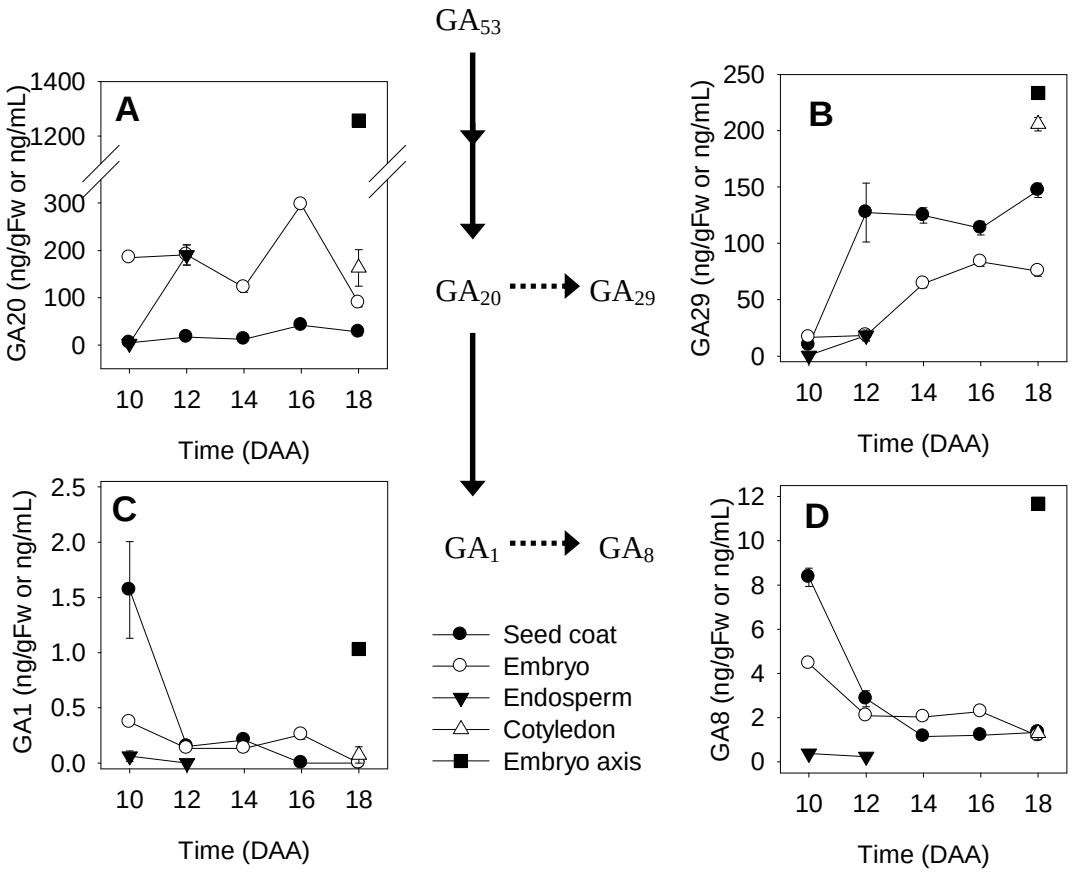

Figure 2.13: Metabolite abundance of 13-hydroxylated GAs in seed tissues from 10 to 18 DAA. Solid arrows indicate biosynthetic reactions and dotted arrows indicate deactivation steps. Results are represented as mean of two independent samples ± standard error (n.d.= endogenous not detected, but internal standard recovered), except for 12 DAA embryo and 20 DAA embryo axis, for which n=1. Results are expressed as ng gfw^{-1} for solid tissues and ng mL^{-1} for liquid endosperm.

GA_{20} was found at lower but biologically significant levels in the seed coat, with minor peaks at 12 and 16 DAA (Figure 2.13A; Table 2.3A), prior to or during the rapid expansion of ground parenchyma cells. Between 10 and 12 DAA, a large increase in GA_{29} levels was observed in the seed coat, and elevated levels of GA_{29} were maintained through 18 DAA in this tissue (Figure 2.13B; Table 2.3A). In the seed coat, steady-state

bioactive GA_1 levels were highest at 10 DAA, decreased 10-fold by 12 DAA, and decreased further to non-detectable levels by 16 DAA (Figure 2.13C; Table 2.3A). The trends in GA_8 levels, the immediate biologically inactive catabolite of GA_1, were similar to those of GA_1 during this developmental period (Figure 2.13D; Table 2.3A,B).

The embryo axis at 18 DAA possessed substantially higher levels of GA_{20}, GA_1, and GA_8 than the cotyledons (Figure 2.13A,C,D; Table 2.3B). Cotyledon levels of GA_{20}, GA_1, and GA_8 were not markedly different from embryo samples (Figures 2.13A,C, and D respectively; Table 2.3A,B); however GA_{29} levels in the 18 DAA cotyledon samples were higher than those of the embryo (Figure 2.13B; Table 2.3A,B). Endosperm GA_1 and GA_8 levels were similar at 10 and 12 DAA (Figure 2.13C and D respectively; Table 2.3C), while marked increases in endosperm GA_{20} and GA_{29} levels were observed from 10 to 12 DAA (Figure 2.13A,B; Table 2.3C).

Table 2.3: Abundance of 13-hydroxylated GAs in developing seed tissues from 10 to 18 DAA. Most results are represented as mean of two independent samples ± standard error (n.d.= endogenous not detected, but internal standard recovered), however for 12 DAA embryo and 20 DAA embryo axis, n=1. Results are expressed as ng gfw^{-1} (A,B) for solid tissues and ng mL^{-1} (C) for liquid endosperm.

A	10 DAA	12 DAA	14 DAA	16 DAA	18 DAA
Embryo GA_1	0.37	0.13 ± 0.01	0.13 ± 0.03	0.26 ± 0.04	n.d.
Embryo GA_8	4.45	2.08 ± 0.03	2.03 ± 0.14	2.27 ± 0.04	1.18 ± 0.01
Embryo GA_{20}	184.94	190.7 ± 21.22	121.80 ± 9.91	297.08 ±0.32	89.21 ± 8.79
Embryo GA_{29}	16.54	18.34 ± 4.92	64.30 ± 3.88	83.65 ± 3.93	75.39 ± 4.46
Seed Coat GA_1	1.57 ± 0.44	0.15 ± 0.03	0.21 ± 0.04	n.d.	n.d.
Seed Coat GA_8	8.35 ± 0.41	2.85 ± 0.36	1.15 ± 0.06	1.20 ± 0.03	1.34
Seed Coat GA_{20}	5.00 ± 0.18	17.05 ± 1.97	12.65 ± 1.97	41.95 ± 4.39	27.79 ± 8.15
Seed Coat GA_{29}	9.66 ±0.16	127.33 ± 26.25	124.77 ± 6.82	113.54 ± 6.02	147.01 ± 6.37

B	GA_1	GA_8	GA_{20}	GA_{29}
18 DAA Embryo axis	1.03	11.69	1256.79	233.62
18 DAA Cotyledon	0.07 ± 0.07	1.30 ± 0.30	163.01 ±38.27	205.83 ± 5.86

C	GA_1	GA_8	GA_{20}	GA_{29}
10 DAA Endosperm	0.06 ± 0.05	0.38 ± 0.09	3.43 ± 0.57	0.66 ± 0.26
12 DAA Endosperm	n.d.	0.24 ± 0.06	190.7 ± 21.22	18.34 ± 4.92

2.3.8 Abscisic Acid

Embryo ABA levels were lower at 10 to 12 DAA, then increased between 12 and 16 DAA, and were maintained at elevated levels to 18 DAA (Figure 2.14A,B). Within the embryo, ABA was at a much higher concentration in the embryo axis (5.2-fold higher) than in the cotyledons (Figure 2.14A,B). ABA levels in the seed coat and the surrounding endosperm increased markedly between 10 and 12 DAA, and seed coat-derived ABA levels remained elevated through 16 DAA, and then decreased by 18 DAA. (Figure 2.14A,B,C).

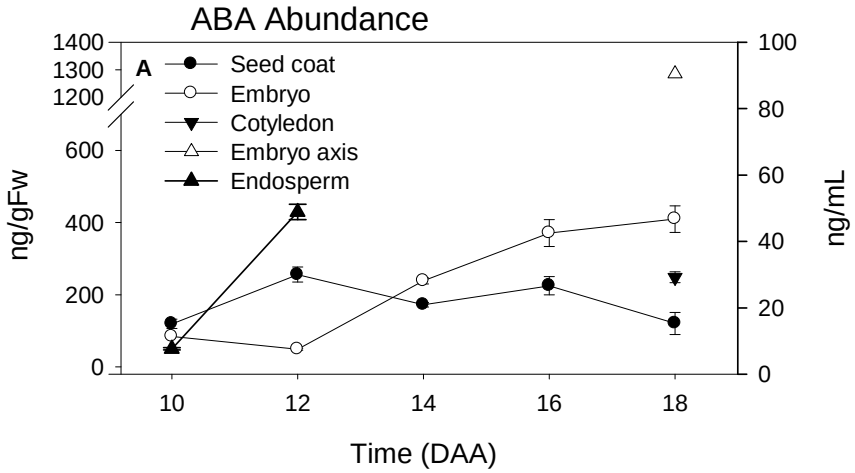

B	10 DAA	12 DAA	14 DAA	16 DAA	18 DAA
Embryo	84.37	48.89 ± 2.28	238.22 ± 8.06	370.96 ± 37.57	409.69 ± 36.75
Cotyledon	-	-	-	-	248.38 ± 14.94
Embryo Axis	-	-	-	-	1285.43
Seed Coat	119.30 ± 12.99	255.89 ± 20.72	172.24 ± 5.95	225.06 ± 25.57	120.60 ± 30.54

C	10 DAA	12 DAA	14 DAA	16 DAA	18 DAA
Endosperm	7.64 ± 0.37	48.89 ± 2.28	-	-	-

Figure 2.14: Abundance of ABA in seed tissues from 10 to 18 DAA. Results are represented as mean of two independent samples ± standard error (n.d.= endogenous not detected, but internal standard recovered) except for 12 DAA embryo and 20 DAA embryo axis, where n=1. Results are expressed graphically as ng gfw^{-1} or ng mL^{-1} (A), ng gfw^{-1} (B) for solid tissues and ng mL^{-1} (C) for liquid endosperm.

2.3.9 Effects of ABA During Early Seed Development

Application of ABA to the seed coats of 10 DAA seeds *in vivo* using a split-pericarp technique altered the expression profile of genes in the GA biosynthesis and catabolism pathway in a tissue-specific manner. Within 6 hours of application, ABA treatment increased *PsGA3ox1* transcript abundance in the seed coats (Figure 2.15A), and decreased the mRNA abundance of both *PsGA2ox* genes in the embryo (Figure 2.15C, D) compared to the controls. Within the endosperm, ABA treatment decreased the mRNA abundance of *PsGA20ox2* (Figure 2.15F). Whole seed *PsGA2ox2* mRNA abundance was higher in control samples than in ABA-treated seeds (Figure 2.15D), but this difference was due to very high transcript abundance in a single control sample, reflected by the large standard error bar, and is not likely physiologically significant.

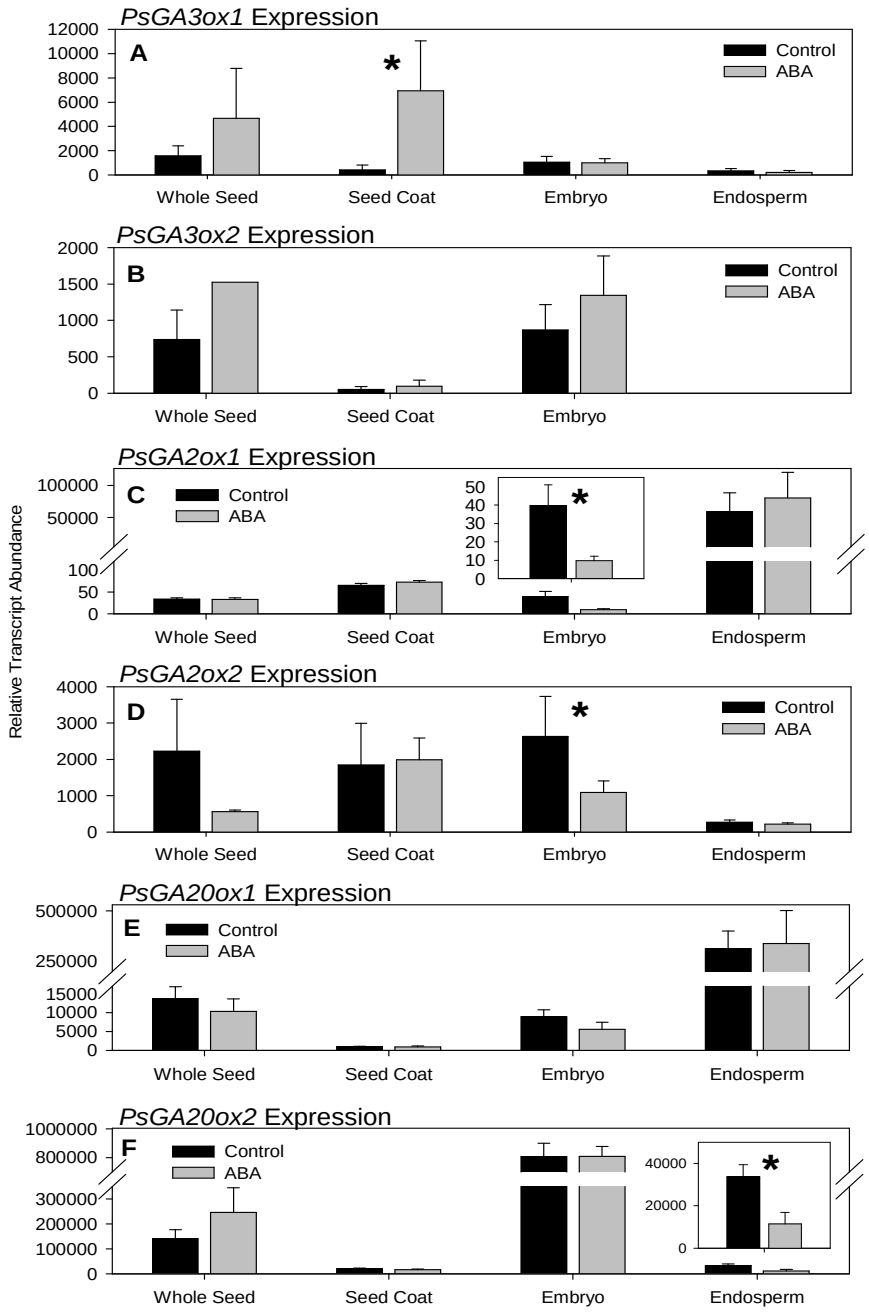

Figure 2.15: Transcript abundance of GA biosynthesis and catabolism genes in seed tissues 6 h after treatment of seeds at 10 DAA with ABA (100 µM in 0.01% aqueous Tween 80) or a control solution (0.01% aqueous Tween 80) using a split-pericarp technique. Results are representative of between 2 and 10 independent samples, except for whole seed *PsGA3ox2*, for which n=1. Significant differences as identified by standard error between control and ABA-treated samples are indicated by an asterisk (*).

The steady-state levels of several GAs were also altered by ABA treatment when assessed 48 hours after ABA application (Table 2.4). In the seed coat, treatment with ABA increased levels of GA_1 1.7 fold and reduced levels of GA_{29} by 3.4-fold. In the embryo, ABA treatment increased the level of GA_{20} 1.8-fold (Table 2.4). Free ABA levels were similar in the treated and control seed coats, likely due to conjugation of free ABA to its glucosyl-ester in ABA-treated seed coat tissue.

Table 2.4: Abundance of 13-hydroxylated GAs and ABA in seed coats and embryos 48 hours after treatment of seeds at 10 DAA with ABA (100 µM in 0.01% aqueous Tween 80) or a control solution (0.01% aqueous Tween 80). ABA and GA levels in seed coats and embryos of untreated (intact) pods harvested at the equivalent time (12 DAA) are also included. Results are expressed as ng gfw^{-1} (n.d.= endogenous not detected, but internal standard recovered).

	ABA	GA_1	GA_8	GA_{20}	GA_{29}
10 DAA control seed coat	218.77 ± 15.67	0.34 ± 0.10	1.56 ± 0.08	19.44 ± 1.08	481.20 ± 66.65
10 DAA ABA seed coat	208.25 ± 20.81	0.50 ± 0.01	1.35 ± 0.02	20.08 ± 5.02	140.20 ± 10.14
Untreated seed coat	255.89 ± 20.72	0.15 ± 0.03	2.85 ± 0.36	17.05 ± 2.43	127.33 ± 26.25
10 DAA control embryo	53.37 ± 2.88	0.14 ± 0.03	2.32 ± 0.34	650.35 ± 159.26	28.94 ± 0.32
10 DAA ABA embryo	74.41 ± 12.84	0.05 ± 0.05	2.60 ± 0.62	1178.88 ± 9.82	46.52 ± 16.56
Untreated embryo	48.89 ± 2.28	0.13 ± 0.01	2.08 ± 0.03	190.70 ± 21.22	18.34 ± 4.92

2.3.10 Effects of ABA During Later Seed Development

Since seeds at 16 DAA have already contacted the pericarp, it was impossible to apply hormone solutions to seed coats without contaminating pericarp tissues. Instead, a small plug of seed coat and cotyledon material was removed and the ABA or control solution was applied directly into the resulting well. In contrast to the previous experiments, in which hormones were applied to the seed coat, this sections describes experiments in which solutions were applied directly to the cotyledon tissue.

Treatment of seeds with ABA at 16 DAA also influenced expression of GA biosynthesis and catabolism genes in both seed coat and embryo tissues when monitored 48 h after ABA application. In the embryo axis, treatment with ABA decreased the mRNA abundance of *PsGA3ox2* (Figure 2.16B), *PsGA20ox1* (Figure 2.16E), and *PsGA20ox2* (Figure 2.16F). In the seed coat, ABA treatment decreased *PsGA2ox1* (Figure 2.16C) and *PsGA20ox2* (Figure 2.16F) transcript abundance. While ABA-treated seed coats had reduced steady-state *PsGA20ox1* mRNA abundance (Figure 2.16E) in comparison to controls, this difference was the result of abnormally high transcript abundance in a single control sample, as reflected by the large standard error.

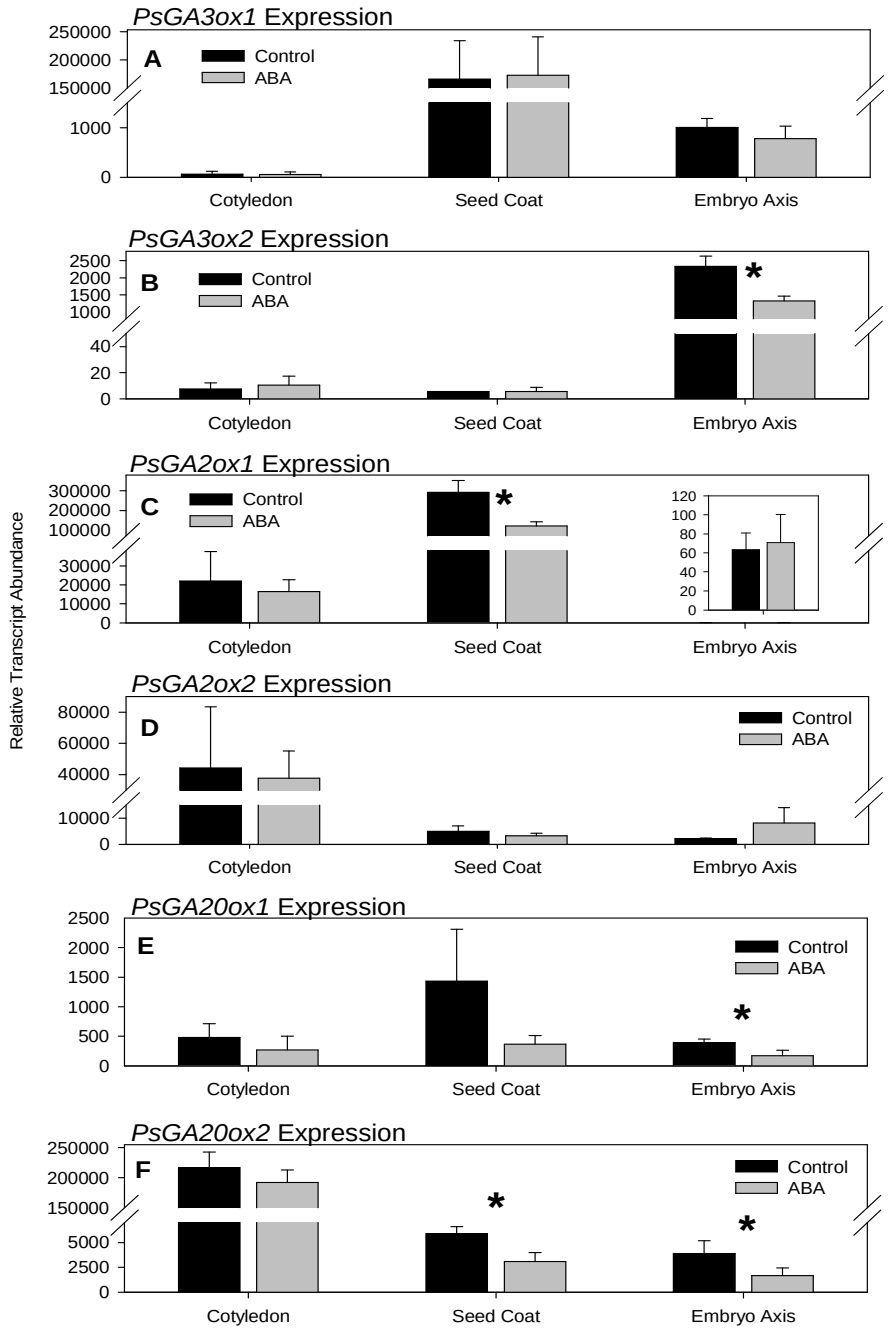

Figure 2.16: Transcript abundance of GA biosynthesis and catabolism genes in seed tissues 48 h after treatment of seeds at 16 DAA with ABA (100 µM in 0.01% aqueous Tween 80) or a control solution (0.01% aqueous Tween 80) using a split-pericarp technique. Results are representative of between 2 and 4 independent samples. Significant differences as identified by standard error between control and ABA-treated samples are indicated by an asterisk (*).

Treatment of 16 DAA seeds with ABA produced slightly higher steady-state levels of seed coat GA_1 and 1.8-fold higher levels of GA_8 than in controls (Table 2.5). Additionally, ABA treatment decreased the abundance of GA_{20} and GA_{29} in the seed coat and GA_{29} levels in the embryo. ABA levels were lower in the seed coat of ABA-treated seeds than in the control (Table 2.5), which may be due to the hormone application method used.

Table 2.5: Abundance of 13-hydroxylated GAs and ABA in seed coats and embryos 48 hours after treatment of 16 DAA seeds with ABA (100 µM in 0.01% aqueous Tween 80) or a control solution (0.01% aqueous Tween 80) using a split-pericarp technique. ABA and GA levels in seed coats and embryos of untreated (intact) pods harvested at the equivalent time (18 DAA) are also included. Data are presented in ng gfw^{-1}. Results are expressed as mean ± standard error, n=2 for each tissue with each treatment (n.d.= endogenous not detected, but internal standard recovered).

	ABA	GA_1	GA_8	GA_{20}	GA_{29}
16 DAA control seed coat	143.03 ± 17.13	0.84 ± 0.01	11.77 ± 3.39	15.53 ± 1.59	213.50 ± 22.72
16 DAA ABA seed coat	87.76 ± 7.00	0.94 ± 0.07	21.16 ± 3.31	11.71 ± 0.22	95.90 ± 4.40
Untreated seed coat	120.60 ± 30.54	n.d.	1.34	27.79 ± 8.15	147.01 ± 6.37
16 DAA control embryo	352.57 ± 6.19	n.d.	2.97 ± 0.48	175.38 ± 22.07	228.87 ± 22.38
16 DAA ABA embryo	290.33 ± 45.08	0.05 ± 0.05	2.28 ± 0.13	116.06 ± 49.31	121.29 ± 58.91
Untreated embryo	409.69 ± 36.75	n.d.	1.18 ± 0.01	89.21 ± 8.79	75.39 ± 4.46

2.4 Discussion

2.4.1 Seed GA Biosynthesis is Time- and Tissue-Specific

The seed coat, embryo and endosperm tissues undergo a variety of changes in physiology and structure as development progresses in order to produce a viable, mature seed. It is likely that extensive coordination must be maintained through tissue-to-tissue signalling in order for normal seed development to occur. Expansion of each of these seed tissues occurred during early seed development (8 to 12 DAA), including rapid increases in seed coat and embryo fresh weight (Figure 2.6A), and endosperm volume (Figure 2.6B). By 14 DAA the endosperm was absorbed by the embryo, and from 14 to 20 DAA, the growth of the embryo was prominent.

Morphology and physiology of developing seed coats

Within the seed coat, each of the five cell types studied proceeded with its own developmental scheme. Similar to that reported by Van Dongen et al. (2003), differentiation of protodermal cells into a palisade of macrosclerids was observed in the seed coat epidermal layer from 10 to 16 DAA (Figure 2.7A,B). Cell wall thickening was observed in the epidermis, particularly from 16 DAA onwards (Figure 2.7A). Organization of the hypodermis also occurred, as cells developed from roughly circular (in cross section) hypodermal cells at 10 DAA to hourglass-shaped cells by 14 DAA (Figure 2.7A). The chlorenchyma cells located just under the hypodermis maintained a relatively constant size from 10 to 18 DAA, but began to be compressed by the expanding embryo by 20 DAA (Figures 2.7B and 2.8A). While containing chloroplasts,

the role of photosynthesis in the seed coat chlorenchyma is likely minor as much of the seed develops in a hypoxic environment (Rolletschek *et al*., 2002), and the chlorenchyma rather fulfill a role in temporary starch synthesis and storage (Rochat and Boutin, 1992). The ground parenchyma towards the interior of the seed coat increased in area from 10 to 14 DAA (Figures 2.7B and 2.8A), concurrent with hypodermal hourglass cell differentiation. Ground parenchyma cell size was maintained between 14 and 16 DAA and then increased markedly from 16 to 18 DAA (Figure 2.8A), concurrent with the onset of the compression of the branched parenchyma by the cotyledons (Figure 2.7B). While ground parenchyma cell size was relatively constant between 14 and 16 DAA, the layer of subtending cells, the branched parenchyma, increased in size notably during this time (Figures 2.7B and 2.8A). The branched parenchyma were irregular in appearance with extensive intercellular spaces from 10 to 14 DAA (Figure 2.7B). This morphology was further supported by the wide variation in cross-sectional area within biological replicates, as cells in various orientations were sectioned (data not shown). These intercellular spaces are both air- and liquid-filled (van Dongen *et al*., 2003), and the branched parenchyma make extensive contacts with the liquid endosperm prior to reabsorption. The dramatic expansion of the branched parenchyma cell layer between 14 and 16 DAA marked one of the most distinctive morphological changes within the seed coat (Figure 2.7B). After embryo contact at approximately 16 DAA, the cells of the seed coat begin being crushed by the cotyledons, beginning with the innermost layer and continuing outwards (Figure 2.7B).

GA gene expression and steady-state GA levels in developing seed coats

Between 8 and 10 DAA, seed coat transcript abundance of *PsGA20ox1* increased notably (Figure 2.10A). Combined with low mRNA levels of the two *PsGA2ox* catabolic genes (Figure 2.11A,C), these data suggest a moderate flux through the GA biosynthesis pathway to bioactive GA_1. Consistent with GA biosynthesis pathway transcription profiles, levels of bioactive GA_1 in the seed coat are elevated at 10 DAA (Figure 2.13C, Table 2.3A), and levels of seed coat GA_{20} increase 3-fold between 10 and 12 DAA (Table 2.3A). The higher flux through the GA biosynthesis pathway to bioactive GA_1 in the seed coat at this developmental stage likely promoted the substantial increase in seed coat fresh weight between 10 and 12 DAA (Figure 2.6A), partially through the increase in ground parenchyma cell expansion (Figure 2.8A).

As seed coat development progressed, the GA biosynthesis and catabolism gene transcript and GA metabolite profiles changed. The transcript abundance of *PsGA3ox1*, the enzyme product of which is capable of converting GA_{20} to bioactive GA_1, increased markedly in the seed coat from 10 to 12 DAA, and peaked at 14 DAA (Figure 2.9A), suggesting an increase in pathway flux to bioactive GA_1 during this period. The peak in *PsGA3ox1* transcript level coincided with the dramatic expansion of the branched parenchyma cells between 14 and 16 DAA (Figures 2.7B and 2.8A), suggesting that seed coat produced GA_1 is involved in the stimulation of rapid branched parenchyma cell expansion at this time. However, transcript abundance of *PsGA2ox1* increased continually from 12 to 20 DAA (Figure 2.11A), likely leading to increased GA_{20} and GA_1 catabolism. Consistent with GA transcription profiles, steady-state levels of GA_1 (Figure 2.13C, Table 2.3A) and the ratio of GA_1 to GA_8 in the seed coat decreased from 10 to 12

DAA (GA_1 to GA_8 ratio of 1:5.3 at 10 DAA, 1:19.0 at 12 DAA), indicating increased GA_1 catabolism. GA_1 levels in the seed coat remained low from 12 to 14 DAA, and were not detectable at 16 to 18 DAA. The gene product of *PsGA2ox1* also efficiently catabolizes GA_{20} to GA_{29}, and levels of the 2β-hydroxylated catabolite GA_{29} increased 13-fold from 10 to 12 DAA, and remained at elevated levels to 18 DAA (Figure 2.13B, Table 2.3A). These data suggest that steady-state levels of seed coat derived GA_1 are tightly controlled by catabolism to GA_8 via the GA 2-oxidase coded for by *PsGA2ox1*, likely a mechanism to aid in the production of a pulse of GA_1 for branched parenchyma expansion.

GA gene expression and steady-state GA levels in the endosperm

In the endosperm, transcript abundance of *PsGA20ox1* increased markedly between 8 and 10 DAA (Figure 2.10B), and at 12 DAA, as the endosperm reached its maximum volume, GA_{20} levels were high (Figure 2.13A, Table 2.3C). At 12 DAA, on a per seed basis (Table 5.4), GA_{20} levels were 4.2-fold higher in the endosperm (7.2 ± 0.8 ng) than in the seed coat (1.7 ± 0.2 ng), and were similar to levels in the embryo (8.3 ± 0.9 ng). Between 10 and 12 DAA, endosperm transcript abundance of both *PsGA3ox1* (Figure 2.9B) and *PsGA2ox1* (Figure 2.11B) increased notably, concurrent with slight decreases in steady-state endosperm GA_1 and GA_8 levels (Table 2.3C), indicating that net GA_1 catabolism is the probable result of these changes in transcript levels. Since the inner branched parenchyma of the seed coat are in contact with the non-cellular endosperm (Marinos, 1970), it is possible that the pool of GA_{20} in the endosperm could be partially transported to the seed coat, as GA_{20} and GA_{29} abundance increases

concurrently in both tissues, and the branched parenchyma could be an important link between seed coat and endosperm GA pools.

Morphology and physiology of developing embryos

Embryo growth as measured by fresh weight was rapid and embryo size increased from 10 to 20 DAA (Figure 2.6A). Between 10 and 14 DAA, the endosperm was absorbed by the embryo as it expanded to fill the seed cavity (Figures 2.5 and 2.6B). The epidermal cell layer of the cotyledons had a relatively higher proportion of cells in prophase or metaphase (as indicated by condensed nuclei) at 10 DAA (Figure 2.7D) compared to later stages, which is suggestive of relatively rapid cell division at this time. Marinos (1970) and van Dongen *et al*. (2003) reported the formation of invaginations of the cell walls of the cotyledonary epidermis prior to endosperm absorption using TEM and cryo-SEM, respectively. The invagination of these epidermal cells produces the cotyledon transfer cells, which are proposed to be important for nutrient uptake from the endospermal cavity (Borisjuk *et al*., 2002b). The resolution afforded by light microscopy in this study did not permit the observation these structures.

While transfer cell formation was not visible, the single layer of cells immediately subtending the cotyledonary epidermis organized into an ordered hypodermis between 10 and 14 DAA (Figure 2.7C). The organization of a cotyledonary hypodermal cell layer in pea has been previously documented (Bain and Mercer, 1966). In contrast to the subtending storage parenchyma cells, which enlarged during the nutrient storage phase of cotyledon development (14 to 20 DAA), the hypodermal cells remained smaller (Figure 2.7C, 20 DAA) and likely serve a similar function to that of the transfer cells of the

epidermis in transferring nutrients from the endospermal cavity to the storage parenchyma cells of the cotyledons (Borisjuk *et al*., 2002b). While the storage parenchyma increase greatly in size as starch and protein storage progresses, the hypodermal cells remain small, and there is a noticeable lack of storage vacuoles in this layer in comparison to the subtending storage parenchyma (Figure 2.7D,E).

The storage parenchyma cells of the cotyledon increased rapidly in area from 10 to 12 DAA (Figure 2.8B) coinciding with rapid cotyledon expansion in volume (Figure 2.5; Figure 2.6B), then more gradually from 12 to 16 DAA as the cotyledons transitioned from the pre-storage growth phase to the storage phase (carbohydrate storage in pea seeds is reviewed in Weber *et al*., 1997). From 16 to 20 DAA, cotyledon storage parenchyma cell area increased more rapidly, coinciding with the onset of the storage phase and cotyledon nutrient accumulation.

GA gene expression and steady-state GA levels in developing embryos

Transcript levels of both *PsGA20ox* genes were high in the embryo during early seed development (8 to 12 DAA, Figure 2.10A; Figure 2.10C). While *PsGA20ox2* mRNA abundance remained at elevated levels until 20 DAA (Figure 2.10C), *PsGA20ox1* transcript levels were lower later in development (Figure 2.10A). Recent qRT-PCR experiments (Ozga *et al*., 2009) have demonstrated that *PsGA20ox1* transcript abundance is higher earlier in development (approximately 3 DAA) and decrease from that point onwards, and the data presented here confirm this trend. The *PsGA20ox* gene expression profiles in the embryo are consistent with high levels of GA_{20} in the embryo from 10 to 18 DAA (Figure 2.13A; Table 2.3A). Additionally, GA_9 abundance in the embryo was

high from 12 to 14 DAA and then decreased (Figure 2.12A,B). GA_9 is the non-13-hydroxylated equivalent to GA_{20} and can be synthesized through the enzymes encoded by *PsGA20ox1* and *PsGA20ox2*, and the decreasing embryo GA_9 abundance is consistent with decreases in *PsGA20ox1* mRNA levels. During pea seed development, large amounts of GA_{20} are produced and stored in the cotyledons. Ayele *et al*. (2006) reported the accumulation of GA_{20} in 20 DAA seeds and mature embryos, consistent with the high levels of GA_{20} observed in 18 DAA cotyledons in this study. Upon germination, this GA_{20} is transported to the embryo axis where *de novo* GA_1 biosynthesis occurs, promoting the rapid growth of the developing seedling (Ayele *et al*., 2006).

Transcript levels of the *PsGA2ox1* catabolism gene were low from 8 to 12 DAA in the embryo (Figure 2.11A), consistent with lower GA_{29} levels in this tissue (Figure 2.13B; Table 2.3A). Embryo *PsGA2ox1* transcript abundance increased 9.7-fold from 12 to 14 DAA (relative transcript abundance 165.20 ± 40.20 at 12 DAA; 1609.90 ± 89.08 at 14 DAA), consistent with a 3-fold increase in embryo GA_{29} during the same time (Figure 2.13B; Table 2.3A). From 14 DAA through 18 DAA, higher GA_{29} levels were maintained in the embryo (Figure 2.3B; Table 2.3A). At 21 DAA (cv. Progress), GA_{29} abundance in the embryo was greater than that of the seed coat, and by 24 DAA, GA_{29} was located almost exclusively in the cotyledons, while seed coat and embryo axis abundance is low (Sponsel, 1983). Feeding studies with labelled GA_{20} demonstrated that in the storage-phase pea seed, embryo-derived GA_{29} is transported to the seed coat for catabolism to GA_{29}-catabolite(Sponsel, 1983). The GA_{29} which accumulates in the pre-storage and transitioning embryo in this study is likely also transported to the seed coat and catabolized through this mechanism after 20 DAA.

Transcript abundance of both *PsGA3ox* genes, the enzyme products of which are capable of converting GA_{20} to bioactive GA_1, was elevated in the early embryo at 10 DAA (Figure 2.9A,C), concurrent with higher GA_1 levels in this tissue (Figure 2.13C; Table 2.3A). The large pool of GA_{20} (Figure 2.13A; Table 2.3A), along with higher levels of both GA_1 (Figure 2.13C; Table 2.3A) and GA_8 (Figure 2.13D; Table 2.3A) and lower levels of GA_{29} (Figure 2.13B; Table 2.3A), suggests comparatively greater flux through the GA biosynthesis pathway in the embryo at 10 DAA, likely to support rapid cell division.

From 10 DAA onwards, both *PsGA3ox1* (Figure 2.9A) and *PsGA3ox2* (Figure 2.9C) transcript abundance decreased in the embryo. Coincident with the initial decrease in *PsGA3ox1* transcript abundance between 10 and 12 DAA, embryo GA_1 decreased 2.8-fold by 12 DAA and remained present at low levels until 16 DAA, after which point it was not detectable in the embryo (Figure 2.13C; Table 2.3A). *PsGA3ox2* was initially reported to be expressed primarily in the roots (Weston *et al*., 2008), but transcript abundance was significant in the embryo at 10 to 12 DAA (Figure 2.9A), identifying a role for this gene in seed development. While *PsGA3ox1* transcript accumulates at very high levels in the seed coat (Figure 2.9A), *PsGA3ox2* transcript is found almost exclusively in the embryo, indicating tissue-specific expression of the *PsGA3ox* genes.

The embryo axis and cotyledons of the embryo execute vastly different developmental programs in the early storage phase (16 to 20 DAA) of seed development. Nutrient storage is accomplished primarily by the cotyledons, and storage-phase cotyledon development is directed primarily to the biosynthesis and storage of starches and proteins. The large size discrepancy between cotyledon and embryo axis (cotyledons

compose approximately 98% of the embryo at 20 DAA, Figure 2.6B) results in the under-representation of embryo axis metabolite and transcript levels in whole embryo samples. The determination of GA biosynthesis gene transcript levels and GA profiles in the cotyledons and embryo axes separately can lead to further understanding of GA metabolism in these developmentally diverse tissues.

Transcript abundance of the *PsGA3ox1* and *PsGA3ox2* genes was minimal in the cotyledons from 14 to 20 DAA, while both *PsGA3ox* transcripts were present at high levels in the embryo axis at 14 to 16 DAA, decreasing as the embryo axis matured to 20 DAA (Figure 2.9B,D). Coincident with higher *PsGA3ox* transcript abundance, levels of GA_1 were notably higher (14.7-fold based on ng gFw^{-1}, Figure 2.13C; Table 2.3A) in the embryo axis than in the cotyledons at 18 DAA, as were levels of its immediate 2β-hydroxylated catabolite, GA_8 (9.0-fold based on ng gFw^{-1}, Figure 2.13D; Table 2.3A). While GA_{20} abundance was 7.7-fold greater in the embryo axis than in the cotyledons at 18 DAA (Figure 2.13A; Table 2.3A), transcript abundance of both *PsGA20ox* genes was lower in the embryo axis from 14 to 20 DAA (Figure 2.10B,D), while *PsGA20ox2* transcript abundance was high in the cotyledons during this time (Figure 2.10D). The high pathway flux to GA_1 in the embryo axis is supportive of the continual growth of this tissue from 16 to 20 DAA (Figure 2.6B), while the accumulation of GA_{20} in the cotyledons and maintained levels of *PsGA20ox2* transcript are likely involved in the storage of GA_{20} for post-germination GA_1 biosynthesis in the embryo axis (Ayele *et al*., 2006), reflecting this tissues role as a storage organ.

Between 18 and 20 DAA, embryo axis *PsGA2ox2* transcript abundance increased markedly (Figure 2.10D), indicating a shift in GA biosynthesis pathway flux in this

tissue. No metabolite profiling data was collected after 18 DAA, so it is not known if this increase in catabolism gene transcript produced a decrease in embryo axis GA_1 levels, although the magnitude of this increase and specificity of the enzyme product of the *PsGA2ox2* gene for GA_1 over GA_{20} (Lester *et al*., 1999) are suggestive of this result. Given the small size of this tissue, no other data on embryo axis GA levels in pea are available, and metabolite profiles of embryo reflect the cotyledon, which makes up approximately 98% of the embryo at 20 DAA (Figure 2.6B). The increase in embryo axis *PsGA2ox2* transcript at 18 DAA is likely maintained until maturity: Ayele *et al*. (2006) reported high levels of *PsGA2ox2* transcript in both 20 DAA and mature embryos, decreasing only after imbibition. The catabolism of GA_1 at this stage is likely a mechanism to limit embryo axis growth and allow embryo maturation to proceed.

2.4.2 ABA Regulation of Early Seed GA Metabolism

Localization of ABA in pea seed tissues

Seed coat ABA increased 2.1-fold from 10 to 12 DAA (Figure 2.14A,B), when the endosperm obtained maximum volume (Figure 2.6B). From 10 to 12 DAA, seed ABA concentration was highest in the seed coat, with seed coat ABA levels 23.3-fold higher than embryo and 44.9-fold higher than endosperm at 10 DAA, and 11.6-fold than the embryo and 13.5-fold higher than endosperm at 12 DAA (on a per seed basis; Table 5.5). Later in development (14 DAA onwards), ABA concentration was highest in the embryo, where per seed levels were 1.8-fold greater at 14 DAA, 2.7-fold greater at 16 DAA, and 6.9-fold greater at 18 DAA than those of the seed coat (Table 5.5). Eeuwens

and Schwabe (1975) found that ABA content in the embryo increased from 12 to 24 DAA, consistent with the increase in embryo ABA levels from 12 to 18 DAA observed in this study. In the storage-phase seed, GC-MS experiments (Wang *et al*., 1987) described a biphasic distribution of ABA, with an initial peak of ABA in the seed coat concomitant with a smaller increase in embryo ABA (when the embryo was approximately 25% of its final fresh weight), followed by a second peak in embryo ABA as the embryo approached its maximum fresh weight. Consistent with embryo and seed coat sizes, the shift in ABA localization from seed coat to embryo observed during this study coincides with the period of time surrounding the first peak. While embryo ABA increased from 12 to 18 DAA (Figure 2.14A,B) and occurred in both the cotyledons and embryo axis at 18 DAA, embryo axis ABA levels were 5.2-fold greater than those of the cotyledons, suggesting a comparatively greater role for ABA in the regulation of processes within the embryo axis at that time.

ABA regulation of seed coat GA metabolism at 10 to 12 DAA

ABA is present at higher levels in the seed coat at 10 to 12 DAA compared to that in other seed tissues (Figure 2.14A,B). Furthermore, seed coat ABA (Figure 2.14A,B) and *PsGA3ox1* transcript abundance (Figure 2.9A) both increased from 10 to 12 DAA, suggesting that ABA may function as a promoter of seed coat GA biosynthesis at this time. Application of ABA (100 μM) to 10 DAA seeds using a split-pericarp technique increased seed coat *PsGA3ox1* transcript abundance 6 hours after hormone treatment (Figure 2.15A) and seed coat GA_1 levels 48 hours after treatment (Table 2.4). These data indicate that at this stage of seed development, ABA promotes synthesis of bioactive GA_1

in the seed coat by increasing the transcript abundance of *PsGA3ox1*, likely resulting in GA_1-induced seed coat growth, both in fresh weight (Figure 2.6A) and ground parenchyma cell expansion (Figure 2.8A).

ABA regulation of embryo GA metabolism at 10 to 12 DAA

In the embryo, ABA also appears to regulate GA metabolism from 10 to 12 DAA. The application of ABA to 10 DAA seed coats using a split-pericarp technique decreased the mRNA abundance of both *PsGA2ox1* (Figure 2.15C) and *PsGA2ox2* (Figure 2.15D) in the embryo 6 hours after treatment. The enzyme products of these genes are capable of removing GA as a substrate for conversion to bioactive GA (converting GA_{20} to GA_{29}), or inactivating bioactive GA (converting GA_1 to biologically inactive GA_8). The changes in embryo transcription profiles in the ABA-treated seeds when compared to controls suggests decreased GA catabolism, and the increased levels of embryo GA_{20} 48 hours after ABA treatment suggests decreased catabolism of GA_{20} to GA_{29} (Table 2.4). Taken together, these data support a role for ABA in decreasing embryo GA catabolism between 10 and 12 DAA.

ABA regulation of endosperm GA metabolism at 10 to 12 DAA

In the endosperm, ABA levels increased 10.3-fold between 10 and 12 DAA (Figure 2.14A,C). Transcript abundance of both *PsGA20ox* genes also increased between 8 and 12 DAA (Figure 2.10B,D), as did the metabolic product of the enzymes coded for by these genes, GA_{20}, which increased in abundance in the endosperm 55.6-fold between 10 and 12 DAA (Figure 2.14A; Table 2.3C). Endosperm *PsGA2ox1* transcript abundance

increased between 10 and 12 DAA, (Figure 2.11B) and endosperm GA_{29} levels increased 27.8-fold during the same period (Figure 2.14B; Table 2.3C). While no metabolite profiling data was collected, the application of ABA to 10 DAA seed coats only decreased transcript abundance of *PsGA20ox2* in the endosperm 6 hours after treatment (Figure 2.15F), suggesting that ABA has a minimal role in the regulation of GA transcript abundance in the endosperm at this time.

2.4.3 ABA Regulation of Later Seed GA Metabolism

ABA regulation of seed coat GA metabolism at 16 to 18 DAA

Between 16 and 18 DAA (during which time the later set of hormone treatments were performed), seed coat ABA levels decreased 1.9-fold (Figure 2.14A,B). The application of ABA to cotyledons at 16 DAA decreased seed coat transcript abundance of both the biosynthesis gene *PsGA20ox2* (Figure 2.16F) and the catabolic gene *PsGA2ox1* (Figure 2.16C). While *PsGA20ox2* transcript levels are low throughout seed coat development from 8 to 20 DAA (Figure 2.10C), *PsGA2ox1* transcript levels increase continually during this period, and are substantial in the seed coat by 16 DAA (Figure 2.11A). Consistent with the reduced transcript levels of *PsGA20ox2*, ABA treatment decreased levels of both GA_{20} (produced by the gene product of *PsGA20ox2*) 48 hours after treatment (Table 2.5). Consistent with reduced transcript levels of *PsGA2ox1*, the immediate catabolite of GA_{20}, GA_{29}, was also reduced (Table 2.5). Additionally, ABA treatment increased seed coat GA_8 (Table 2.5), suggesting a shift in the GA biosynthesis pathway from earlier metabolites (GA_{20}, GA_{29}) to bioactive GA_1 and GA_8, which may be

the result of ABA-dependant downregulation of *PsGA2ox1* mRNA levels. The ability of ABA to act as both a promoter (via downregulation of *PsGA2ox1*, leading to increased GA_8) and inhibitor (via downregulation of *PsGA20ox2*, leading to decreased GA_{20} and GA_{29}) of GA biosynthesis suggests that the regulation of the seed coat GA biosynthesis pathway between 16 and 18 DAA is complex.

ABA regulation of embryo GA metabolism at 16 to 18 DAA

The high abundance of ABA in the embryo axis at 18 DAA (Figure 2.14A,B) combined with the rapid increase in embryo axis *PsGA2ox2* transcript abundance between 18 and 20 DAA suggested that ABA may serve as a regulator of embryo axis GA catabolism at this stage of development. The application of ABA to 16 DAA cotyledons reduced transcript abundance of three biosynthesis genes in the embryo axis: *PsGA3ox2* (Figure 2.16B), *PsGA20ox1* (Figure 2.16E), and *PsGA20ox2* (Figure 2.16F) 48 hours after treatment. ABA treatment also decreased embryo GA_{29} 48 hours after treatment (Table 2.5) in comparison to controls. In the embryo axis, both *PsGA3ox1* and *PsGA3ox2* transcript abundance decreases from 14 DAA onwards, but ABA was not observed to regulate *PsGA3ox1* in these experiments, possibly because of differences in the timing of *PsGA3ox* decrease: by 18 DAA (time of harvesting of hormone-treated pods) *PsGA3ox1* transcript has already reached minimal levels (Figure 2.9B), while *PsGA3ox2* abundance continues to decrease (Figure 2.9D). Metabolite profiling confirmed that ABA served to decrease GA biosynthesis pathway flux, as lower levels of GA_{29} were detected in ABA treated embryos 48 hours after treatment (Table 2.5).

While no changes in embryo GA_1 or GA_8 levels were detected (Table 2.5), this may be because the embryo sample consists of approximately 98% cotyledonary tissue (Figure 2.6B), so small to moderate changes in GA pathway flux in the embryo axis may not be reflected. It must be noted that while ABA altered GA biosynthesis pathway flux through the regulation of biosynthesis genes in the embryo axis, GA catabolism was unaffected (while ABA-treated embryo axis *PsGA2ox2* levels, Figure 2.16D, appear higher than controls, this was due to high transcript abundance in a single ABA-treated sample (n=3), and was not replicated). Additional experiments with increased ABA dosage and different timing also had no effect on embryo axis GA catabolism gene transcript abundance between 16 and 18 DAA, indicating that the drastic increase in *PsGA2ox2* transcript between 18 and 20 DAA likely responds to another developmental queue, while ABA serves primarily to down-regulate the GA biosynthesis machinery.

2.5 Literature Cited

Aach, H., H. Bode, D. Robinson, and J. Graebe. (1997). *ent*-Kaurene synthetase is located in proplastids of meristematic shoot tissues. *Planta* **202**:211-219.

Appleford, N., D. Evans, J. Lenton, P. Gaskin, S. Croker, K. Devos, A. Phillips, and P. Hedden. (2006). Fucntion and transcript analysis of gibberellin-biosynthetic enzymes in wheat. *Planta* **223**: 568-582.

Ayele, B., J. Ozga, L. Kurepin, and D. Reinecke. (2006). Developmental and embryo axis regulation of gibberellin biosynthesis during germination and young seedling growth of Pea. *Plant Physiol.* **142**: 1267-1281.

Bain, J., and F. Mercer. (1966). Subcellular organization of the developing cotyledons of *Pisum sativum* L. *Aust. J. Biol. Sci.* **19**:49-67.

Bick, J. and B. Lange. (2003). Metabolic cross talk between cytosolic and plastidial pathways of isoprenoid biosynthesis: unidirectional transport of intermediates across the chloroplast envelope membrane. *Arc. Biochem. Biophys*. **415**: 146-154.

Borisjuk, L., T. Wang, H. Rolletschek, U. Wobus, and H. Weber. (2002a). A pea seed mutant affected in the differentiation of the embryonic epidermis leads to deregulated seed maturation and impaired embryo growth. *Development* **129**:1595-1607.

Borisjuk, L., S. Walenta, H. Rolletschek, W. Mueller-Klieser, U. Wobus, and H. Weber. (2002b). Spatial analysis of plant metabolism: sucrose imaging within *Vicia faba* cotyledons reveals specific developmental patterns. *Plant J.* **29**:521-530.

Chrispeels, M., and J. Varner. (1967). Gibberellic acid-enhanced synthesis and release of α-amylase and ribonuclease by isolated barley and aleurone layers. *Plant Physiol.* **42**:398-406.

Cosgrove, D., and S. Sovonick-Dunford. (1989). Mechanism of gibberellin-dependent stem elongation in Peas. *Plant Physiol.* **89**: 184-191.

Davidson, S., J. Smith, C. Helliwell, A. Poole, and J. Reid. (2004). The Pea gene *LH* encodes *ent*-kaurene oxidase. *Plant Physiol.* **134**:1123-1134.

Dill., A., S. Thomas, J. Hu, C. Steber, and T. Sun. (2004). The *Arabidopsis* F-box protein SLEEPY1 targets gibberellin signalling repressors for gibberellin induced degradation. *Plant Cell* **16**:1392-1405.

Eeuwens, C., and W. Schwabe. (1976). Seed and pod wall development in *Pisum sativum*, L. in relation to extracted and applied hormones. *J. Exp. Bot.* **26**:1-14.

Fleet, C., S. Yamaguchi, A. Hanada, H. Kawaide, C. David, Y. Kamiya, and T. Sun. (2003). Overexpression of *AtCPS* and *AtKS* in *Arabidopsis* confers increased *ent*-kaurene production but no increase in bioactive gibberellins. *Plant Physiol.* **132**:830-839.

Frey, A., B. Godin, M. Bonnet, B. Sotta, A. Marion-Poll. (2004). Maternal synthesis of abscisic acid controls seed development and yield in *N. plumbaginifolia*. *Planta* **218**:958-964.

Fu, X., D. Richards, T. Ait-ali, L. Hynes, H. Ougham, J. Peng, and N. Harberb. (2002). Gibberellin-mediated proteasome-dependent degradation of the barley DELLA protein SLN1 repressor. *Plant Cell* **14**:3191-3200.

Garcia-Martinez, J., I. Lopez-Diaz, M. Sanchez-Beltran, A. Phillips, D. Ward, P. Gaskin, and P. Hedden. (1997). Isolation and transcript analysis of gibberellin 20-oxidase genes in pea and bean in relation to fruit development. *Plant Mol. Biol.* **33**:1073-1084.

Gaskin, P., and J. Macmillan. (1991). GC-MS of the gibberellins and related compounds. *Methodology and a library of spectra.* Bristol, UK: University of Bristol (Cantock's Enterprises).

Gilroy, S., and R. Jones. (1994). Perception of gibberellin and abscisic acid at the external face of the plasma membrane of barley (*Hordeum vulgare* L.) aleurone protoplasts. *Plant Physiol.* **104**:1185-1192.

Gray, W., J. del Pozo, L. Walker, L. Hobbie, E. Risseeuw, T. Banks, W. Crosby, M. Yang, H. Ma, and M. Estelle. (1999). Identification of an SCF ubiquitin-ligase complex required for auxin response in *Arabidopsis thaliana*. *Genes Dev.* **13**:1678-1691.

Griffiths, J., K. Murase, I. Rieu, R. Zentella, Z. Zhang, S. Powers, F. Gong, A. Phillips, P. Hedden, T. Sun, and S. Thomas. (2006). Genetic characterization and functional analysis of the GID1 gibberellin receptors in *Arabidopsis*. *Plant Cell* **18**:3399-3414.

Hedden, P. (1987). Gibberellins. In: Rivier, L. and A. Crozier, eds. *Principles and practice of plant hormone analysis*, Vol. 1. London: Academic Press, 9-110.

Helliwell, C., J. Sullivan, R. Mould, J. Gray, W. Peacock, and E. Dennis. (2001). A plastid envelope location of *Arabidopsis ent*-kaurene oxidase links the plastid and endoplasmic reticulum steps of the gibberellin biosynthesis pathway. *Plant J.* **28**:201-208.

Jacobsen, J., D. Pearce, A. Poole, R. Pharis, and L. Mander. (2002). Abscisic acid, phaseic acid, and gibberellin contents associated with dormancy and germination in barley. *Physiologica Plantarum* **115**:428-441.

Kamiya, Y., and J. Graebe. (1983). The biosynthesis of all major pea gibberellins in a cell-free system from *Pisum sativum*. *Phytochem.* **22**:681-689.

Karssen, C., D. Brinkhorst-van der Swan, A. Breekland, and M. Koornneef. (1983). Induction of dormancy during seed development by endogenous abscisic acid: studies of abscisic acid deficient genotypes of *Arabidopsis thaliana* (L.) Heynh. *Planta* **157**:158-165.

Kasahara, H., A. Hanada, T. Kuzuyama, M. Takagi, Y. Kamiya, and S. Yamaguchi. (2002). Contribution of the mevalonate and methylerythritol phosphate pathways to the biosynthesis of gibberellins in *Arabidopsis*. *J. Biol. Chem.* **277**:45188-45194.

Koshioka, M., K. Takeno, F. Beall, and R. Pharis. (1983) Purification and separation of gibberellins from their precursors and glucosyl conjugates. *Plant. Phys.* **73**:398-406.

Lee, D., and J. Zeevart. (2005). Molecular cloning of GA *2-oxidase3* from spinach and its ectopic expression in *Nicotiana sylvestris*. *Plant Physiol.* **138**:243-254.

Lester, D., J. Ross, T. Ait-Ali, D. Martin, and J. Reid. (1996). A gibberellin 20-oxidase cDNA (Accession No. U58830) from Pea Seed. *Plant Physiol.* **111**:1353.

Lester, D., J. Ross, J. Davies, and J. Reid. (1997) Mendel's stem length gene (*Le*) encodes a gibberellin 3β-hydroxylase. *Plant Cell* **9**:1435-1443.

Lester, D., J. Ross, J. Smith, R. Elliott, and J. Reid. (1999). Gibberellin 2-oxidation and the SLN gene of *Pisum sativum*. *Plant J.* **19**:65-73.

Livak, K., and T. Schmittgen. (2001). Analysis of relative gene expression data using real-time quantitative PCR and the 2(-Delta Delta C(T)) method. *Methods* **25**:402-408.

MacMillan, J., P. Gaskin, and S. Croker. *Plant-Hormones: gibberellin structural and mass spectral information*. Accessed 14 March 2009, <http://www.plant-hormones.info/ga1info.htm>

MacMillan, J., J. Seaton, and P. Suter. (1962). Plant Hormones-II: Isolation and structures of Gibberellin A_6 and Gibberellin A_8. *Tetrahedron* **18**: 349-355.

Marinos, N. (1970). Embryogenesis of the pea (*Pisum sativum*). I. The cytological environment of the developing embryo. *Protoplasma* **70**:261-279.

Martin, D., M. Proebsting, and P. Hedden. (1999). The *SLENDER* gene of Pea encodes a gibberellin 2-oxidase. *Plant Physiol.* **121**:775-781.

Nelson, D., M. Schular, S. Paquette, D. Werck-Reichhart, and S. Bak. (2004). Comparative genomics of rice and *Arabidopsis*. Analysis of 727 cytochrome P450 genes and pseudogenes from a monocot and a dicot. *Plant Physiol.* **135**:756-772.

Owen, D., L. Mander, J. Storey, R. Huntley, P. Gaskin, J. Lenton, D. Gage, and J. Zeevaart. (1998). Synthesis and confirmation of structure for a new gibberellin, 2 beta-hydroxy-GA12 (GA110), from spinach and oil palm. *Phytochem.* **47**:331-337.

Ozga, J., R. van Huizen, and D. Reinecke. (2002). Hormone and seed-specific regulation of pea fruit growth. *Plant Phys* **128**:1379-1389.

Ozga, J., J. Yu, and D. Reinecke. (2003). Pollination-, development-, and auxin-specific regulation of gibberellin 3β-Hydroxylase gene expression in pea fruit and seeds. *Plant Phys* **131**:1137-1146.

Ozga, J., D. Reinecke, B. Ayele, P. Ngo, C. Nadeau, and A. Wickramarathna. (2009). Developmental and Hormonal Regulation of Gibberellin Biosynthesis and Catabolism in Pea Fruit. *Plant Physiol.* **150:**448-462.

Patrick, J., and C. Offler. (1995). Post-sieve element transport of sucrose in developing seeds. *Aust. J. Plant Physiol.* **22**:681-702.

Pfaffl, M. (2006). "Relative quantification" in Real-time PCR (T. Dorak ed.) Published by International University Line, 63-82.

Rochat, C., and J-P. Boutin. (1992). Temporary storage compounds and sucrose-starch metabolism in seed coats during pea seed development. *Phys. Plant.* **85**:567-572.

Rodrigo, M., J. García-Martinez, C. Santes, P. Gaskin, and P. Hedden. (1997). The role of gibberellins A_1 and A_3 in fruit growth of *Pisum sativum* L. and the identification of gibberellins A_4 and A_7 in young seeds. *Planta* **201**:446-455.

Rolletschek, H., L. Borisjuk, M. Koschorreck, U. Wobus, and H. Weber. (2002). Legume embryos develop in a hypoxic environment. *J. Exp. Bot.* **53**:1099-1107.

Schneider, G., E. Jensen, C. Spray, and B. Phinney. (1992). Hydrolysis and reconjugation of gibberellin A_{20} glucosyl ester by seedlings of *Zea mays* L. *Proc Nat Acad Sci USA* **89**:8045-8048.

Schneider, G., and W. Schliemann. (1994). Gibberellin conjugates-an overview. *Plant Growth Regul.* **15**:247-260.

Silverstone, A., C. Ciampaglio, and T. Sun. (1998). The *Arabidopsis* RGA gene encodes a transcriptional regulator repressing the gibberellin signal transduction pathway. *Plant Cell* **10**:155-169.

Soler, E., M. Clastre, B. Bantignies, G. Marigo, and C. Ambid. (1993). Uptake of isopentenyl diphosphate by plastids isolated from *Vitis vinifera* L. cell suspensions. *Planta* **191**:324-329.

Sponsel, V. (1983). The localization, metabolism and biological activity of gibberellins in maturing and germinating seeds of *Pisum sativum* cv. Progress No. 9. *Planta* **159**:454-468.

Spurr, A. (1969). A low-viscosity epoxy resin embedding medium for electron miscroscopy. *J. Ultrastruct. Res.* **26**:31-43.

Sun, T., and Y. Kamiya. (1994). The *Arabidopsis GA1* locus encodes the cyclase *ent*-kaurene synthetase A of gibberellin biosynthesis. *Plant Cell* **6**: 1509-1518.

Sun, T., and Y. Kamiya. (1997). Regulation and cellular localization of ent-kaurene synthesis. *Physiol. Plant.* **101**:701-708.

Talon, M., M. Koornneef, and J. Zeevart. (1990). Endogenous gibberellins in *Arabidopsis thaliana* and possible steps blocked in the biosynthetic pathways of the semidwarf ga4 and ga5 mutants. *Proc. Nat. Acad. Sci. USA* **87**:7983-7987.

Thomas, S., A. Phillips, and P. Hedden. (1999). Molecular cloning and functional expression of gibberellin 2- oxidases, multifunctional enzymes involved in gibberellin deactivation. *Proc. Nat. Acad. Sci. USA* **96**:4698-4703.

Ueguchi-Tanaka, M., M. Ashikari, M. Nakajima, H. Itoh, E. Katoh, M. Kobayashi, T. Chow, Y. Hsing, H. Kitano, I. Yamaguchi, and M. Matsuoka. (2005). *GIBBERELLIN INSENSITIVE DWARF1* encodes a soluble receptor for gibberellin. *Nature* **437**:693-698.

van Dongen, J., A. Ammerlaan, M. Wouterlood, A. van Aelst, and A. Borstlap. (2003). Structure of the developing pea seed coat and the post-phloem transport pathway of nutrients. *Ann. Bot.* **91**:729-737.

Varbanova, M., S. Yamaguchi, Y. Yang, K. McKelvey, A. Hanada, R. Borochov, F. Yu, Y. Jikumaru, J. Ross, D. Cortes, C. Ma, J. Noel, L. Mander, V. Shulaev, Y. Kamiya, S. Rodermel, D. Weiss, and E. Pichersky. (2007). Methylation of gibberellins by *Arabidopsis* GAMT1 and GAMT2. *Plant Cell* **19**:32-45.

Wang, T., S. Cook, R. Francis, M. Ambrose, and C. Hedley. (1987). An analysis of seed development in *Pisum sativum*: VI. Abscisic acid accumulation. *J. Exp. Bot.* **38**:1921-1932.

Weber, H., L. Borisjuk, U. Wobus. (1997). Sugar import and metabolism during seed development. *Trends Plant Sci.* **2**:169-174.

Weston, D., R. Elliott, D. Lester, C. Rameau, J. Reid, I. Murfet, and J. Ross. (2008). The Pea DELLA proteins LA and CRY are important regulators of gibberellin synthesis and root growth. *Plant Physiol*. **147**:199-205.

Willige, B., S. Ghosh, C. Nill, M. Zourelidou, E. Dohmann, A. Maier, and C. Schwechheimer. (2007). The DELLA domain of GA INSENSITIVE mediates the interaction with the GA INSENSITIVE DWARF1A gibberellin receptor of *Arabidopsis*. *Plant Cell* **19**:1209-1220.

Yabuta, T., and Y. Sumiki. (1938). On the crystal of gibberellin, a substance to promote plant growth. *J. Agric. Chem. Soc. Japan* **14**:1526.

Zhu, Y., T. Nomura, Y. Xu, Y. Zhang, Y. Peng, B. Mao, A. Hanada, H. Zhou, R. Wang, P. Li, X. Zhu, L. Mander, Y. Kamiya, S. Yamaguchi, and Z. He. (2006). *ELONGATED UPPERMOST INTERNODE* encodes a cytochrome P450 monooxygenase that epoxidizes gibberellins in a novel deactivation reaction in rice. *Plant Cell* **18**:442-456.

Chapter 3

Regulation of Auxin Sensitivity in Pea Fruit

3.1 Background

3.1.1 Auxins in Plants

Auxins as a class of phytohormones are defined by function, and as such contain structurally diverse members. The most ubiquitous natural auxin is a bi-cyclic molecule known as indole-3-acetic acid (IAA), synthesized from tryptophan, indole or indole-3-glycerol phosphate via multiple parallel biochemical pathways (reviewed in Bartel, 1997). A second naturally occurring auxin in pea is indole-3-butyric acid (Schneider *et al*., 1985), which can be converted to IAA *in vivo* (Nordström *et al*., 1991). A third naturally occurring auxin, 4-chloroindole-3-acetic acid (4-Cl-IAA), has been identified in a number of legumes but seems to be restricted to only certain genera including *Pisum sativum* (Marumo *et al*., 1968; Katayama et al., 1988) and *Vicia amurensis* (Katayama *et al*., 1987), but not in the closely related *Phaseoleae* genus (Katayama *et al*., 1987).

Auxins occur in plants as free acids and in conjugated forms. Auxin conjugates identified in plants include auxin linked to single amino acids or to mono- or disaccharides (Bandurski *et al*., 1995). It has also been demonstrated that IAA can be

covalently bound to proteins (Bialek and Cohen, 1989). Auxin conjugation has been implicated as a storage mechanism, where, in addition to *de novo* synthesis, free auxin can be generated upon cleavage from these bound forms (Bandurski *et al*., 1995; Woodward and Bartel, 2005). Conjugated auxins identified in pea include amide conjugates such as indole-3-acetylaspartic acid (Law and Hamilton, 1982) and esterified compounds, such as 1-O-indole-3-acetyl-β-D-glucose (Jakubowska and Kowalczyk, 2004). The ratio between amide and ester conjugates varies between tissues (Bandurski and Schulze, 1977; Magnus *et al*. 1997), suggesting a developmental role for auxin conjugation in pea.

In pea, 4-Cl-IAA has been implicated as a specific fruit growth promoting auxin (Reinecke *et al*., 1995; Reinecke *et al*., 1999; Ozga and Reinecke, 2003), and the further understanding of the biological roles of 4-Cl-IAA in this system could have significant agricultural implications.

3.1.2 Auxin Signal Perception

Most research in auxin signalling has been performed in *Arabidopsis*. Shortly after application of auxins to *Arabidopsis* seedlings, a group of transcriptional repressors (the Aux/IAA genes) are upregulated (Leyser, 2002). Aux/IAA proteins are transcriptional repressors and contain four domains; an N-terminal transcriptional repressor called domain I (Tiwari *et al.*, 2001), domain II, involved in protein stability and degradation (Park *et al.*, 2002), and two C-terminal dimerization domains named domains III and IV.

A second family of proteins involved in auxin signal transduction are the Auxin Response Factors (ARF). ARF proteins are similar to the Aux/IAA proteins in structure (Ulmasov *et al*., 1999), and also consist of four domains; an N-terminal DNA-binding domain, an RNA polymerase II interaction domain (Hagen and Guilfoyle, 2002), and two dimerization domains similar in structure to domains III and IV of the Aux/IAA repressors. The DNA-binding domain recognizes a sequence that consists minimally of a conserved sequence (5'-TGTCTC). This sequence, combined with a secondary constitutive element in some genes (Ulmasov *et al*., 1995), constitutes the auxin responsive element (ARE), which is both necessary and sufficient to confer auxin inducibility to reporter genes.

Whereas the Aux/IAA proteins are transcriptional repressors, ARFs can act as either transcriptional repressors or activators (Hagen and Guilfoyle, 2002). These two groups of proteins are capable of both homo- and heterodimerization freely with one another. In the absence of auxin, a heterodimer consisting of one Aux/IAA repressor and one ARF protein (either a repressor or an activator) is bound at the ARE of an auxin-inducible gene, inhibiting transcription. Upon auxin induction, the Aux/IAA protein of that dimmer is degraded, which allows the formation of a new homo- or heterodimer, effecting changes in gene transcription.

The degradation of Aux/IAA proteins relies on the SCF complex, named for its major components: Skp1, Cullin, and F-box (Gray *et al*., 1999; Figure 3.1). The SCF complex is an E3 ubiquitin ligase involved in several signal transduction pathways, including those for the phytohormones gibberellin and jasmonic acid. Skp1 is a scaffold protein, and interacts with two of the other members of this complex. Cullin is a protein

which transfers ubiquitin subunits from an E2 ubiquitin conjugating enzyme to a specific target protein, and functions as a heterodimer with a fourth protein, RBX1. The F-box proteins are a diverse family of proteins containing two characteristic features; a protein-protein interaction domain which interacts with Skp1 called the F-box, and a variety of C-terminal protein-protein interaction domains which confer target specificity to the complex (leucine rich repeats for the AFB family of F-box proteins (Gagne *et al*., 2002), although a variety of other domain types are present in other groups of F-box proteins).

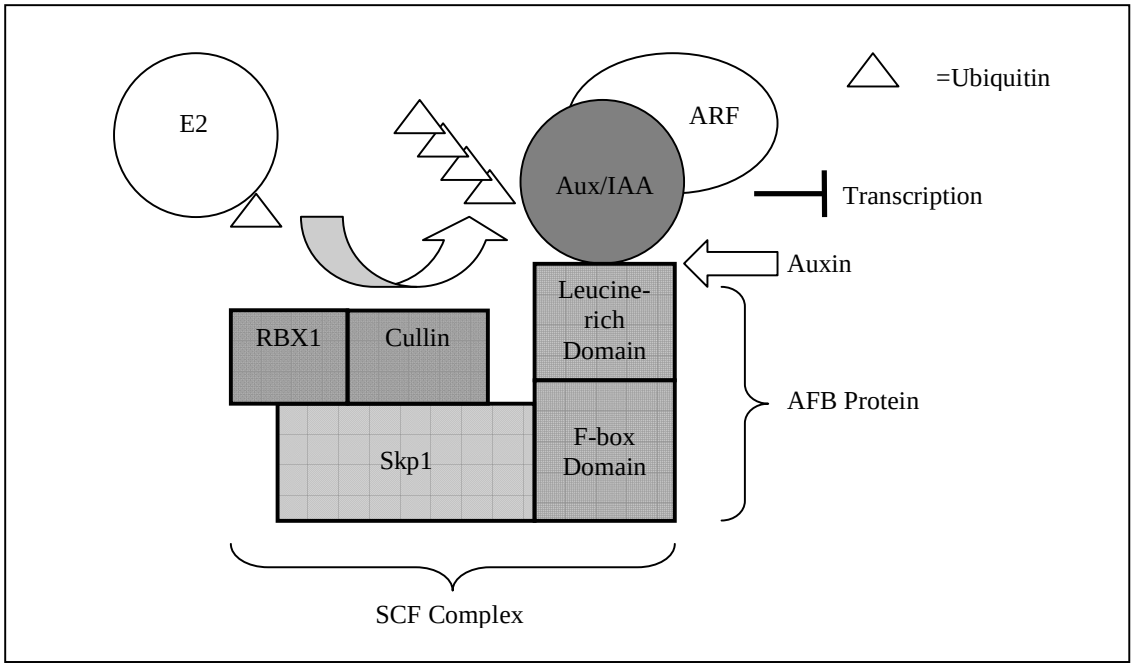

Figure 3.1: Schematic of SCF complex indicating interactions with key components of auxin signalling pathway. Upon auxin binding directly to the F-box protein, conformational changes allow the binding and ubiquitin-mediated degradation of Aux/IAA proteins, which in turn allows the dimerization of ARF proteins, altering gene transcription.

In addition to contributing target specificity to the SCF complex, the F-box proteins TIR1, AFB2, and AFB3, function as auxin receptors (Dharmasiri *et al*., 2005a). Kepinski and Leyser (2005) demonstrated that the AFB F-box proteins bind auxins directly, and that the formation of the auxin-AFB complex is a necessary condition for the binding of Aux/IAA proteins by the SCF. Recently the crystal structure of the TIR1 protein in Arabidopsis both in the presence and absence of auxin was obtained (Tan *et al.*, 2007). While the F-box region of the AFB proteins interact with the SCF scaffold protein (ASK1 in Arabidopsis), the C-terminal leucine rich repeats form an open pocket. The auxin molecule sits in the proximal end of the pocket and acts as a molecular glue, mediating contact between the AFB protein and the targeted Aux/IAA protein. This binding is likely promoted by van der Waals, hydrophobic, and hydrogen-bonding interactions, and may help to explain why a number of relatively hydrophobic molecules of approximately the same size and general structure can serve as auxins.

Upon the introduction of auxin into the nucleus, a series of events unfolds which culminate in the alteration of transcription profiles of auxin regulated genes. Initially, auxin binds to the LRR region of the AFB protein of the SCF complex. The auxin molecule mediates interactions between the AFB protein of the SCF complex and the target Aux/IAA protein, which may be part of an inhibitory Aux/IAA-ARF heterodimer. The Cullin subunit of SCF then transfers, iteratively, ubiquitin peptides from E2 ubiquitin conjugating enzymes to a site in domain II of the Aux/IAA protein (Dharmasiri and Estelle, 2004). The ubiquitinated Aux/IAA protein is shuttled to the 26s proteasome for degradation (Gray *et al*., 2001), freeing the formerly bound ARF protein to interact with other subunits. Another ARF subunit or a second Aux/IAA protein (if more are

available) can then dimerize with the pre-existing ARF protein, either promoting or inhibiting transcription of the auxin-responsive gene in question, leading to a variety of physiological and developmental changes (Dharmasiri *et al*., 2005b; Figure 3.2).

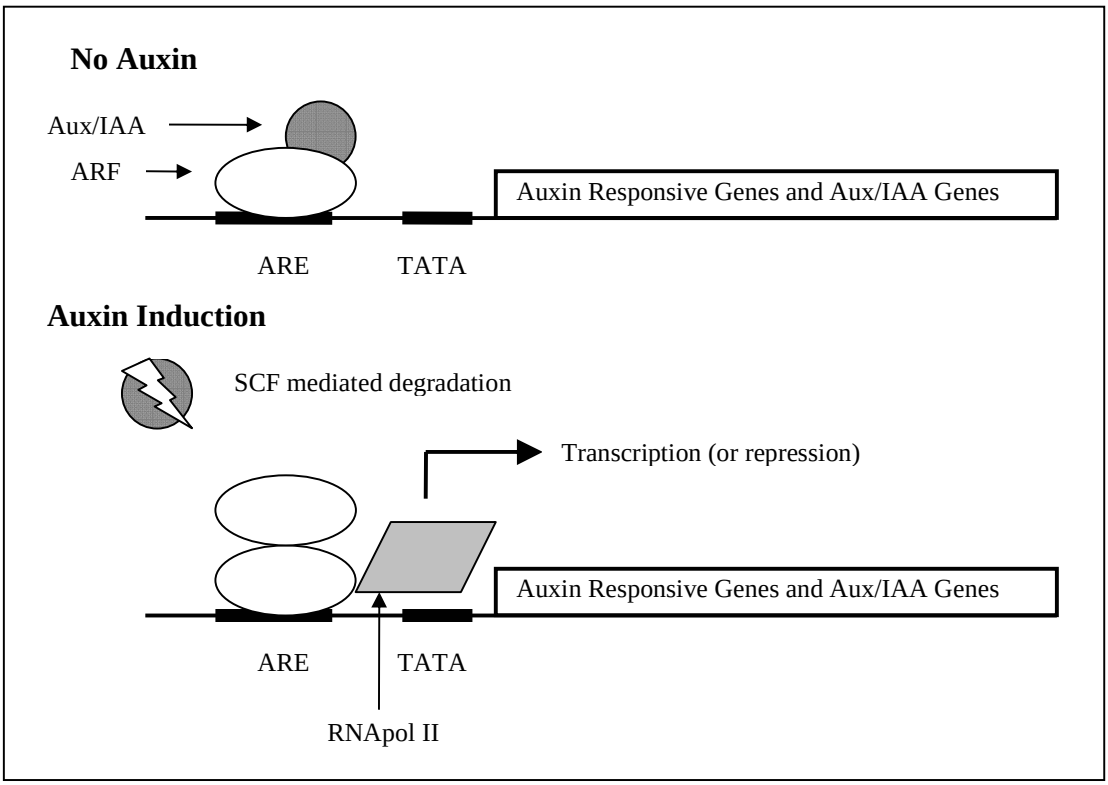

Figure 3.2: Schematic of auxin regulation of gene transcription. In the absence of an appropriate auxin, an ARF-Aux/IAA heterodimer binds the upstream ARE sequence, preventing transcription. Upon degradation of the Aux/IAA protein by the auxin-activated SCF complex, an ARF homodimer can form, recruiting RNApol II and increasing transcription.

3.1.2 Auxins in *Pisum* Fruit Development

Auxins play vital roles in the coordination of seed and fruit growth in pea. The presence of viable, developing seeds is a prerequisite for pericarp development. Seed removal early in fruit development retards pericarp growth (Ozga *et al*., 1992), eventually

leading to pericarp senescence. Mounting evidence supports the hypothesis that seed-derived signals promote pericarp growth in pea. While the application of bioactive GA_3 or GA_1 to the endocarp of deseeded pericarps can stimulate pericarp growth (Ozga and Reinecke, 1999), GA transport from the seeds to the pericarp is likely minimal. In the pea GA biosynthesis mutant *na*, which possesses a loss of function mutation in an *ent*-kaurene oxidase gene (*PsKO1*) primarily expressed in vegetative tissues (producing a severely dwarfed plant), the presence of the wildtype seed expressed *PsKO2* homolog allows seeds of *na* mutant plants to develop with normal GA levels, while GA levels in the pod are severely reduced (Davidson *et al*., 2003). A similar lack of apparent seed to pericarp GA transport was observed in the *ls-1* GA biosynthesis mutant (partial loss of the ability to convert GGDP to CPP early in the GA biosynthesis pathway), where pericarp GA_1 levels were significantly lower than in wildtype plants while seed GA_1 was comparable to wildtype levels (Reid and Ross, 1993).

While transport of bioactive GAs from the seeds to the pericarp as a growth-inducing signal are likely minimal, 4-Cl-IAA can substitute for seeds in many aspects of pericarp growth, and may be a primary seed-to-pericarp growth signal in pea. 4-Cl-IAA accumulates in both the seeds and pericarps of pea (Magnus *et al*., 1997), and in the absence of viable seeds, 4-Cl-IAA can stimulate pericarp growth (Reinecke *et al*., 1995). 4-Cl-IAA-stimulated pericarp growth is mediated partially by GAs through the local upregulation of the GA biosynthesis pathway in the pericarp. While $[^{14}C]GA_{12}$ is efficiently metabolized to GA_{19} and GA_{20} by pericarps with intact seeds, in deseeded pericarps $[^{14}C]GA_{19}$ accumulates, but $[^{14}C]GA_{20}$ does not, indicating that seeds have a role in the conversion of GA_{19} to GA_{20} within the pericarp (Ozga *et al*., 1992). A similar

pattern was observed in the profile of endogenous GAs in the pericarp. In pericarp with seeds, GA_{19}, GA_{20}, GA_1, and GA_8 were detected; however, in deseeded pericarps, GA_{19} accumulated, while GA_{20}, GA_1, and GA_8 were not detected, suggesting a block in the GA pathway at the oxidation step between GA_{19} and GA_{20} due to seed removal (Ozga *et al*., 1992). When applied to the pericarp via a split-pericarp technique, [^{14}C]GA_{19} was readily converted to [^{14}C]GA_{20} and [^{14}C]GA_{29} in fruit with seeds, while in deseeded pericarps, the production of [^{14}C]GA_{20} and [^{14}C]GA_{29} was reduced (van Huizen *et al*., 1995). Steady-state pericarp transcript abundance of *PsGA20ox1*, the enzyme product of which can convert GA_{19} to GA_{20}, was lower in deseeded pericarps than in pericarps with seeds, confirming the results of the [^{14}C]GA_{12} metabolism studies which indicate that seeds are important for pericarp GA_{20} biosynthesis (van Huizen *et al*., 1997).

The application of 4-Cl-IAA to deseeded pericarps stimulated the conversion of radiolabelled GA_{12} or GA_{19} to GA_{20} (van Huizen *et al.*, 1995; Ozga *et al*., 2009), and increased steady-state transcript levels of *PsGA20ox1* (van Huizen *et al.*, 1997; Ozga *et al*., 2009), mimicking the presence of the seeds. In addition to promoting the production of pericarp GA_{20}, seeds are also involved in the regulation of GA 3β-hydroxylase activity: steady-state *PsGA3ox1* transcript abundance was significantly reduced in deseeded pericarps in comparison to controls with viable seeds. The application of 4-Cl-IAA to deseeded pericarps once again increased steady-state *PsGA3ox1* mRNA levels (Ozga *et al*., 2003), much as with *PsGA20ox1*. Additionally, upon treatment with 4-Cl-IAA, deseeded pericarps were able to convert [^{14}C]GA_{12} to [^{14}C]GA_1, which did not occur in the absence of 4-Cl-IAA treatment, indicating the restoration of GA pathway flux in the pericarp by this auxin (Ozga *et al.*, 2009). Furthermore, transcript abundance

of the catabolic gene *PsGA2ox1* was elevated in pericarps lacking seeds, and 4-Cl-IAA, but not IAA, reduced *PsGA2ox1* transcript to levels comparable to those in pericarps containing viable seeds (Ozga *et al*., 2009). Between 2 and 3 DAA, pericarps with viable seeds displayed a transitory increase in transcript abundance of the catabolic gene *PsGA2ox2*, possibly as part of a regulatory mechanism to support the transition between developmental programs of fruit set and sustained pericarp growth. While *PsGA2ox2* transcript levels do not increase in deseeded pericarps, the application of 4-Cl-IAA (but not IAA) to the pericarp can mimic the seed-induced transitory increase in pericarp *PsGA2ox2* transcript (Ozga *et al*., 2009). Taken together, these data present a compelling role for seed-derived 4-Cl-IAA in the regulation of fruit development.

The presence of two natural auxins with varying developmental roles provides a unique system in which to study the relationship between physiological activity and auxin structure. Using a split-pericarp pod elongation assay, Reinecke *et al*. (1995) tested the ability of a variety of halogenated auxins (4-, 5-, 6-, and 7-chloro- and fluoroindole-3-acetic acid) to promote deseeded pericarp growth. While 4-Cl-IAA stimulated pericarp growth, the other auxins tested generally did not stimulate growth. Similar research using a variety of 4-substituted auxins (4-H-IAA, 4-Cl-IAA, 4-Fl-IAA, 4-Me-IAA, and 4-Et-IAA) found that 4-Me-IAA was also capable of stimulating the expansion of deseeded pericarps, but not to the same extent as 4-Cl-IAA (Reinecke *et al*., 1999). The most recent data on structure-activity relationships in pea pericarp suggests that the position, size, and lipophilicity of the indole-substituent are important for determining biological activity, with optimal activity obtained with a hydrophobic substituent of approximately

the same size as a chlorine atom at the 4-position of the indole ring (see Reinecke *et al*., 1999 for lipophilicity and sterimol parameters).

While the variance in biological activity of 4-Cl-IAA and other indole-substituted auxins may be explained by differences in transport or stability, specificity may lie in the binding kinetics of 4-Cl-IAA and the AFB proteins. The first steps to understanding receptor 4-Cl-IAA interactions and their greater role in whole plant physiology are to identify putative auxin receptor genes. Once cloned and expressed, structure-function assays, site-directed mutagenesis, and x-ray crystallography can be employed to further study this unique hormone and its signal perception machinery. Additionally, the spatial and temporal localization of auxin receptor transcripts may yield interesting insights into the modulation of auxin sensitivity and its interactions in other hormone networks.

3.1.3 Goals

This study will employ a variety of RNA-based cloning strategies to identify and isolate members of the AFB family of auxin receptors from *Pisum sativum* L. The possible roles of these receptors in seed and fruit development will be examined through transcription profiling with qRT-PCR. Additionally, the response of steady-state mRNA levels of these genes to auxins and gibberellins will be evaluated, in order to identify possible hormone regulation of auxin sensitivity via the modulation of AFB gene transcript abundance. The correlation between endogenous IAA and 4-Cl-IAA and auxin receptor transcript abundance in seed tissues will also be examined. These data should provide clues as to the roles of these genes in fruit and seed development, and will serve as the starting point for future studies in receptor kinetics and structure.

3.2 Methods

3.2.1 Plant Material

Plants (*Pisum sativum* L. I_3 Alaska-type) were grown under the same conditions as described in Chapter 2. To obtain RNA for cDNA generation, whole seeds at 14 days after anthesis (DAA), ovaries with seeds at 2 DAA, pericarps (seeds removed) at 2 DAA, and funiculi at 10 DAA were harvested. To determine the expression profiles of the AFB genes during early fruit development, pericarp and whole seeds were harvested at -2, -1, 0, 1, 2, 3, 4, 5, 6, 7, 8, 10, and 12 DAA. To investigate the role of fertilization and the presence of developing seeds on AFB transcript levels in the pericarp, flowers were emasculated at -2 DAA and pericarps were harvested at the equivalent to -1, 0, 1, 2, and 3 DAA for RNA extraction.

To determine the expression profiles of the AFB genes in developing seed tissues, seeds were harvested whole or dissected into seed coat, endosperm and embryo at 8, 10, and 12 DAA. At 14, 16, 18, and 20 DAA, seeds were dissected into seed coat and embryo or seed coat, cotyledons, and embryo axis (see Chapter 2 for details). To examine the spatial expression of the AFB genes within the pericarp while seeds were rapidly expanding, pods were harvested at 8, 10, 12, 14, 16, 18, and 20 DAA and dissected into three regions (Figure 3.3). The dorsal and ventral vascular suture regions were approximately 1 to 2 mm in width, and extended along most of the pericarp (regions where no seeds were present were omitted; Figures 3.3A and D). The pericarp wall samples were approximately 2 to 3 mm in width, and were taken from the mid-pericarp wall region extending the majority of the length of the pericarp (Figure 3.3B). Funiculi

were also harvested from 8 to 20 DAA fruits. All tissues for cDNA generation and expression profiling were harvested into liquid nitrogen and stored at -80^{o}C until RNA extraction

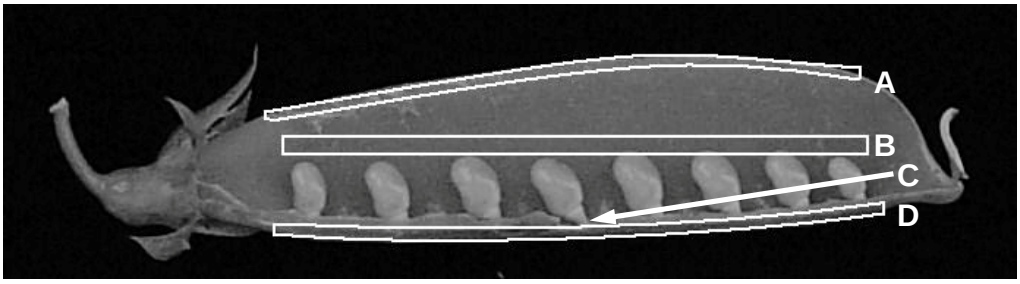

Figure 3.3: Dissection schematic detailing the approximate location of tissues used to study localization of transcripts in the pericarp vascular suture tissues, pericarp wall, and funiculus. RNA for qRT-PCR was isolated from the dorsal vascular suture traces (A), pericarp wall lacking vascular suture traces (B), the funiculus (between ventral trace and seed; C), and the ventral vascular suture traces (D).

3.2.2 Hormone Treatments

To examine the hormonal regulation of pericarp AFB mRNA levels, the pea split-pericarp assay was used (Ozga et al., 1992). Fruit at 2 DAA were split along the dorsal suture. Seeds were removed and pericarps were left for 12 hours prior to hormone application to reduce residual seed effects. IAA, 4-Cl-IAA, or GA_3 was applied to the inside of the pericarp (endocarp) at a concentration of 50µM in 0.1% aqueous Tween 80 in a total volume of 30 µL. For split-pod, no seed controls (SPNS), 30 µL of 0.1% aqueous Tween 80 was applied. For split-pod controls (SP), seeds were not removed after the dorsal suture was opened, but 30 µL of 0.1% aqueous Tween 80 was applied 12 hours after pericarp splitting. As a further control for the split-pericarp procedure, intact

pods were also harvested at the appropriate times. All fruit subjected to split-pericarp treatments were covered with plastic to maintain humidity, and all manipulations were carried out while pericarps remained on the plant. Intact controls were harvested at the 0 hour and 12 hour treatment timing, while all split-pericarp treatments were harvested at 12, 14, 20, and 24 hours after pericarp splitting (0, 2, 8, and 12 hours after hormone treatment).

3.2.3 Degenerate PCR and Cloning

cDNA was synthesized using multiple protocols from several tissues to maximize chances of obtaining at least one pool with high levels of the genes of interest. The first protocol utilized total RNA isolated from 14 DAA whole seeds, 2 DAA ovaries, 2 DAA pericarps, or 10 DAA funiculi. RNA isolation procedures were as described in Chapter 2. To generate cDNA from total RNA, 1250 ng RNA was mixed with oligo-dT (12-18 bases in length, final concentration 2.14 µM), and nucleotides (0.71 mM each dNTP), brought to a final volume of 35 µL with water, heated at 65°C for 5 minutes to minimize any secondary structures, and cooled to 4°C for the remainder of the reaction assembly. SuperScript III reverse transcriptase (250 u; Invitrogen), dithiothreotol (DTT, final concentration 5 mM) and the supplied buffer were added to the reaction and cDNA synthesis was performed at 50°C for one hour, after which point the reaction was halted by heating to 70°C for 15 minutes.

The second protocol utilized RNA isolated from both 2 DAA pericarp and 6 DAA whole seeds. RNA was isolated as previously described and mRNA was selected for with a poly-T cellulose column (Poly-A purist, Ambion) as per the manufacturer's

directions. To generate cDNA from poly-A mRNA, 500 ng of RNA was mixed with oligo-dT (final concentration 2.5 µM), nucleotides (0.5 mM each dNTP), brought to a final volume of 13 µL with water, and heated as previously described. SuperScript III reverse transcriptase (400 U; Invitrogen), DTT (final concentration 5 mM), and the supplied buffer were added to the reaction and cDNA synthesis was performed as previously described. cDNA generated with either protocol was checked for concentration (A_{260}) and quality (A_{260}/A_{280} and A_{260}/A_{230}) via a spectrophotometer and by agarose gel electrophoresis.

Some cDNA samples were treated with RNAse to remove RNA-cDNA duplexes that could potentially inhibit PCR. In this protocol approximately 500 ng of cDNA was incubated with 2 u of RNAse H (Invitrogen) for 80 minutes at 37°C. As the sample was already reverse transcribed, no RNAse deactivation was performed. Additionally some cDNA samples were purified through a phenol/chloroform extraction as follows. Samples (20 µL) were mixed with 20 µL phenol/chloroform/isoamyl alcohol (25:24:1 v/v/v, saturated with 10 mM TRIS, pH 8.0, 1 mM EDTA, Sigma-Aldrich), and the aqueous phase was removed and partitioned against 20 µL chloroform. cDNA was precipitated with sodium acetate (950 mM final concentration), glycogen (1 µL per 63 µL precipitation), and 95% ethanol (40 µL per 63 µL precipitation) at -80°C for 2.5 hours. The precipitation was spun with a table-top microcentrifuge at 13 000 rpm for 10 minutes, then the pellet was washed twice with 100 µL 70% ethanol. The pellet was dried and resuspended in 15 µL DEPC-treated water.

PCR primers were designed by Dr. Dennis Reinecke with the CODEHOP algorithm, a program which generates degenerate primers when supplied with blocks of

protein sequence (Rose *et al.*, 2003). The protein sequences of 58 AFB genes from both angiosperms and gymnosperms were used to generate the two primers used to obtain initial sequence data (Table 3.1). PCR was successfully carried out with 150 ng of cDNA from 14 DAA whole seed and 2 DAA ovary tissues using Taq polymerase (0.56 µL per reaction; Invitrogen,), the forward and reverse CODEHOP primers (50 pmol each per reaction, Table 3.1), nucleotides (0.5 mM final concentration), magnesium chloride (4 mM final concentration), and the supplied buffer (final concentration 1x) in a total reaction volume of 20 µL. Reactions were carried out with the following thermocycling program: denaturation at 95°C for 5 minutes, 35 cycles of denaturation at 94°C for 30 seconds, annealing at 50°C for 30 seconds, and polymerization at 72°C for 70 seconds, followed by a final extension phase at 72°C for 7 minutes. Products were analyzed with agarose gel electrophoresis.

Table 3.1: Degenerate primers used for amplification of interior sections of AFB genes.

Primer	Sequence	Purpose
AFB-F	5'-TGG TGT AGA AGG AAA GTG ATT GGN A	Forward CODEHOP Primer
AFB-R	5'-CAT CAG CGA AAG GAC AAT CTC TAA TYT CN	Reverse CODEHOP Primer

PCR products of the appropriate length were cloned via T/A overhangs into the pCR8 vector using the pCR8/GW/TOPO kit (Invitrogen). Briefly, 2 µL of the appropriate DNA was mixed with 0.5 µL high salt solution (1.2 M NaCl and 0.06 M $MgCl_2$) and 0.5 µL of the supplied linearized, topoisomerase I bound vector. The ligation reaction was held at room temperature for between 15 and 30 minutes then incubated

with 50 µL competent TOP10 *E. coli* (Invitrogen) on ice for 20-40 minutes. Cells were heat shocked at 42°C for 30 seconds and returned to 4°C to cool, then incubated with 125 µL S.O.C. medium at 37°C for approximately one hour. Cells were plated on LB agar plates containing 100 µg/mL spectinomycin and grown overnight at 37°C.

Individual colonies were picked from plates and grown overnight in 5 mL LB containing 100 µg mL^{-1} spectinomycin at 37°C with agitation at 250 rpm. Cells were collected by centrifugation in either an Avanti J-E centrifuge (Beckman-Coulter) or a benchtop microcentrifuge and excess media was drained off. Plasmid DNA was isolated with either the GenElute miniprep kit (Sigma-Aldrich) or QiaQuick spin miniprep kit (Qiagen) as recommended by the manufacturers. Plasmids were screened for insert size by restriction digestion with EcoRI followed by agarose gel electrophoresis. The inserts of clones containing appropriately sized fragments were sequenced from the T3 and T7 or M13 primer sites within the vector using the BigDye Terminator v3.1 Cycle Sequencing kit and 3730 DNA Analyzer (Applied Biosystems) at the University of Alberta Molecular Biology Service Unit as per the manufacturer's recommendations. Sequence editing and alignment was performed in BioEdit.

3.2.4 Random Amplification of cDNA Ends of *PsAFB2*

RNA-ligase mediated RACE (RLM-RACE) was used to generate cDNA for PCR amplification of the ends of *PsAFB2*. The 3' RACE cDNA pool was generated from 14 DAA whole seeds, 2 DAA ovaries, 2 DAA pericarps, and 10 DAA funiculi with a primer consisting of poly-T and a unique sequence (Figure 3.4, across from primers E and F),

which was later used along with a gene specific primer (Figure 3.4, primer G) to amplify the unknown 3' end.

In the first stage of 5' RACE cDNA synthesis, poly-A selected RNA from 14 DAA whole seeds, 2 DAA ovaries, 2 DAA pericarps, and 10 DAA funiculi was treated with a calf intestinal phosphatase to cleave the 5' phosphate group from any remaining rRNA, tRNA, DNA, and fragmented mRNA. The sample was then treated with tobacco alkaline pyrophosphatase, which cleaves the 5' 7-methylguanine cap from full-length mRNA, leaving a free 5' phosphate. A single-strand ligation was performed between these molecules and a synthetic RNA containing a unique sequence (Figure 3.4, across from primers C and D), then cDNA synthesis was performed from random decamers. The unique sequence was later used with an internal gene specific primer (Figure 3.4, multiple internal primers were used in this study, A and B) to amplify the unknown 5' end.

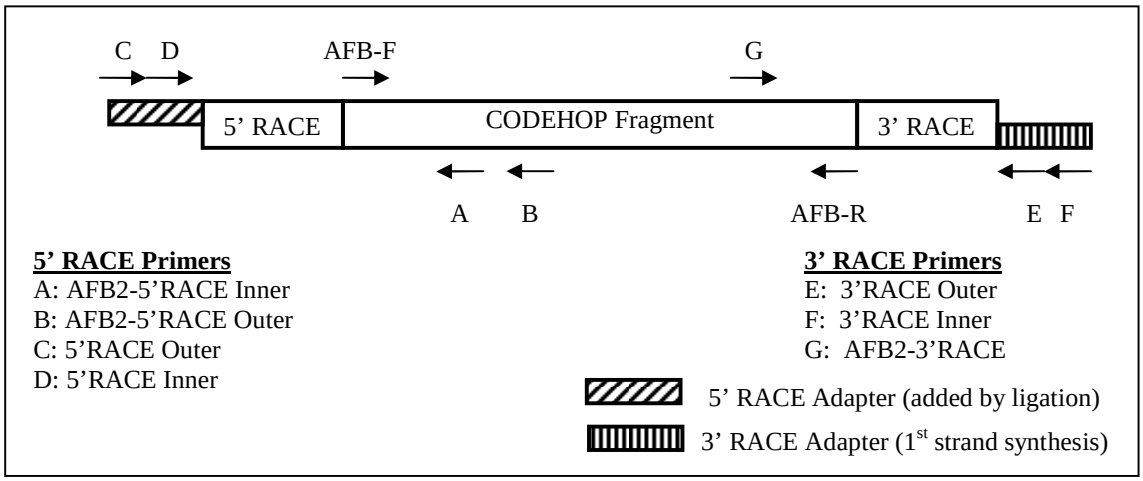

Figure 3.4: Schematic of cloning strategy used to obtain *PsAFB2*. While displayed as one molecule, the schematic represents both the 5' (5' RACE Adapter to undetermined points within the CODEHOP fragment) and 3' (3' RACE Adapter to undetermined points within the CODEHOP fragment) cDNA pools, which are used separately for amplification of each end.

The RNA used for RLM-RACE was the same poly-A selected RNA used in the previously described CODEHOP experiments. Generation of cDNA pools was performed using the FirstChoice RLM-RACE system (Ambion) according to the manufacturer's directions.

The 5' region of *PsAFB2* was amplified in three stages of nested PCR from the 5' RLM-RACE cDNA pools as follows. Template cDNA (1 µL) was mixed with nucleotides (final concentration 0.2 mM each), 20 pmol of AFB2-5'RACE outer gene specific primer, 20 pmol of supplied 5' RACE Outer primer (FirstChoice RLM-RACE kit, Ambion), $MgCl_2$ (final concentration 1.4 mM), 1.25 U Taq polymerase (Invitrogen), and the supplied reaction buffer in a final volume of 25 µL. Thermocycling consisted of denaturation at 94°C for 3 minutes, 35 cycles of 94°C for 15 seconds, 50°C for 20 seconds, and 72°C for 30 seconds, and final extension at 72°C for 5 minutes. The second stage of nested PCR was carried out using 1 µL of the first reaction products. Template DNA was mixed with nucleotides (final concentration 0.2 mM each), 20 pmol of AFB2-5'RACE outer gene specific primer, 20 pmol of the 5' RACE Inner primer (FirstChoice RLM-RACE kit, Ambion), $MgCl_2$ (final concentration 1.8 mM), 1.25 U Taq polymerase (Invitrogen), and the supplied reaction buffer in a final volume of 25 µL. Thermocycling consisted of denaturation at 94°C for 5 minutes, 35 cycles of 94°C for 1 minute, 55°C for 1 minute, and 72°C for 1 minute, and final extension at 72°C for 5 minutes. The third stage of nested PCR was carried out using 2 µL of the reaction products of the second stage PCR. Template DNA was mixed with nucleotides (final concentration 0.2 mM each), 20 pmol of AFB2-5'RACE inner gene specific primer, 20 pmol of 5' RACE Inner primer (FirstChoice RLM-RACE kit, Ambion), $MgCl_2$ (final concentration 1.8 mM),

1.25 U Taq polymerase (Invitrogen), and the supplied reaction buffer in a final volume of 25 µL. Thermocycling consisted of denaturation at 94°C for 5 minutes, 40 cycles of 94°C for 1 minute, 55°C for 1 minute, and 72°C for 1 minute, and final extension at 72°C for 5 minutes. The 5' RACE PCR reaction products were analyzed by agarose gel electrophoresis, and bands of the appropriate size were excised. DNA was extracted using a gel extraction kit (QIAquick, Qiagen), then ligation, transformation, plating, and fragment analysis proceeded as previously noted.

The 3' region of *PsAFB2* was amplified in two stages of nested PCR from the 3' RLM-RACE cDNA pools as follows (primers listed in Table 3.2). Template cDNA (1 µL) was mixed with nucleotides (final concentration 0.8 mM each), 8 pmol of AFB2-3'RACE gene specific primer, 8 pmol of the 3' RACE Outer primer (FirstChoice RLM-RACE kit, Ambion), $MgCl_2$ (final concentration 1.75 mM), 0.5 U Taq polymerase (Invitrogen), and the supplied reaction buffer in a final volume of 20 µL. The thermocycling consisted of an initial denaturation of 5 minutes at 94°C followed by 35 cycles of denaturation at 94°C for 15 seconds, primer annealing at 55°C for 15 seconds, and extension at 72°C for 25 seconds, and a final elongation at 72°C for 3 minutes. The second stage was performed using 5 µL of the first-stage reactions as template. Template DNA was mixed with nucleotides (final concentration 0.8 mM each), 20 pmol of AFB2-3'RACE gene specific primer, 20 pmol of the 3' RACE Inner primer (FirstChoice RLM-RACE kit, Ambion), $MgCl_2$ (final concentration 1.75 mM 1.25 U Taq polymerase (Invitrogen), and the supplied reaction buffer in a final volume of 50 µL. Thermocycling for the second phase consisted of initial denaturation at 94°C for 5 minutes, and 35 cycles of denaturation at 94°C for 30 seconds, annealing at 55°C for 30 seconds, and primer

extension at 72°C for 45 seconds, and a final extension at 72°C for 5 minutes. The 3' RACE PCR reaction products were analyzed by agarose gel electrophoresis, and bands of the appropriate size were excised. DNA was extracted using a gel extraction kit (QIAquick, Qiagen), then ligation, transformation, plating, and fragment analysis proceeded as previously noted.

Table 3.2: Primers used for *PsAFB2* RLM-RACE. 5'RACE Adapter is an RNA molecule, and thus contains uracil. All other primers used are DNA oligonucleotides.

Primer	Sequence	Purpose
AFB2-5'RACE outer	5'-AGC TAC AGC AGC AAG TCC ATC AGT	Gene specific primer for *AFB2* 5'RACE (B)
AFB2-5'RACE inner	5'-AAC CTA AGC TCC TCC AAC CCA ACT	Gene specific primer for *AFB2* 5'RACE (A)
AFB2-3'RACE	5'-CAA TGC AGC CAC TGG ATG AAG GTT	Gene specific primer for *AFB2* 3'RACE (G)
5' RACE Adapter	5'-GCU GAU GGC GAU GAA UGA ACA CUG CGU UUG CUG GCU UUG AUG AAA	RNA oligo ligated to 5' end of decapped transcripts
3' RACE Adapter	5'- GCG AGC ACA GAA TTA ATA CGA CTC ACT ATA GGT12 VN	Primer for 1st strand synthesis
5' RACE Outer	5'-GCT GAT GGC GAT GAA TGA ACA CTG	5' RACE PCR (not gene specific; C)
5' RACE Inner	5'-CGC GGA TCC GAA CAC TGC GTT TGC TGG CTT TGA TG	As above (D)
3' RACE Outer	5'-GCG AGC ACA GAA TTA ATA CGA CT	3' RACE PCR (not gene specific; E)
3' RACE Inner	5'-CGC GGA TCC GAA TTA ATA CGA CTC ACT ATA GG	As above (F)

3.2.5 Random Amplification of cDNA Ends of *PsAFB6A*

A template-switching method was used to construct cDNA for PCR amplification of the ends of *PsAFB6A*. The 3' RACE cDNA pools were generated with a primer consisting of poly-T and a unique sequence (Figure 3.5, across from primer B), which was later used along with a gene specific primer (Figure 3.5, primer E) to amplify the unknown 3' end. The first strand synthesis of the 5' RACE cDNA pool was generated from poly-T using a reverse transcriptase which adds several non-template cytosine bases to the end of the strand. Second strand synthesis was then carried out from a primer consisting of a unique sequence (Figure 3.5, across from primer B) ending in three G bases, which allow it to pair with the first-strand cDNA. This unique sequence was later used with another gene specific primer (Figure 3.5, primer D) to amplify the unknown 5' end. Primer sequences are listed in Table 3.3.

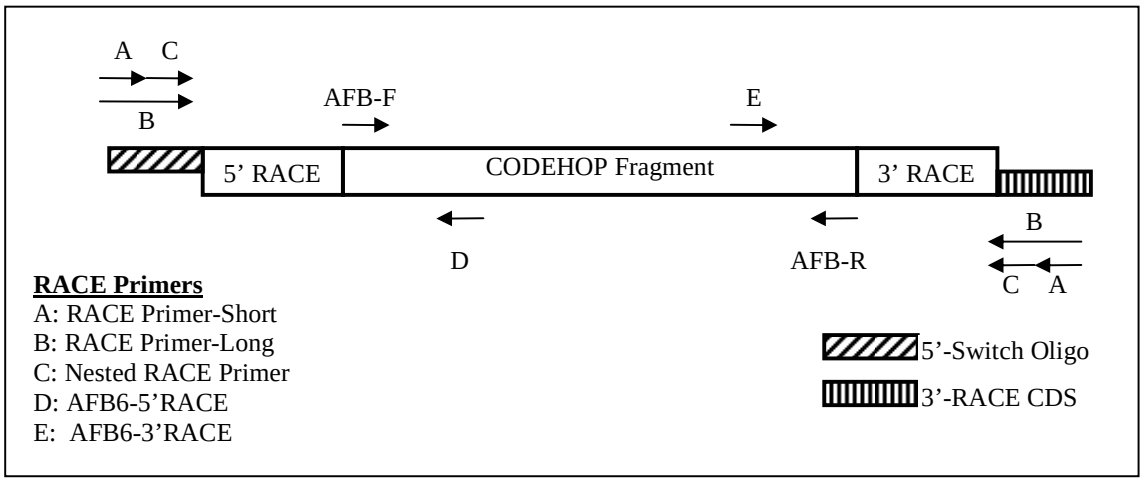

Figure 3.5: Schematic of cloning strategy used to obtain *PsAFB6A*. While displayed as one molecule, the schematic represents both the 5' (5'-Switch Oligo to undetermined points within the CODEHOP fragment) and 3' (3'-RACE CDS, complementary DNA sequence, to undetermined points within the CODEHOP fragment) cDNA pools, which are used separately for amplification of each end.

Between 250 and 1200 ng of total RNA isolated from 14 DAA whole seed, 2 DAA ovaries, 2 DAA pericarps, or 10 DAA funiculi, in a total volume of 4 µL were used for both 5' and 3' RACE. For 5' RACE, 12 pmol each of the 5'-RACE CDS and 5'Switch Oligo (for second strand priming) were added to the RNA. For 3' RACE, 12 pmol of the 3'-RACE CDS and water (to a final volume of 6 µL) were added to the reaction. The reactions were incubated at 72°C for 2 minutes to eliminate secondary structures, then were transferred to ice for the remainder of reaction assembly. Nucleotides (final concentration 1 mM each), 200 U reverse transcriptase (H- MMLC reverse transcriptase, Fermentas), and the supplied reaction buffer (final concentration 1x) were added, and the reaction was carried out at 42°C for 90 minutes. Reactions were diluted with 100 µL water, and stopped by incubation for 10 minutes at 72°C.

The 5' region of *PsAFB6A* was amplified from 300 ng of 5'RACE cDNA using touchdown PCR as follows. Template was mixed with nucleotides (final concentration 0.5 mM each), 50 pmol of AFB6-5'RACE gene specific primer (Figure 3.5D), 37.5 pmol of RACE Primer-Short, 7.5 pmol of RACE Primer-Long, $MgCl_2$ (final concentration 2.75 mM), 0.4 µL Taq polymerase (Invitrogen), and water in a final volume of 20 µL. The thermocycling conditions consisted of an initial denaturation at 94°C for 3 minutes, touchdown PCR for 10 cycles (denaturation at 94°C for 30 seconds, primer annealing for 30 seconds at 61°C minus 0.5°C per cycle, and extension at 72°C for 2 minutes), followed by normal PCR for 20 cycles (denaturation at 94°C for 30 seconds, primer annealing for 30 seconds at 55°C, and extension at 72°C for 2 minutes), followed by a final elongation at 72°C for 5 minutes.

The 3’ region of *PsAFB6A* was amplified from 300 ng of 3’ RACE cDNA using touchdown PCR as follows. Template was mixed with nucleotides (final concentration 0.5 mM each), 30 pmol of AFB6-3’RACE gene specific primer (Figure 3.5E), 30 pmol of RACE Primer-Short, 6 pmol of RACE Primer-Long, $MgCl_2$ (final concentration 2.25 mM), 0.3 µL Taq polymerase (Invitrogen), and water in a final volume of 20 µL. The thermocycling consisted of an initial denaturation of 3 minutes at 94°C followed by 30 cycles of denaturation at 94°C for 30 seconds, primer annealing at 70°C for 30 seconds (minus 0.5°C per cycle), and extension at 72°C for 2 minutes, and a final elongation at 72°C for 5 minutes.

Both 5’ and 3’ RACE PCR reaction products were analyzed by agarose gel electrophoresis, and bands of the appropriate size were excised. DNA was extracted using a gel extraction kit (QIAquick, Qiagen), then ligation, transformation, plating, and fragment analysis proceeded as previously noted.

Table 3.3: Primers used for *PsAFB6A* RACE.

Primer	Sequence	Purpose
5'-RACE CDS	5'-TTT TTT TTT TTT TTT TTT TTT TTT TVN	First strand cDNA synthesis from poly-A tail
5'-Switch Oligo	5'-AAG CAG TCG TAT GAA CGC AGA GTA CGC GGG	Second strand cDNA synthesis from non-template C's
3'-RACE CDS	5'-AAG CAG TCG TAT GAA CGC AGA GTA CTT TTT TTT TTT TTT TTT TTT TTT TTT TVN	First strand cDNA synthesis from poly-A tail
RACE Primer-Short	5'-CTA ATA GCA CTC ACT ATA GGG C	Amplification from 5' or 3' RACE cDNA (not gene specific; A)
RACE Primer-Long	5'-CTA ATA GCA CTC ACT ATA GGG CAA GCA GTC GTA TGA ACG CAG AGT	Same as above, but allows second round of PCR from nested primer to amplify weak signal (B)
Nested RACE Primer	5'-AAG CAG TCG TAT GAA CGC AGA GT	Second round of PCR for weak 5' or 3' RACE products (C)
AFB6-5'RACE	5'-GCT TTC TGG GAA GCA ACT CAA CCA	Gene specific primer for AFB6 5'RACE (D)
AFB6-3'RACE	5'-AGG ATG CCG GAA GCT TCA CTA TGT	Gene specific primer for AFB6 3'RACE (E)

3.2.6 Amplification of full-length cDNA

Full length *PsAFB2* was amplified as follows from poly-A cDNA prepared from 2 DAA pericarps and 14 DAA seeds with the previously described methods. cDNA template (300 ng) was mixed with nucleotides (final concentration 0.5 mM each), 50 pmol of the PsAFB2 FWD primer, 50 pmol of the PsAFB2 REV primer (Table 3.4), $MgCl_2$ (final concentration 2.25 mM), 3.1 u Taq polymerase (Invitrogen), and the

supplied buffer in a final volume of 20 µL. The thermocycling consisted of an initial denaturation of 5 minutes at 94°C followed by 30 cycles of denaturation at 94°C for 30 seconds, primer annealing at 50°C for 30 seconds, and extension at 72°C for 90 seconds, followed by a final elongation at 72°C for 7 minutes. Products were analysed with agarose gel electrophoresis, then were cloned into the PCR8 gateway vector as previously described. Clones were analyzed as previously described, and clones containing the complete *PsAFB2* gene were sequenced across completely in several overlapping fragments from both direction using the T3, T7, PsAFB2 FWD, PsAFB2 REV (Table 3.4), and two internal primers generated to region of *PsAFB2* isolated via the CODEHOP procedure using the sequencing protocols previously noted. All attempts to amplify and clone the full-length *PsAFB6A* gene were unsuccessful.

Table 3.4: Primers used to amplify full-length coding region of *PsAFB2*.

Primer	Sequence	Purpose
PsAFB2 FWD	5'-ATG AAT TAT TTT CCA GAC GAG GTA ATA GAA CA	Amplification of full length coding region
PsAFB2 REV	5'-CTA CAG AGT CCA TAC ATA GTC TGG TG	Amplification of full length coding region

3.2.7 qRT-PCR

All transcript quantification was performed on a StepOnePlus sequence detector (Applied Biosystems) using the reaction conditions described in Chapter 2. Probes were labelled with the same fluorophores and 18s rRNA controls were performed and analyzed as previously detailed in Chapter 2. Primers and probes for *PsAFB2* and *PsAFB6A* were designed with the Primer Express software package (Applied Biosystems). In addition to

the amplicon used for quantification, a larger amplicon for each gene was generated with the same probe, but different primers (listed in Table 3.5) which bind to regions outside of the quantification amplicon. A series of samples was assayed with both the inner and outer primers in tandem, and both primer sets yielded the same trends in relative transcript abundance, increasing confidence that the correct RNA was amplified. Additionally, reactions with both the quantification and outer validation sets of primers produced single bands of the appropriate sizes when qRT-PCR reaction products were separated on a 2.5% agarose gel. Results of database searches with the target amplicons are presented in appendix 5.5. Relative transcript levels were calculated using the ΔCt method with the formula described in Chapter 2. Reaction efficiency was calculated for each amplicon after validation experiments using the formula detailed in Chapter 2.

Table 3.5: Primer and probe sequences used in qRT-PCR assays. Probes for *PsAFB6A* and *PsAFB2* were labelled at the 5' end with FAM (6-carboxyfluorescein) and at the 3`end with the MGB quencher (Applied Biosystems). Probe for 18s rRNA was labelled at the 5`end with VIC and at the 3` end with the TAMRA quencher (Applied Biosystems).

Gene		Sequence	Amplicon length
PsAFB2	Forward	5'-TCG ATG CAA CAA AAC CTG ACT	80 bp
	Reverse	5'-TCG TTT GCA TGA CTG TAC GAT	
	Probe	5'-TGC AGC CAC TGG AT	
PsAFB6A	Forward	5'-TGT CGC TAC CGT AGT CCA AA	52 bp
	Reverse	5'-TGC AGA GGC GGA AAT GA	
	Probe	5'-CTG CCC CGA CTT TA	
PsAFB2	Forward	5'-CAG TAG CCA AGA ACT GTC CA	159 bp
(validation)	Reverse	5'-TCA ACT GAC CGG AGA GTG AT	
	Probe	5'-TGC AGC CAC TGG AT	
PsAFB6A	Forward	5'-GTC GTC AAA TGA CCA ATG CTG	114 bp
(validation)	Reverse	5'-GTT CGT CCG TCA GGT AAT CTT G	
	Probe	5'-CTG CCC CGA CTT TA	
18s rRNA	Forward	5'-ACG TCC CTG CCC TTT GTA CA	62 bp
	Reverse	5'-CAC TTC ACC GGA CCA TTC AAT	
	Probe	5'-ACC GCC CGT CGC TCC TAC CG	

3.2.8 Hormone Extraction, HPLC, and GC-MS

All metabolite extraction and quantification was performed by Dr. Leon Kurepin at the department of Biological Sciences of the University of Calgary. Plant tissues were dissected and processed using the methods mentioned in Chapter 2. Metabolite extraction used the same process as described previously, but internal standards of 400 ng

[$^{13}C_6$] IAA (available from Cambridge Isotope Laboratories, Inc.) and 50-300 ng of [$^{2}H_4$] 4-Cl-IAA (gift from Dr. J. Cohen) were added to the MeOH extract prior to filtering.

The HPLC apparatus, solvents, and program are identical to those previously described for the isolation of GAs and ABA in Chapter 2. Fractions from C_{18} HPLC were collected at 9.53 min for IAA and 11.11 min for 4-Cl-IAA. These fractions were subsequently methylated by ethereal CH_2N_2 and derivatized to their trimethylsilyl ethers for GC-MS as described in Chapter 2.

Endogenous auxins were identified by GC-MS-SIM via comparisons of GC-retention times of auxins and internal standards and by the relative intensities of molecular ion (M^+) pairs. Relative intensities of at least one other characteristic m/z ion pair for each auxin and its standard (IAA/[$^{13}C_6$]-IAA, 202/208 and 261/267; 4-Cl-IAA/[$^{2}H_4$] 4-Cl-IAA, 236/240 and 295/299) were also compared. Quantification was accomplished using the peak areas of the 202/208 ions for IAA/[$^{13}C_6$]-IAA, and the peak areas of the 236/240 ions for 4-Cl-IAA/[$^{2}H_4$] 4-Cl-IAA in the equations for isotope dilution analysis from Gaskin and MacMillan (1991) as adapted by DW Pearce (Jacobsen *et al.*, 2002).

3.3 Results

3.3.1 Sequences of Auxin Receptor Genes

The interior regions of two *Pisum* AFB homologues were obtained via PCR amplification with the degenerate CODEHOP primers. Several successive experiments produced 13 clones of one gene with high sequence similarity to members of the AFB2/3

group of receptors, and one clone belonging to the AFB6 group of receptors. While the AFB2/3 clade is fairly ubiquitous amongst investigated plants, with many species possessing two or more members, AFB6 is restricted to fewer species, including the legumes *Pisum sativum* and *Medicago truncatula* (BAC sequence mth2-32m30, Cannon *et al*., 2006).

The 5' region of *PsAFB2* not amplified by the CODEHOP primers, consisting of putative coding sequence and part of the 5' UTR, was amplified in three independent clones. The 3' region of *PsAFB2* not amplified by the CODEHOP primers, consisting of part of the putative coding region and 3' UTR, was also amplified in three independent clones. All 3' and 5' RACE products overlapped with the interior fragment isolated with the CODEHOP primers, and represented one unique 5' and one unique 3' sequence. The coding region of the entire *PsAFB2* gene was amplified and cloned into the PCR8 vector for later transfer to expression systems, and 3 clones were sequenced end-to-end to confirm the sequence. The putative coding region of this cDNA is 1716 nucleotides long (Figure 3.6), and codes for a protein with an expected length of 571 amino acids (Figure 5.2).

***PsAFB2* cDNA Sequence**

```
  1- ATGAATTATT TTCCAGACGA GGTAATAGAA CATGTGTTTG ACTATGTGGT GTCACATAGC
                ------------------------------F-BOX-------------------

 61- GACAGAAACA GTTTGTCTTT GGTATGCAAA AGTTGGTATA GAATAGAGGG ATTTACAAGG
     ---------------------F-BOX---------------------------------------

121- AAAAGGGTGT TCATAGGAAA CTGTTACTCT ATTAGTCCTG AGAGGTTGGT AGAGAGGTTT
     ------F-BOX-----

181- CCTGATTTCA AATCTTTAAC TCTAAAGGGA AAACCTCATT TTGCTGACTT CAGTTTGGTT

241- CCTCATGGTT GGGGTGGTTT TGTTTATCCA TGGATTGAAG CTCTTGCTAA GAGTAGAGTT
                                                                --LRR-
```

***PsAFB2* cDNA Sequence**

```
 301- GGGTTGGAGG AGCTTAGGTT GAAGAGGATG GTTGTGTCAG ATGAGAGCCT GGAGCTACTG
      ---------------------------------LRR------------------------------

 361- TCTCGTTCTT TCATGAATTT TAAGTCTTTA GTTCTTGTTA GCTGTGAAGG GTTCACCACT
      ---------------------------------LRR------------------------------

 421- GATGGACTTG CTGCTGTAGC TGCAAATTGC AGGTCTCTTA GGGAGCTAGA TTTGCAAGAG
      --------LRR------------------

 481- AATGAAGTTG AAGATCACAA AGGACAGTGG CTAAGTTGTT TTCCGGAAAA CTGTACATCA

 541- CTCGTCGCTC TTAATTTTGC TTGCCTTAAA GGAGAGATTA ACGTGGGAGC ACTTGAGAGA

 601- CTTGTGGCAA GATCGCCTAA CCTCAAGACT CTAAGGTTAA ACCGTTCCGT GCCGGCTGAT

 661- GCACTTCAAA GGATACTAAT GCGAGCGCCT CAAATAGCAG ATTTGGGTAT TGGATCATTT

 721- ATCCATGATC TCAATTCAGA GGCCTACATA AAGCTTAAGA ATACCATTCT TAGATGCCGG

 781- TCAATAACGA GTTTGTCCGG ATTTTTGGAA GTGGCTCCTT TTAGCCTTGC TGCTGTGTAT

 841- CCAATTTGCC GGAACTTAAC ATCCTTGAAC TTGAGCTATG CAGCAAGCAT TCAGGGCGCT
            -------------------------LRR------------------------------

 901- GAGCTTATTA AACTTATTCG CCATTGCGGC AAACTACAGC GCTTATGGAT AATGGATTGC
      ---------------------------------LRR------------------------------

 961- ATTGGAGACA AAGGACTAGT TGCTGTAGCT ACTATATGTA AAGAGTTGCA AGAATTGAGG
      ---------------------------------LRR------------------------------

1021- GTATTTCCAT CGGCACCATT TGGAAATCAA GCAGCTGTTA CCGAAGTAGG ACTTGTTGCG
      ---------------------------------LRR------------------------------

1081- ATATCAAAGG GATGCCCAAA GCTCCACTCG TTACTCTACT TCTGCCACCA GATGACAAAT
      ---------------------------------LRR------------------------------

1141- GCTGCTCTCA TAACAGTAGC CAAGAACTGT CCAAATTTTA TCCGATTTAG GTTATGCATC
      ------------LRR--------------
                   ----FWD Validation--->

1201- CTCGATGCAA CAAAACCTGA CTCCGACACA ATGCAGCCAC TGGATGAAGG TTTTGGGGCA
       ------FWD Primer------>          -----Probe-----

1261- ATCGTACAGT CATGCAAACG ACTGAGGCGG CTATCACTCT CCGGTCAGTT GACCGACCAG
                   ------------------LRR------------------------------
      <------REV Primer------            <----REV Validation---

1321- GTCTTCCTTT ACATTGGAAT GTACGCGGAG CAGCTTGAAA TGCTATCTAT TGCTTTTGCT
      ----------LRR-------------

1381- GGCGAGAGTG ACAAGGGAAT GCTCTATGTA TTGAATGGTT GCAAAAAGCT TCGCAAGCTC
                                                 -----------LRR---------

1441- GAGATAAGAG ACTGCCCTTT CGGCGACACA GCACTTCTGA CAGACGTAGG GAAGTATGAA
      ---------------------------------LRR----------------------------
```

***PsAFB2* cDNA Sequence**

```
1501- ACAATGCGAT CCCTTTGGAT GTCGTCGTGT GAGGTGACTG TAGGAGCATG CAAGACATTG
1561- GCGAAGAAGA TGCCGAGTTT GAATGTGGAG ATCTTCAATG AAAGTGAACA AGCAGATTGT
1621- TATGTGGAAG ATGGGCAAAG AGTGGAGAAG ATGTATTTGT ATCGTTCTGT GGCTGGTAAA
1681- AGGGAAGATG CACCAGACTA TGTATGGACT CTGTAG
```

Figure 3.6: cDNA sequence of the putative coding region of *PsAFB2* (sense strand). Regions corresponding to putative F-box and LRR domains in the predicted protein are identified underneath the sequence (Table 5.6; Figure 5.2), and qRT-PCR primer and probe binding sites (Table 3.5) are additionally underlined.

The 5' region of *PsAFB6A* not amplified by the CODEHOP primers, consisting of putative coding sequence and part of the 5' UTR, was amplified in two independent clones. While both of these clones contained the same fragment of the coding region, one possessed an additional ~20 bp within the 5' UTR. The 3' region of *PsAFB6A* not amplified by the CODEHOP primers, consisting of part of the putative coding region and 3' UTR, was obtained in two independent clones. While both of the 3' RACE clones consisted of the same coding region and 3' UTR, one was slightly longer and contained part of the poly-A tail. All 3' and 5' RACE products overlapped with the interior fragment isolated with the CODEHOP primers. The putative coding region of this cDNA is 1725 nucleotides long (Figure 3.7), and encodes a putative protein of 574 amino acids length (Figure 5.3). All attempts to amplify and clone the entire *PsAFB6A* coding region were unsuccessful.

***PsAFB6A* cDNA Sequence**

```
   1- ATGGAACCAC AAACCATGAA TCCCAGTTCA GTCTTTCCAG ATGAAGTGCT GGAGAGAATT
                          ------------------F-BOX---------------------

  61- CTCAGCATGG TGAAGTCACG CAAAGACAAG AGTTCGGTTT CATTGGTTTG CAAAGACTGG

 121- TTCGACGCTG AAAGATGGTC GAGAAAGAAT GTGTTCATAG GTAACTGTTA TTCCGTTACA

 181- CCAGAGATCT TGACTCAAAG ATTTCCGAAT GTTCGAAGTG TTACATTGAA AGGGAAGCCA

 241- CGTTTCTCTG ATTTCAACTT GGTTCCTGCT AATTGGGGTG CTGATATTCA TCCATGGCTT

 301- GTTGTTTTCG CTGAAAAGTA CCCTTTTCTT GAAGAGTTAA GGCTTAAGAG AATGGTTGTT
                          --------------------LRR----------------------

 361- ACTGATGAGA GTTTAGAGTT TCTGGCTTTT TCGTTTCCGA ATTTTAAAGC TCTTTCTCTT
      -------------------------------LRR--------------------------------

 421- TTGAGCTGTG ATGGATTTAG CACTGATGGT TTAGCTGCTG TTGCTACTAA TTGCAAGAAC
      ------------------LRR-----------------------------------

 481- TTAACTGAGC TTGACATACA AGAGAATGGT ATCGAAGACA AAAGCGGTAA CTGGTTGAGT

 541- TGCTTCCCAG AAAGCTTTAC ATCATTGGAA GTGTTGAACT TTGCCAACCT AACCAATGAA

 601- GTAAACATCG ACGCGCTAGA GAAACTTGTT GGTAGGTGCA AATCATTGAA GACTTTGAAG

 661- GTTAACAAAA GCGTAACGCT GGAACAGTTG AAAAAACTTC TTGTTCGCGC CCCTCAGTTA

 721- TGTGAGCTTG GCAGTGGCTC ATTTTCGCAA GAGCTGACAT CTCAGCAGTA TGCAGAGCTC

 781- GAAACCGCGT TCAAAAATTG TAAAAGCCTT CACACCCTGT CTGGTTTATG GGTGGCTTCA

 841- GCGCGATATC TTCAAGTTCT ATACCCTGCG TGCGCGAATC TGACTTTTTT GAATTTTAGC

 901- TATGCTCCTC TTGACAGTGA AGATCTTACC AAGATTCTTG TTCACTGTCC TAATCTTCGA
                                                      ------LRR-------

 961- CGTCTTTGGG TTGTTGACAC CGTTGAAGAC AAGGGACTTG AAGCGGTTGG ATCGAACTGT
      -------------------------------LRR----------------------------

1021- CCATTGCTTG AGGAACTGCG TGTTTTTCCT GCAGATCCGT TTGACGAGGA AGCTGAAGGC

1081- GGGGTGACTG AATCGGGGTT TGTTGCTGTC TCTGAAGGAT GCCGGAAGCT TCACTATGTT
                                              --------------LRR------

1141- CTCTACTTTT GTCGTCAAAT GACCAATGCT GCTGTCGCTA CCGTAGTCCA AAACTGCCCC
      -------------------------------LRR-----------------------
                 ----FWD Validation----> ------FWD Primer-----> --Probe

1201- GACTTTACTC ATTTCCGCCT CTGCATAATG AACCCTGGCC AGCAAGATTA CCTGACGGAC
      Probe-- <---REV Primer-----                   <----REV Validation

1261- GAACCTATGG ACGAGGCCTT CGGAGAAGTT GTTAAGAACT GCACTAAACT TCAGAGGCTC
      ----                                      --------------LRR------
```

***PsAFB6A* cDNA Sequence**

```
1321- GCTGTATCAG GTTATCTAAC GGACCTCACA TTCGAGTATA TAGGAAAGTA TGCCAAAAAC
      --------------------------------LRR----------------------

1381- TTGGAAACGC TTTCGGTGGC TTTTGCAGGA AGCAGTGATT GGGGAATGGA GTGTGTACTG

1441- GTCGGATGTC CGAAACTGAG AAAACTCGAG ATAAGAGACA GTCCATTCGG AAATGCAGCG
            ------------------------------------LRR-----------------

1501- CTTTTGGCAG GTTTGGAGAA GTACGAGTCG ATGAGGTCAC TTTGGATGTC GTCCTGCAGA
      -------------LRR-------

1561- CTGATGATGA ATGGATGTAG ATTTTTGGCA GGAGAAAAGC CGAGGTTGAA TGTCGAAGTA

1621- ATGCAGGAAG AAGGAGGCGA TGATAGTCGG GCCGAAAAAC TTTATGTTTA TCGATCTGTT

1681- GCCGGGCCAA GAAGGGATGC ACCTCCTTTT GTTCTCACTC TCTGA
```

Figure 3.7: cDNA sequence of the putative coding region of *PsAFB6A* (sense strand). Regions corresponding to putative F-box and LRR domains in the predicted protein are identified underneath the sequence (Table 5.6; Figure 5.3), and qRT-PCR primer and probe binding sites (Table 3.5) are additionally underlined.

In silico translation of *PsAFB2* and *PsAFB6A* and alignment with the 58 protein sequences used to generate the CODEHOP primers was used to name the two cDNAs according to standard *Pisum sativum* nomenclature, and an unrooted tree generated with ClustalW2 is displayed below (Figure 3.8). Domain prediction was performed with the SMART (Simple Modular Architecture Research Tool) program (Schultz *et al.*, 1998, Letunic *et al.*, 2005), and identified C-terminal F-boxes and multiple LRRs (Table 5.6). There were no major differences in the position or length of these putative domains between the putative AFB gene products isolated here and their corresponding homologues (see Figures 5.2 and 5.3 for alignments of putative proteins).

Figure 3.8: Phylogram of putative and experimentally verified AFB proteins. Known homologues in pea are indicated with arrows. Distances computed with BLOSUM matrix and NJ clustering in ClustalW2. Tree designed in PhyloDraw. Presentation style was chosen for ease of reading, no root is implied.

3.3.2 Transcription Profiling of Auxin Receptor Genes

Reaction efficiency for the AFB amplicons was determined for use in the calculation of relative transcript abundance. The efficiency of the *PsAFB6A* amplicon was somewhat higher than that of the *PsAFB2* amplicon (Table 3.6), and in both cases the calculated regressions had r^2 values greater than 0.990.

Table 3.6: Reaction efficiency of *PsAFB2* and *PsAFB6A* qRT-PCR Assays

Amplicon	Efficiency	r^2
PsAFB2	93.6%	0.999
PsAFB6A	99.1	0.994

Early in development, whole seed *PsAFB2* mRNA abundance was highest immediately post-fertilization (Figure 3.9). Whole seed *PsAFB2* mRNA levels decreased substantially between 2 and 6 DAA, and remained low through 12 DAA (Figure 3.9). Pericarp *PsAFB2* transcript abundance was higher from -2 to 1 DAA, then decreased by 5 DAA and remained at this lower level until 20 DAA (Figures 3.9 and 3.10E). In pericarps from non-pollinated ovaries (flowers emasculated at -2 DAA), *PsAFB2* transcript abundance was elevated from -1 DAA to 3 DAA in comparison to pericarps from pollinated ovaries, (Figure 3.9).

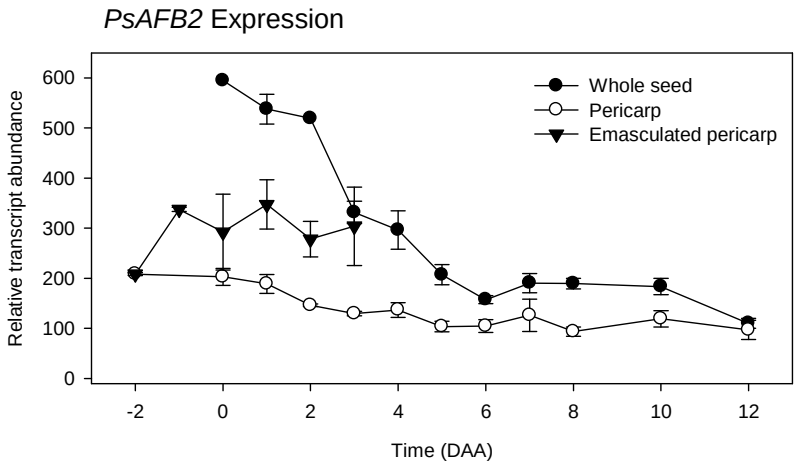

Figure 3.9: Steady-state transcript abundance of *PsAFB2* during early fruit development in whole pericarps, seeds, and pericarps from flowers emasculated at -2 DAA. Data are expressed as mean ± standard error. Where standard error is too small, error bars may be obscured by symbols. Samples are representative of between 2 and 3 independent replicates, except for 0 DAA whole seed (n=1) and 6 DAA pericarp (n=4).

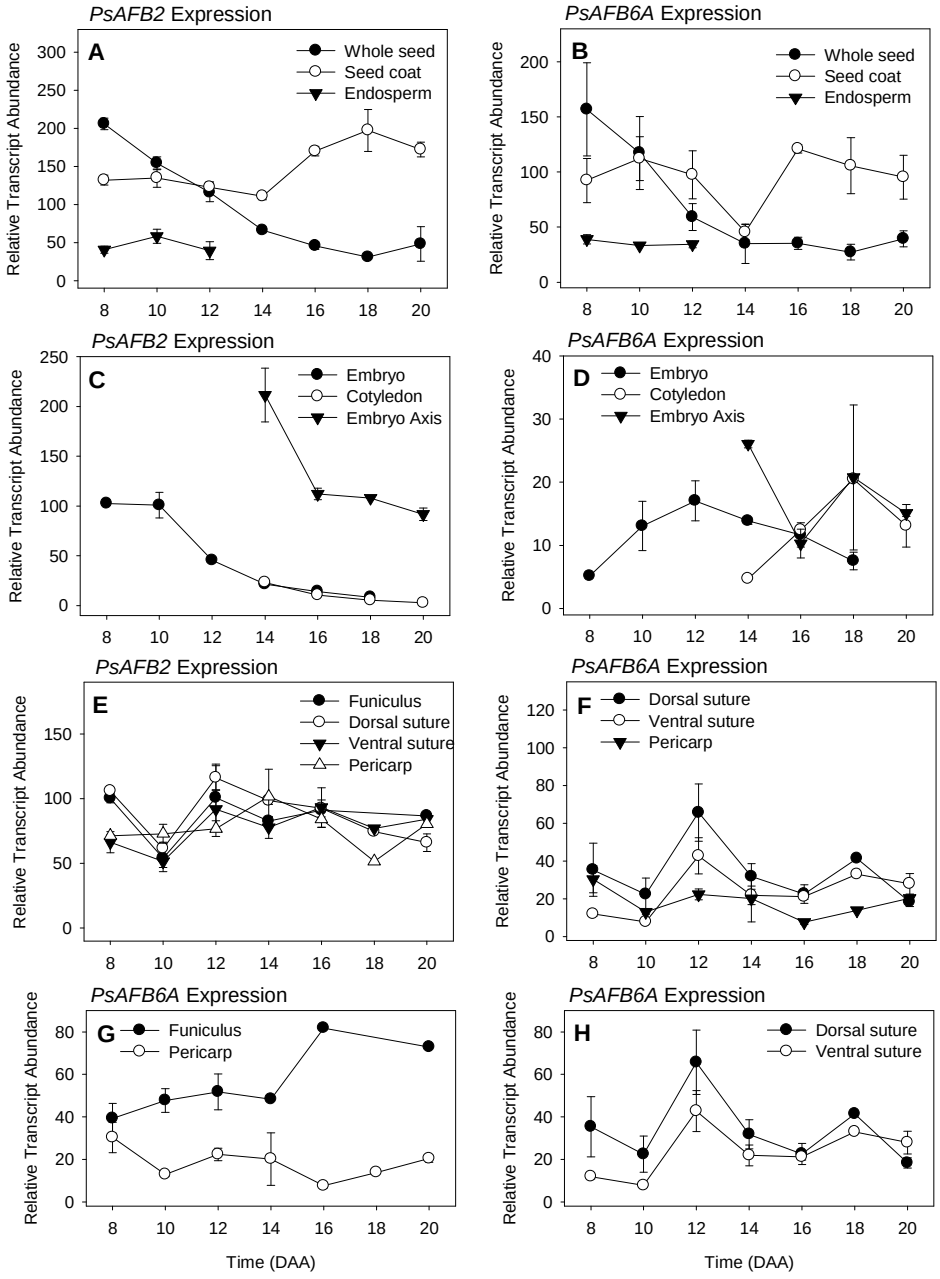

Figure 3.10: Transcript abundance of the putative auxin receptor genes *PsAFB2* and *PsAFB6A* in seed and fruit tissues during development. Data are expressed as mean ± standard error. Where standard error is too small, error bars may be obscured by symbols. Samples are representative of between 2 and 5 independent samples, except for all vascular suture tissues at 18 DAA, pericarp at 8 DAA, and embryo at 8 DAA, for which n=1, and whole seed at 16 DAA, for which n=6. All samples are normalized to the same scale, allowing comparison between all tissues of the same gene.

Trends in transcript abundance of *PsAFB6A* were similar to those of *PsAFB2* in seeds and pericarps from -2 to 12 DAA. Whole seed *PsAFB6A* transcript abundance was higher immediately after fertilization (Figure 3.11) then decreased until 20 DAA (Figures 3.11 and 3.10B). Pericarp *PsAFB6A* transcript levels were elevated prior to pollination (-2 DAA), then decreased 4.1-fold by 1 DAA, after pollination and fertilization of the ovary (Figure 3.11). From 2 to 20 DAA, pericarp *PsAFB6A* transcript levels were relatively constant (Figures 3.11 and 3.10F). *PsAFB6A* mRNA abundance was slightly elevated in emasculated pericarps within 24 hours of emasculation (Figure 3.11), as was the case with *PsAFB2*. However, whereas *PsAFB2* mRNA levels remained constant after this initial increase, *PsAFB6A* abundance markedly increased between 1 and 3 DAA in emasculated pericarps (Figure 3.11), indicating that pericarp transcript levels of these two genes are regulated differentially.

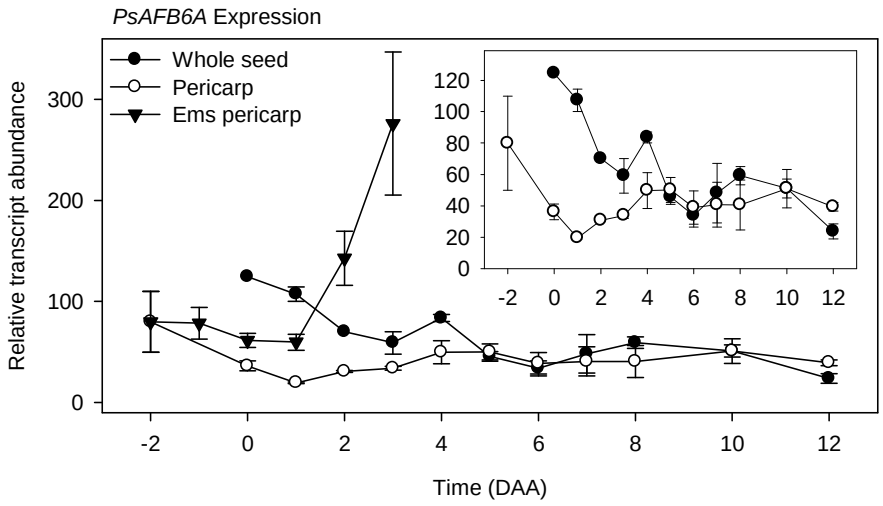

Figure 3.11: Steady-state transcript abundance of *PsAFB6A* during early fruit development in whole pericarp, seeds, and pericarp from flowers emasculated at -2 DAA (Ems peri). Data are expressed as mean ± standard error. Where standard error is too small, error bars may be obscured by symbols. Samples are representative of between 2 and 3 independent replicates, except for 0 DAA whole seed (n=1) and 6 DAA pericarp (n=4).

Steady-state transcript abundance of both *PsAFB* genes was maintained at relatively low levels in the endosperm from 8 to 12 DAA (Figure 3.10A,B). In whole seeds both *PsAFB2* (Figure 3.9) and *PsAFB6A* (Figure 3.11) transcript levels were higher earlier in development and decreased over time, however mRNA levels of these two genes varied in a tissue-specific manner over development from 8 to 20 DAA.

In early development (8 DAA), *PsAFB2* mRNA was present at approximately equal levels in the seed coat and embryo (Figure 3.10A,C). While embryo *PsAFB2* transcript abundance decreased from 10 DAA onwards (Figure 3.10C), seed coat *PsAFB2* mRNA levels were maintained during this period, and slightly increased between 14 and 16 DAA (Figure 3.10A). Within the embryo, *PsAFB2* mRNA localized primarily to the embryo axis from 14 to 20 DAA, as steady-state abundance was significantly higher in this tissue than in cotyledon or whole embryo samples (Figure 3.10C). Steady-state transcript abundance of *PsAFB2* was similar in the tissues of the pericarp (dorsal and ventral vascular trace sutures and pericarp wall tissue), and pericarp *PsAFB2* transcript abundance remained relatively constant from 8 to 20 DAA (Figure 3.10E). *PsAFB2* transcript abundance in the funiculus was also similar to that of the pericarp tissues (Figure 3.10E).

While *PsAFB2* mRNA levels were approximately equal in the early (8 DAA) seed coat and embryo, *PsAFB6A* transcript abundance was 17.9-fold greater in the seed coat than in the embryo at this time (Figure 3.10B,D). *PsAFB6A* mRNA was maintained at relatively constant levels in the seed coat between 8 and 20 DAA (Figure 3.10B). Steady-state *PsAFB6A* mRNA abundance was low in the embryo at 8 DAA, then increased between 8 and 12 DAA before decreasing between 12 and 18 DAA (Figure

3.10D). While *PsAFB6A* transcript abundance was 5.5-fold higher in the embryo axis than in the cotyledons at 14 DAA, by 16 DAA mRNA levels in these tissues were equivalent and remained so until 20 DAA (Figure 3.10D).

In contrast to *PsAFB2* transcript levels, *PsAFB6A* steady-state mRNA abundance varied in a tissue-specific manner between 8 and 20 DAA within the pericarp and funiculus tissues. *PsAFB6A* transcript levels were generally higher in the funiculus than in any of the pericarp (Figure 3.10F,G) or seed (Figure 3.10D,G) tissues. Additionally, funiculus *PsAFB6A* mRNA levels increased as the fruit matured (Figure 3.10G). While *PsAFB2* mRNA was present at approximately equal levels in the three pericarp tissues (Figure 3.10E), *PsAFB6A* transcript abundance was higher in the two vascular sutures than in the pericarp wall (Figure 3.10F). Furthermore, *PsAFB6A* transcript abundance was generally higher in the dorsal than in the ventral vascular suture of the pericarp (seeds are attached to the pericarp via the funiculus at the ventral suture; Figure 3.10H).

3.3.3 Hormonal Regulation of Auxin Receptor Genes

PsAFB2 transcript abundance was approximately equal in pericarps with (SP) or without seeds (SPNS; Figure 3.12A). Treatment of deseeded pericarps with 4-Cl-IAA, IAA, or GA_3 did not significantly affect steady-state *PsAFB2* transcript abundance (Figure 3.12A,C,E) in this tissue. These data suggest that *PsAFB2* mRNA levels are largely unregulated by the presence of seeds, pericarp splitting, or the addition of IAA, 4-Cl-IAA, or GA_3.

PsAFB6A transcript abundance was similar in both split-pericarps with seeds (SP) and intact controls, indicating that the split-pericarp procedure did not influence steady-

state abundance of this gene (Figure 3.12B). Removal of seeds markedly increased *PsAFB6A* transcript abundance in the pericarp at all times assessed (12 to 24 hours after seed removal; Figure 3.12B). Two hours after IAA was applied to deseeded pericarps, pericarp *PsAFB6A* mRNA abundance was similar to that of the SP control (Figure 3.12D). However, 8 hours after IAA application, pericarp *PsAFB6A* transcript abundance increased to that observed in the SPNS pericarps, and remained at this elevated level until 12 hours after hormone treatment (Figure 3.12D). In contrast to the transitory reduction of *PsAFB6A* steady-state mRNA abundance by IAA in deseeded pericarps, 4-Cl-IAA treatment reduced *PsAFB6A* mRNA abundance to levels similar to those found in SP controls throughout the developmental time course (Figure 3.12D). GA_3 was found to have no effect on *PsAFB6A* steady-state transcript abundance in these experiments (Figure 3.12F).

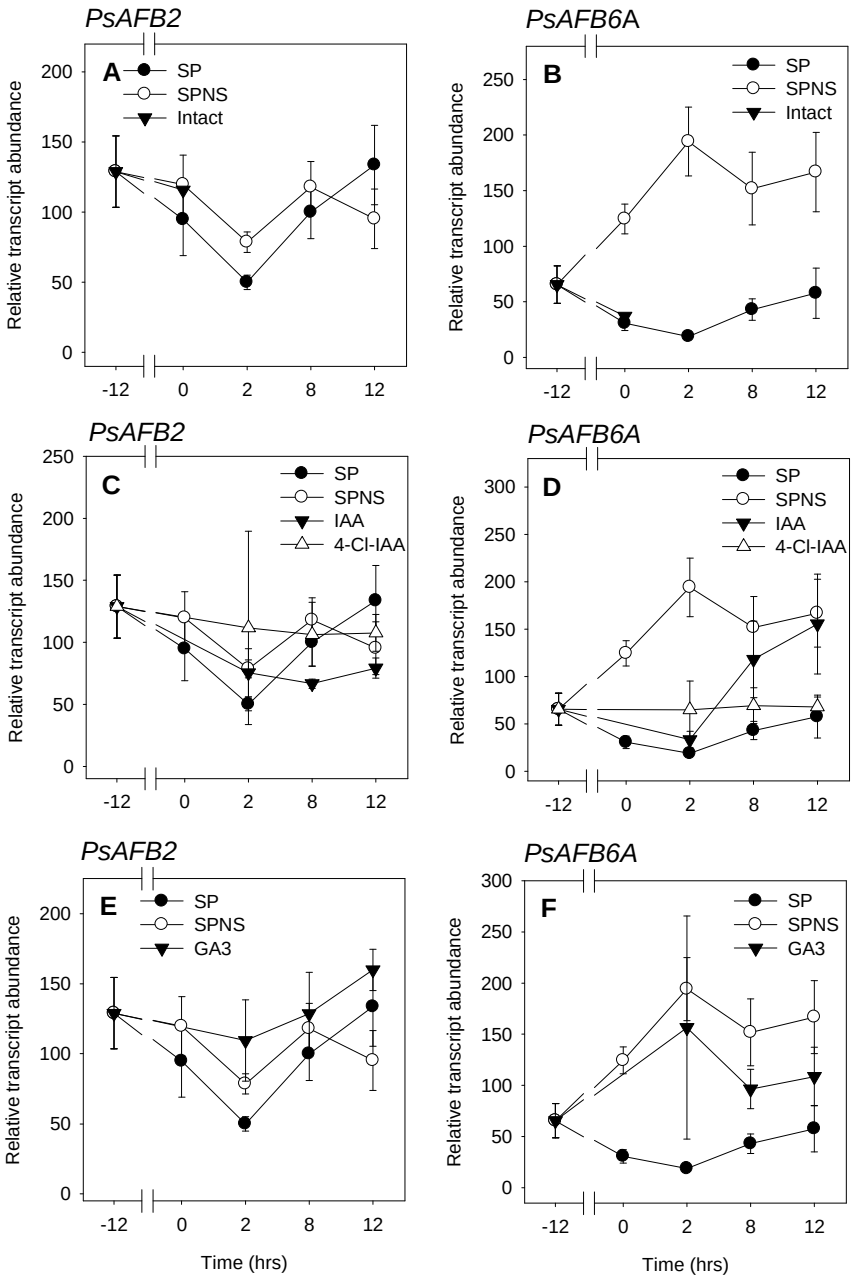

Figure 3.12: Steady-state mRNA abundance of *PsAFB2* (A, C, E) and *PsAFB6A* (B, D, F) genes in pericarps with and without seeds, and deseeded pericarps treated with hormones. Two DAA pericarps were left intact, split (SP), split and deseeded (SPNS), or split and deseeded then treated with 50 μM IAA (C, D), 4-Cl-IAA (C, D) or GA_3 (E, F). Hormones were applied to pericarps 12 hours after deseeding and the effects of hormone application on transcript abundance were monitored 2, 8 and 12 h after application (14, 20, and 24 h after deseeding). Data are presented as mean ± standard error, n=2 to 4 at each point.

3.3.4 Auxins in Seed Tissues

Embryo IAA levels were initially high at 10 DAA, and then decreased with a small peak in levels observed at 16 DAA (Table 3.7A). At 18 DAA, levels of IAA were 8.4-fold (based on ng gFw^{-1}) higher in the embryo axis than in the cotyledons (Table 3.7A). Like the embryo, seed coat IAA was also highest at 10 DAA and decreased as the seed developed (Table 3.7A).

The tissue localization and relative concentrations of 4-Cl-IAA were significantly different to those of IAA. Levels of 4-Cl-IAA were significantly higher than that of IAA in both the seed coat and embryonic tissues from 10 to 18 DAA (Table 3.7A). Embryo 4-Cl-IAA levels increased markedly between 12 and 14 DAA, during which time the endosperm is completely absorbed by the embryo as it expands to fill the seed cavity (Table 3.7A). Subsequently, embryo 4-Cl-IAA levels decreased (between 16 and 18 DAA; Table 3.7A). Like IAA, the concentration of 4-Cl-IAA was higher in the embryo axis than that in the cotyledons at 18 DAA (Table 3.7A). 4-Cl-IAA was very abundant in the seed coat at 10 DAA, and decreased as the seed developed (Table 3.7A).

The concentrations of both auxins increased between 10 and 12 DAA in the endosperm, when it reached maximum volume (Table 3.7B). In contrast to the other seed tissues, where 4-Cl-IAA was much more abundant than IAA, levels of IAA and 4-Cl-IAA were comparable in this tissue (Table 3.7B).

Table 3.7: IAA and 4-Cl-IAA content in developing pea seed tissues from 10 to 18 DAA. Results are presented as means of two independent samples ± standard error (n.d.= not detected, although internal standard added at tissue homogenization was recovered), with a few exceptions where n=1.. Results are expressed as ng gFw^{-1} (A) for solid tissues and ng mL^{-1} (B) for liquid endosperm

A	10 DAA	12 DAA	14 DAA	16 DAA	18 DAA
Embryo IAA	86.22	28.55 ± 2.42	19.80 ± 1.83	36.35 ± 8.46	14.56 ± 2.36
Cotyledon IAA	-	-	-	-	8.46 ± 1.06
Embryo Axis IAA	-	-	-	-	71.20
Seed Coat IAA	54.95 ± 10.80	20.05 ± 1.34	8.47 ± 1.15	10.05 ± 1.96	5.71 ± 1.04
Embryo 4-Cl-IAA	141.68	102.55	661.68 ± 261.71	653.97	137.7 ± 49.35
Cotyledon 4-Cl-IAA	-	-	-	-	84.18 ± 6.44
Embryo Axis 4-Cl-IAA	-	-	-	-	265.03
Seed Coat 4-Cl-IAA	840.99	486.27	128.41 ± 21.25	295.22	196.08

B	10 DAA	12 DAA	14 DAA	16 DAA	18 DAA
Endosperm IAA	89.35 ± 19.34	244.04 ± 11.04	-	-	-
Endosperm 4-Cl-IAA	148.67 ± 33.38	238.95	-	-	-

3.4 Discussion

3.4.1 Spatial and Temporal Regulation of AFB Expression in the Seed

In whole seeds, transcript abundance of both *PsAFB2* (Figure 3.9, Figure 3.10A) and *PsAFB6A* (Figure 3.11, Figure 3.10B) was highest immediately following fertilization (0 DAA), and gradually decreased to 20 DAA, a 12.4-fold and 3.2-fold decrease over this developmental period, respectively. These transcript abundance profiles suggest that initial seed development is more sensitive to auxin than later seed developmental stages.

AFB gene expression and steady-state auxin levels in the seed coat

In the seed coat, transcript levels of both *PsAFB2* and *PsAFB6A* did not markedly change from 8 to 20 DAA (Figure 3.10A,B). During this period however, levels of free IAA and 4Cl-IAA in the seed coat changed significantly: seed coat IAA decreased 9.6-fold and seed coat 4-Cl-IAA decreased 4.3-fold between 10 and 18 DAA (Table 3.7A). These data suggest that changes in free auxin levels may be the main mechanism for regulating auxin-related growth and development in the seed coat during this developmental period (10 to 20 DAA).

AFB gene expression in the embryo

In the embryo, *PsAFB2* transcript abundance was higher earlier in development and decreased with embryo maturation (Figure 3.10C). *PsAFB2* transcript levels were also higher in the embryo axis than in the cotyledons from 14 to 20 DAA (Figure

3.10C,D). Experiments using end-point RT-PCR and promoter::GUS fusion constructs have demonstrated that the *AtAFB2* and *AtAFB3* genes are expressed in developing embryos, floral organs, and siliques in *Arabidopsis* (Dharmasiri *et al*., 2005b). Additionally, auxin signalling is vital to early embryo patterning (reviewed in Jenik *et al*., 2007), and mutation of the AFB genes prevents normal embryo formation (Dharmasiri *et al*., 2005b). The expression studies conducted here are consistent with the roles of AFB2/3 as a necessary regulator of embryo development. The *PsAFB2* expression profiles suggest that higher expression of *PsAFB2* occurs earlier in development (Figure 3.10C) when the embryo tissues undergo rapid growth, during which time developmental patterning and cell division are important processes. Additionally in the liquid endosperm, a non-cellular multinucleate tissue with no internal spatial patterning, transcript abundance of *PsAFB2* was lower than in either the seed coat or the embryo from 8 and 12 DAA (Figure 3.10A,C).

In contrast to *PsAFB2* expression, *PsAFB6A* transcript abundance was lower in the embryo than in the endosperm from 8 to 12 DAA (Figure 3.11B,D). Furthermore, the embryo *PsAFB6A* transcript profile also differed from that of *PsAFB2* in that higher transcript abundance was observed later (10 to 14 DAA) during development, and higher *PsAFB6A* levels were observed in the embryo axis (compared to the cotyledons) only at 14 DAA (Figure 3.11D). These data suggest that transcript abundance of the auxin receptor *PsAFB6A* is regulated differently than that of *PsAFB2* in these seed tissues.

As no investigation into the ability of the PsAFB2 or PsAFB6A proteins to interact with auxin , the SCF complex, or Aux/IAA proteins has been performed, any discussion of the roles of these genes in the context of auxin-signalling remains

hypothetical. While the *PsAFB2* gene was clustered with other homologues with demonstrated roles in auxin-perception (including *AtAFB2* and *AtAFB3;* Dharmasiri *et al*., 2005b), comparatively little investigation has been carried out on members of the AFB6 family of F-box proteins, so further evidence is required to demonstrate that *PsAFB6A* codes for a functional auxin receptor.

3.4.2 Endogenous IAA and 4-Cl-IAA Profiles in the Seed

Endogenous 4-Cl-IAA levels were higher than those of IAA in the embryo and seed coat at all development stages studied (10 to 18 DAA; Table 3.7A), however the levels of these endogenous auxins were approximately equal in the 10 to 12 DAA endosperm (Table 3.7B). The comparatively high abundance of 4-Cl-IAA in the embryo and seed coat suggests that this hormone serves a major role in auxin regulated processes in these tissues during this phase of seed development.

Endogenous auxin profiles in the embryo

Embryo IAA abundance in general decreased over seed development (10 to 18 DAA) with a small peak in levels observed at 16 DAA (Table 3.7A). In contrast, embryo 4-Cl-IAA levels peaked at 14 to 16 DAA, and at levels 18.0- to 33.4-fold greater than those of IAA (Table 3.7A), concomitant with the transition of the embryo from the pre-storage phase (characterized primarily by growth and development) to the reserve accumulation phase (characterized by nutrient storage, although embryo growth still occurs; Figure 2.6). These endogenous auxin profiles suggest that the specific roles of 4-Cl-IAA and IAA in the embryo likely differ during the stages of growth studied, and that

increases in embryo 4-Cl-IAA abundance may be involved in the regulation of embryo processes during the transition from the pre-storage to storage phase.

Endogenous auxin profiles in the seed coat

Seed coat IAA abundance decreased from 9.6-fold from 10 to 18 DAA (Table 3.7A), similar to the IAA profile of the developing embryo during this time. Seed coat 4-Cl-IAA levels were highest earlier in development (10 DAA) then decreased 6.5-fold by 14 DAA before increasing somewhat by 16 to 18 DAA (Table 3.7A). In contrast to the embryo, in which 4-Cl-IAA accumulates as the seed enters the storage phase at approximately 14 to 18 DAA, 4-Cl-IAA accumulates earlier in seed coat development and is relatively low at 14 DAA (Table 3.7A). While final seed size in pea is related to cotyledon cell number (Davies, 1975), the seed coat may also exert influences on seed growth, both as a mechanical limiter to embryo expansion and as a source of regulatory compounds. The high abundance of 4-Cl-IAA in the seed coat from 10 to 12 DAA may be important for regulating seed coat growth (seed coat fresh weight and ground parenchyma cell size increase greatly between 10 and 12 DAA; see Figures 2.6A, 2.7B, and 2.8A), and/or 4-Cl-IAA may be transported to either the pericarp or embryo to regulate developmental processes in those tissues.

Endogenous auxin profiles in the endosperm

In the endosperm, both IAA and 4-Cl-IAA levels increase from 10 to 12 DAA (Table 3.7B) as the endosperm reaches its maximum volume (Figure 2.6B). Whereas in the embryo and seed coat 4-Cl-IAA was more abundant than IAA (Table 3.7A), both

hormones are found at similar concentrations in the liquid endosperm (Table 3.7B). In *Zea mays*, the liquid endosperm produces large quantities of IAA, and early increases in liquid endosperm IAA production promote increases in chromosome endoreduplication (Lur and Setter, 1993). While the development of the endosperm in pea differs significantly from that of maize (pea endosperm is liquid, non-cellular, and absorbed by the embryo long before maturity, while maize endosperm is cellular and present in the mature seed), it is also characterized by increases in ploidy: endosperm nuclei are normally 3n, but 6n and even 12n nuclei are observed (Kapoor, 1966), and the relatively high levels of IAA may promote similar processes in pea endosperm.

3.4.3 Seed and Auxin Regulation of Pericarp *PsAFB* Expression

Pollination and fertilization events (-2 to 1 DAA) did not affect pericarp transcript abundance of *PsAFB2* (Figure 3.9), but reduced transcript abundance of *PsAFB6A* (Figure 3.11). The emasculation of flowers at -2 DAA increased transcript abundance of both *PsAFB2* (Figure 3.9) and *PsAFB6A* (Figure 3.11) by anthesis (0 DAA), and additionally produced a marked increase in *PsAFB6A*, but not *PsAFB2*, transcript levels after 1 DAA (Figure 3.11). Between 1 and 3 DAA, transcript abundance of *PsAFB6A* in emasculated pericarps increased 4.6-fold, while levels in pollinated pericarps increased only 1.7-fold, and at 3 DAA transcript levels of *PsAFB6A* were 8.2-fold greater in non-pollinated pericarps than in pollinated pericarps (Figure 3.11). By 4 DAA, non-pollinated pea fruit will normally become flaccid and subsequently senesce (Ozga *et al*., 2003). Therefore, in pea, the presence of fertilized seeds is required for pericarp growth

(Eeuwens and Schwabe, 1975; Ozga *et al*., 1992), and appears to repress the expression of the auxin receptor *PsAFB6A* in the pericarp.

To further test the hypothesis that seeds are required for repression of pericarp *PsAFB6A* transcript levels, the mRNA abundance of both *PsAFB* genes in pericarps with and without seeds post-anthesis was monitored. Seed removal from 2 DAA fruits increased the transcript abundance of pericarp *PsAFB6A* (Figure 3.12B), but not *PsAFB2* (Figure 3.12A), confirming trends observed in non-pollinated pericarps.

Hormone regulation of AFB transcript abundance

Previous work has shown that the application of 4-Cl-IAA, but not IAA, to 2 DAA deseeded pericarps can mimic the presence of the seeds with respect to stimulation of pericarp growth (Reinecke *et al*., 1995). Bioactive GAs, GA_1 and GA_3 also stimulate deseeded pericarp growth (Ozga and Reinecke, 1999). To test if the auxin 4-Cl-IAA can specifically mimic the effect of the seeds on *PsAFB6A* transcript abundance, and determine if bioactive GAs also can affect the expression of these auxin receptor genes, transcript abundance was monitored in deseeded pericarps treated with 4-Cl-IAA, IAA and GA_3. Pericarp *PsAFB6A* transcript levels were initially reduced by both 4-Cl-IAA and IAA treatment (2 h after hormone application; Figure 3.12D). However, by 8 hours after hormone application, *PsAFB6A* transcript levels were significantly greater in the IAA-treated deseeded pericarps than the pericarp with seeds (SP) and transcript levels remained elevated through the 12 hour time point (Figure 3.12D). In contrast, 4-Cl-IAA treated deseeded pericarps had lower levels of PsAFB6A transcript throughout the 12 hour period analyzed (Figure 3.12D). Bioactive GA_3 had no effect on pericarp *PsAFB6A* transcript abundance (Figure 3.12F). Pericarp *PsAFB2* transcript abundance was not

affected by seed removal (Figure 3.12A) or treatment with IAA, 4-Cl-IAA (Figure 3.12C), or GA_3 (Figure 3.12E). These data support the hypothesis that, in addition to stimulating pericarp growth (Reinecke *et al*., 1999) and GA biosynthesis (Ozga *et al*., 2009), 4-Cl-IAA can mimic the presence of seeds in the repression of transcript levels of the putative auxin receptor *PsAFB6A* in the pericarp.

In pea, seed-derived 4-Cl-IAA promotes pericarp growth through several mechanisms. In addition to promoting pericarp GA biosynthesis (Ozga *et al*., 2002) and inhibiting pericarp GA catabolism (Ozga *et al*., 2009), 4-Cl-IAA also inhibits ethylene response (Johnstone *et al*., 2005). Previous work has demonstrated that the application of IAA to deseeded pericarp further decreases growth as measured by fresh weight, through the stimulation of ethylene biosynthesis (Johnstone *et al*., 2005). While both IAA and 4-Cl-IAA stimulated pericarp ethylene evolution, 4-Cl-IAA additionally inhibited ethylene response (Johnstone *et al*., 2005). The ability of 4-Cl-IAA to inhibit pericarp ethylene response may involve the repression of the auxin receptor *PsAFB6A*, the gene product of which could serve as a promoter of ethylene sensitivity or response via SCF-mediated degradation of specific Aux/IAA regulators. Orzáez *et al*. (1999) observed that the putative ethylene receptor *PsERS* was upregulated in emasculated pericarps compared to pericarps with fertilized seeds. Orzáez *et al*. (1999) also found that both ethylene levels and ACC oxidase transcript (codes for a key enzyme in the ethylene biosynthesis pathway) were higher in emasculated pericarps between -2 and 3 DAA, suggesting a role for ethylene in non-pollinated pea fruit senescence.

The role of 4-Cl-IAA and viable seeds in promoting pericarp GA biosynthesis and growth has been well-documented, and the seed signal(s) is required for normal pericarp

development (Ozga and Brenner, 1992, Ozga *et al*., 2003, Ozga *et al*., 2009). In the absence of these signals, pericarp senescence occurs, and it is possible that the localized upregulation of *PsAFB6A* is a mechanism to ensure that pericarp senescence does not proceed in the presence of viable seeds. Under this hypothesis, seed-derived 4-Cl-IAA serves to limit *PsAFB6A* gene expression, while in the absence of this signal (absence of ovule fertilization) *PsAFB6A* transcript levels increase. In the case of partial ovule fertilization within the fruit, the upregulation of pericarp *PsAFB6A* would heighten the local pericarp tissues sensitivity to ethylene, and reduce pericarp growth locally around non-fertilized ovules (local pericarp growth is restricted around non-fertilized ovules or aborted seeds in pea; Ozga, personal communication). This mechanism would serve to adjust pericarp growth to the number of developing seeds.

3.4.4 Localization of *PsAFB* Transcripts within the Pericarp

Following fruit set, pericarp transcript abundance of both *PsAFB2* (Figure 3.9; Figure 3.10E) and *PsAFB6A* (Figure 3.11; Figure 3.10F) was relatively constant from 2 to 20 DAA. While transcript abundance of *PsAFB2* was similar in the vascular sutures, funiculus, and pericarp wall (Figure 3.10E), transcript abundance of *PsAFB6A* was greater in the dorsal and ventral vascular sutures than in the pericarp wall (Figure3.10F). Furthermore, the pericarp dorsal vascular suture had in general slightly higher *PsAFB6A* mRNA levels than the pericarp ventral vascular suture (seeds are attached at the ventral vascular suture via the funiculus; Figure 3.10F,H) and the funiculus, which is rich in vascular tissue, had higher levels of *PsAFB6A* transcript than the pericarp tissues from 8 to 20 DAA (Figure 3.10G). Both the vascular sutures and the funiculus can form

abscission zones, either between each half of the pericarp (in the case of the sutures) or between the fruit and seed (in the case of the funiculus). Ethylene serves as an inducer of abscission (reviewed in Patterson, 2001), and the higher levels of *PsAFB6A* mRNA in the pericarp vascular suture tissues and in the funiculus may serve a possible developmental role in heightening auxin-induced ethylene sensitivity in these tissue, allowing for the prompt formation of abscission zones when ethylene is present.

3.5 Literature Cited

Bandurski, R., and A. Schulze. (1977). Concentration of Indole-3-acetic acid and its derivatives in plants. *Plant Physiol.* **60**:211-213.

Bandurski, R., J. Cohen, J. Solvin, and D. Reinecke. (1995). Auxin biosynthesis and metabolism. *In* PJ Davies, ed, *Plant Hormones: Physiology, Biochemistry and Molecular Biology 2nd edition.* Kluwer Academics Publishers, Dordrecht, The Netherlands pp. 649-670

Bartel, B. (1997). Auxin biosynthesis. *Ann. Rev. Plant Physiol. Plant Mol. Biol.* **48**:51-66

Bialek, K., and J. Cohen. (1989). Quantitation of indoleacetic acid conjugates in bean seeds by direct tissue hydrolysis. *Plant Physiol*. **90**:398-400

Cannon, S., L. Sterck., S. Rombauts, S. Sato, F. Cheung, J. Gouzy, X. Wang, J. Mudge, J. Vasdewani, T. Schiex, M. Spannagl, E. Monaghan, C. Nicholson, S. Humphray, H. Schoof, K. Mayer, J. Rogers, F. Quetier, G. Oldroyd, F. Debelle, D. Cook, B. Roe, C. Town, S. Tabata, Y. van de Peer, and N. Young. (2006). Legume evolution viewed through the *Medicago truncatula* and *Lotus japonicus* genomes. *Proc. Nat. Acad. Sci. USA* **103**:14959-14964.

Davidson, S., R. Elliott, C. Helliwell, A. Poole, and J. Reid. (2003). The pea gene *NA* encodes *ent*-kaurenoic acid oxidase. *Plant Physiol*. **131**:335-344

Davies, D. (1975). Studies of seed-development in Pisum sativum. I. Seed size in reciprocal crosses. *Planta* **124**:303-309

Dharmasiri, N., and M. Estelle. (2004). Auxin signalling and regulated protein degradation. *Trends Plant Sci.* **9**:302-308

Dharmasiri, N., S. Dharmasiri, and M. Estelle. (2005a). The F-box protein TIR1 is an auxin receptor. *Nature* **435**:441-445

Dharmasiri, N., S. Dharmasiri, D. Weijers, E. Lechner, M. Yamada, L. Hobbie, J. Ehrismann, G. Jürgens, and M. Estelle. (2005b). Plant development is regulated by a family of auxin receptor F box proteins. *Dev. Cell* **9**:109-119

Gagne, J., B. Downes, S. Shiu, A. Durski, and R. Vierstra. (2002). The F-box subunit of the SCF E3 complex is encoded by a diverse superfamily of genes in *Arabidopsis*. *Proc. Nat. Acad. Sci. USA* **99**:11519-11524

Gaskin, P., and J. Macmillan. (1991). GC-MS of the gibberellins and related compounds. *Methodology and a library of spectra.* Bristol, UK: University of Bristol (Cantock's Enterprises).

Gray, W., J. del Pozo, L. Walker, L. Hobbie, E. Risseeuw, T. Banks, W. Crosby, M. Yang, H. Ma, and M. Estelle. (1999). Identification of an SCF ubiquitin-ligase complex required for auxin response in *Arabidopsis thaliana*. *Genes Dev.* **13**:1678-1691

Gray, W., S. Kepinski, D. Rouse, O. Leyser, and M. Estelle. (2001). Auxin regulates SCF(TIR1)-dependant degradation of AUX/IAA proteins. *Nature* **414**:271-276

Hagen, G., and T. Guilfoyle. (2002). Auxin-responsive gene expression: genes, promoters and regulatory factors. *Plant Mol. Biol.* **49**:373-385

Jacobsen, J., D. Pearce, A. Poole, R. Pharis, and L. Mander. (2002). Abscisic acid, phaseic acid, and gibberellin contents associated with dormancy and germination in barley. *Physiologica Plantarum* **115**:428-441.

Jakubowska, A., and S. Kowalczyk. (2004). The auxin conjugate 1-O-indole-3-acetyl-β-D-glucose is synthesized in immature legume seeds by IAGIc synthase and may be used for modification of some high molecular weight compounds. *J. Exp. Bot.* **55**:791-801

Jenik, P., C. Gillmor, and W. Lukowitz. (2007). Embryonic patterning in *Arabidopsis thaliana*. *Annu. Rev. Cell Dev. Biol.* **23**:207-236

Johnstone, M., D. Reinecke, and J. Ozga. (2005). The auxins IAA and 4-Cl-IAA differentially modify gibberellin action via ethylene response in developing pea fruit. *J. Plant Growth Reg.* **24:214-225.**

Kapoor, B. (1966). Contributions to the cytology of endosperm in angiosperms – XII. *Pisum sativum* L. *Genetica* **37**:557-568

Katayama, M., S. Thiruvikraman, and S. Marumo. (1987). Identifiation of 4-chloroindole-3-acetic acid and its methyl ester in immature seeds of *Vicia amurensis* (the tribe *Vicieae*), and their absence from three species of *Phaseoleae*. *Plant Cell Physiol.* **28**: 383-386

Katayama, M., S. Thiruvikraman, and S. Marumo. (1988). Localization of 4-chloroindole-3-acetic acid in seeds of *Pisum sativum* and its absence from all other organs. *Plant Cell Physiol.* **29**:889-891

Kepinski, S., and O. Leyser. (2005). The Arabidopsis F-box protein TIR1 is an auxin receptor. *Nature* **435**:446-451

Law, D., and R. Hamilton. (1982). A rapid isotope dilution method for analysis of indole-3-acetic acid and indoleacetyl aspartic acid from small amounts of plant tissue. *Biochem. Biophys. Res. Comm.* **106**:1035-1041

Letunic, I., R. Copley, B. Pils, S. Pinkert, J. Schultz, and P. Bork. (2005). SMART 5: domains in the context of genomes and networks. *Nuc. Acid Res.* **34**: D257-D260

Leyser, O. (2002). Molecular genetics of auxin signaling. *Ann. Rev. Plant Biol.* **53**:377-398

Lur, H.-S., and T. Setter. (1993). Role of auxin in maize endosperm development: timing of nuclear DNA endoreduplication, zein expression, and cytokinin. *Plant Physiol.* **103**:273-280

Magnus, V., J. Ozga, D. Reinecke, G. Pierson, T. Larue, J. Cohen, and M. Brenner. (1997). 4-chloroindole-3-acetic and indole-3-acetic acids in *Pisum sativum*. *Phytochem.* **46**:675-681

Marumo, S., H. Hattori, H. Abe, and K. Munakata. (1968). Isolation of a novel auxin, methyl 4-chloroindoleacetate from immature seeds of *Pisum sativum*. *Agr. Biol. Chem.* **32**:117-118.

Nordström, A-C., F. Jacobs, and L. Eliasson. (1991). Effect of exogenous indole-3-acetic acid and indole-3-butyric acid on internal levels of the respective auxins and their conjugation with aspartic acid during adventitious root formation in pea cuttings. *Plant Physiol.* **96**:856-861.

Orzáez, D., R. Blay, and A. Granell. (1999). Programme of senescence in petals and carpels of Pisum sativum L. flowers and its control by ethylene. *Planta* 208:220-226.

Ozga, J., D. Reinecke, B. Ayele, P. Ngo, C. Nadeau, and A. Wickramarathna. (2009). Developmental and Hormonal Regulation of Gibberellin Biosynthesis and Catabolism in Pea Fruit. *Plant Physiol.* **150:**448-462.

Ozga J., and M. Brenner. (1992). The effect of 4-CI-IAA on growth and GA metabolism in deseeded pea pericarp. *Plant Physiol.* **99**:S-12.

Ozga, J., and D. Reinecke. (1999). Interaction of 4-chloroindole-3-acetic acid and gibberellins in early pea fruit development. *Plant Growth Reg.* **27**:33-38.

Ozga, J., M. Brenner, and D. Reinecke. (1992). Seed effects on gibberellin metabolism in pea pericarp. *Plant Physiol.* **100**:88-94.

Ozga, J., J. Yu, and D. Reinecke. (2003). Pollination-, development- and auxin-specific regulation of gibberellin 3β-hydroxylase gene expression in pea fruit and seeds. Plant Physiol. **131**:1137-1146.

Park, J., H. Kim, and J. Kim. (2002). Mutation in domain II of IAA1 confers diverse auxin-related phenotypes and represses auxin-activated expression of Aux/IAA genes in steroid regulator-inducible systems. *Plant J.* **32**:669-683

Patterson, S. (2001). Cutting loose. Abscission and dehiscence in *Arabidopsis*. *Plant Physiol.* **126**:494-500

Reid, J., and J. Ross. (1993). A mutant-based approach, using *Pisum sativum*, to understanding plant growth. *Int. J. Plant Sci*. **154**:22-34.

Reinecke, D., J. Ozga, and V. Magnus. (1995). Effect of halogen substitution of indole-3-acetic acid on biological activity in pea fruit. *Phytochem.* **40**:1361-1366.

Reinecke, D., J. Ozga, N. Ilić, V. Magnus, and B. Kojić-Prodić. (1999). Molecular properties of 4-substituted indole-3-acetic acids affecting pea pericarp elongation. *Plant Growth Reg.* **27**:39-48

Rose, T., J. Henikoff, and S. Henikoff. (2003). CODEHOP (COnsensus-DEgenerate Hybrid Oligonuceotide Primer) PCR primer design. *Nuc. Acid Res.* **31**:3763-3766

Schneider, E., C. Kazakoff, and F. Wightman. (1985). Gas chromatography-mass spectrometry evidence for several endogenous auxins in pea seedlings organs. *Planta* **165**:232-241

Schultz, J., F. Milpetz, P. Bork, and C. Ponting. (1998). SMART, a simple modular architecture research tool: Identification of signalling domains. *Proc. Nat. Acad. Sci. USA* **95**:5857-5864

Tan., X., L. Calderon-Villalobos, M. Sharon, C. Zheng, C. Robinson, M. Estelle, and N. Zheng. (2007). Mechanism of auxin perception by the TIR1 ubiquitin ligase. *Nature* **446**:640-645.

Tiwari, S., X. Wang, G. Hagen, and T. Guilfoyle. (2001). AUX/IAA proteins are active repressors, and their stability and activity are modulated by auxin. *Plant Cell* **13**:2809-2822

Ulmasov, T., Z. Liu, G. Hagen, and T. Guilfoyle. (1995). Composite structure of auxin responsive elements. *Plant Cell* **7**:1611-1623

Ulmasov, T., G. Hagen, and T. Guilfoyle. (1999). Dimerization and DNA binding of auxin response factors. *Plant J.* **19**:309-319

van Huizen, R., J. Ozga, D. Reinecke, B. Twitchen, and L. Mander. (1995). Seed and 4-chloroindole-3-acetic acid regulation of gibberellin metabolism in pea pericarp. *Plant Phys.* **109**:1213-1217

van Huizen, R., J. Ozga, and D. Reinecke. (1997). Seed and hormonal regulation of Gibberellin-20 oxidase expression in pea pericarp. *Plant Phys.* **128**:1379-1389

Woodward, A., and B. Bartel. (2005). Auxin: regulation, action, and interaction. *Ann. Bot.* **95**:707-735

Chapter 4

Conclusions

4.1 Regulation of GA metabolism in developing seeds

This research has presented metabolite and GA biosynthesis gene transcript profiles in conjunction with microscopy and growth data, and has identified several processes in seed development in which GAs may serve important roles. Additionally, the ability of ABA to act as a regulator of GA metabolism has been examined (summarized in Figure 4.1). Together, these data examine the links between GA metabolism, ABA, and seed morphology, and suggest several possible directions for future research.

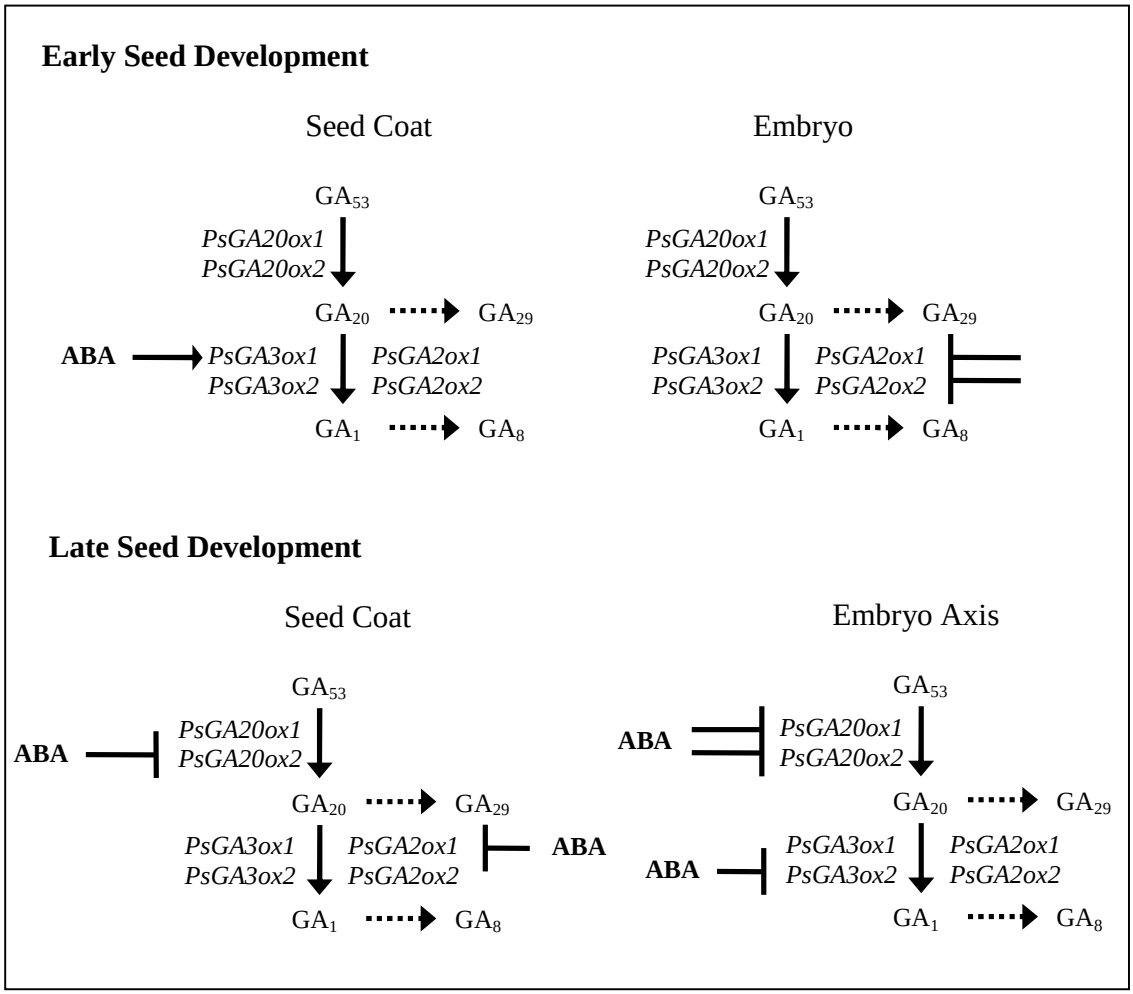

Figure 4.1: Model of regulation of GA biosynthesis by ABA in developing pea seeds. In the pre-storage phase seed (10 to 12 DAA), ABA promotes bioactive GA1 synthesis by upregulating *PsGA3ox1*, while it inhibits GA catabolism in the embryo by repressing the catabolic *PsGA2ox* genes. In the early storage phase seed (16 to 18 DAA), ABA reduces both GA biosynthesis (via repressing *PsGA20ox2*) and GA catabolism (via repressing *PsGA2ox1*), while it inhibits GA biosynthesis in the embryo axis by downregulating both *PsGA20ox* genes and *PsGA3ox2*. Biosynthetic reactions are indicated by solid arrows, while deactivation or catabolism reactions are indicated with dashed arrows.

Transcript and metabolite profiling has identified several periods in development during which GA metabolism may promote tissue development. While the evidence presented here suggests that ABA-induced GA_1 biosynthesis may be an important promoter of branched parenchyma expansion, a direct link between ABA-induced GA_1 production and branched parenchyma expansion has not been noted. The seed coat morphology of ABA-treated 10 DAA seeds could be investigated: increases in branched parenchyma thickness or cell size due to ABA application would serve as additional evidence that ABA-induced GA_1 production promotes branched parenchyma expansion. While the the stimulation of seed coat GA biosynthesis by ABA during early development has been examined from both GA metabolism gene transcript abundance and hormone abundance and is supported by endogenous transcript and metabolite profiles, a direct link between ABA application and enzyme activity would further support the hypothesis that ABA promotes early seed coat GA biosynthesis. To this end, 10 DAA seeds could be treated with ABA as described in Chapter 2, and radiolabelled GA_{20} could be applied after 6 hours (when increased *PsGA3ox1* transcript levels were observed). After an incubation to allow metabolism, levels of radiolabelled GA_{20}, GA_{29}, GA_1, and GA_8 could be examined. If the ABA-induced upregulation of *PsGA3ox1* results in increased GA 3β-hydroxylase activity, high levels of radiolabelled GA_1 and/or GA_8 should be observed.

While the increase of GA catabolism between 18 and 20 DAA in the embryo axis is a proposed mechanism to limit growth and allow maturation, the effect of increased embryo axis *PsGA2ox2* transcript on GA metabolite profiles has not been demonstrated. The examination of GA levels in 20 to 22 DAA embryo axes would determine whether

the increase in embryo axis GA catabolism gene expression between 18 and 20 DAA results in decreased embryo axis GA_1 abundance.

4.2 Roles of *PsAFB6A* in fruit and seed development

The data presented here suggest a role for *PsAFB6A* in the regulation of pericarp development. Seed-derived 4-Cl-IAA is transported to the pericarp, where it has multiple actions including the upregulation of GA biosynthesis (Ozga *et al*., 2009) and inhibition of ethylene signalling (Johnstone *et al*., 2005), both of which promote pericarp growth. The modulation of auxin sensitivity through the regulation of the *PsAFB6A* receptor by 4-Cl-IAA may be an important factor in the regulation of both of these processes in pericarp development.

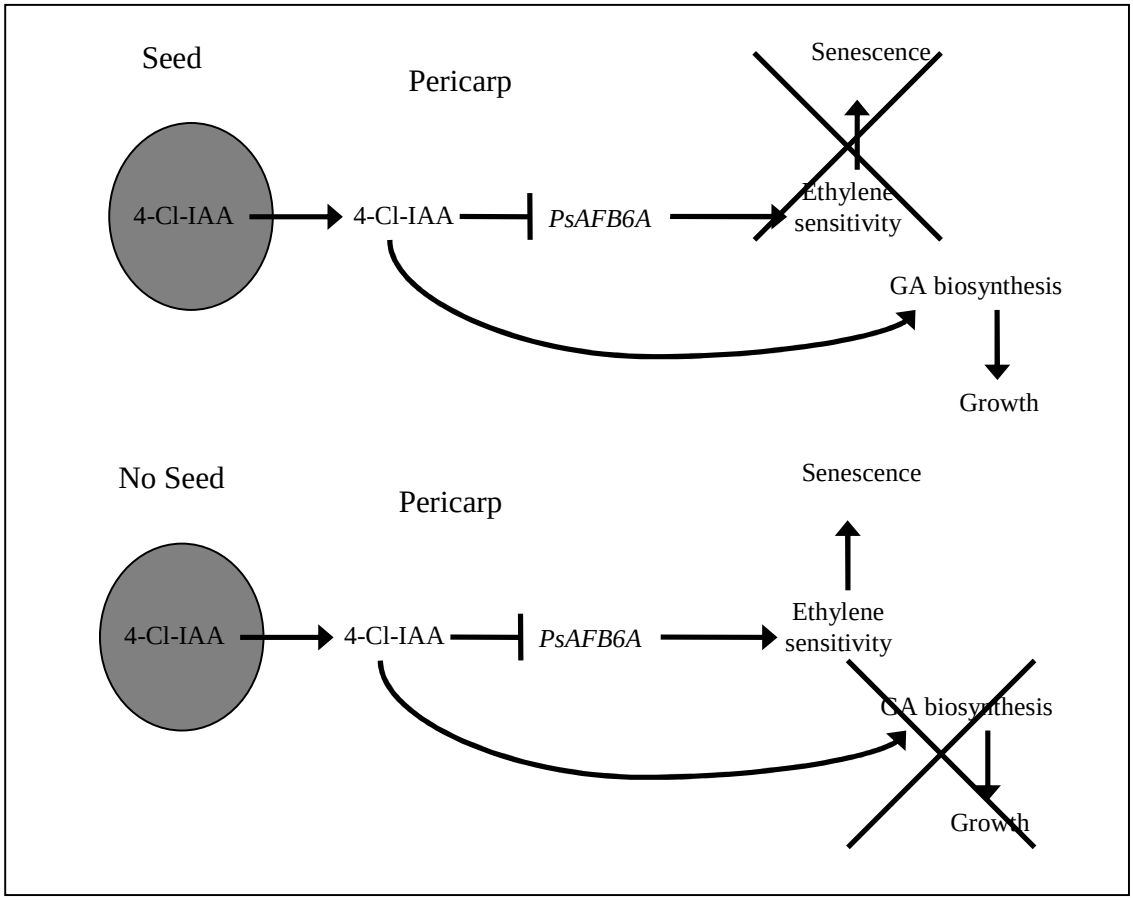

Figure 4.1: Working model of hormone regulation of early pea fruit development. Seed-derived 4-Cl-IAA is transported to the pericarp, where it represses transcription of *PsAFB6A*, part of its signal perception machinery. In the absence of auxin, *PsAFB6A* could serve to increase ethylene sensitivity, promoting pericarp senescense when no seed-derived 4-Cl-IAA is present. Under this hypothesis, the 4-Cl-IAA-induced repression of *PsAFB6A* may be a mechanism to limit ethylene-induced processes including abscission when viable seeds are present.

By repressing *PsAFB6A* transcription, 4-Cl-IAA downregulates its own signal perception, providing that *PsAFB6A* serves as an auxin receptor with the ability to bind 4-Cl-IAA. The downregulation of auxin perception by seed-produced 4-Cl-IAA could be a mechanism to moderate pericarp development in the presence of variable seed count. Under this hypothesis, auxin sensitivity is heightened when few seeds (and thus little 4-

Cl-IAA signal) are present, allowing the pericarp to maintain growth even with low seed count. The role of seed-induced *PsAFB6A* regulation could be better understood through the use of transgenic plants. While wildtype pea fruit normally have between 4 and 7 seeds, a recently characterized line with a constitutively expressed *PsGA3ox1* transgene is capable of maintaining fruit growth with fewer (1 to 3) seeds. Greater pericarp *PsAFB6A* transcript in fruit with fewer seeds would support the role of *PsAFB6A* regulation as a mechanism to adjust pericarp growth to variable seed count.

The localization of *PsAFB6A* transcript to the abscission zones of the pea fruit suggests a role for this gene in the 4-Cl-IAA mediated repression of ethylene signalling. In this model, *PsAFB6A* promotes ethylene signalling, and the repression of *PsAFB6A* by 4-Cl-IAA reduces ethylene sensitivity, preventing abscission and ethylene-induced repression of GA biosynthesis. In the absence of 4-Cl-IAA, increased *PsAFB6A* transcript leads to increased ethylene sensitivity, priming abscission zones for ethylene perception and inhibiting pericarp GA biosynthesis (Figure 4.1). The role of *PsAFB6A* as a regulator of ethylene response could be examined through the transcription profiling of ethylene receptors (*PsERS*) and members of the ethylene signal transduction pathway (*Pisum* orthologue(s) of *AtEIN2*), and by examining the response of these genes to seeds and auxin signals.

The regulation of *PsAFB6A* transcript levels by 4-Cl-IAA and viable seeds, while *PsAFB2* remains largely unresponsive, raises the possibility that *PsAFB6A* serves as a 4-Cl-IAA specific receptor. Given that 4-Cl-IAA is not a naturally occurring auxin in *Arabidopsis*, the specificity of AFB receptors for alternate endogenous auxins has not been thoroughly investigated. Isolation of the gene product of *PsAFB6A* from a relevant

protein expression system and binding assays with 4-Cl-IAA, IAA, and the other indole-substituted auxins used by Reinecke *et al.* (1999) should provide further insights into auxin-receptor specificity.

4.3 Literature Cited

Johnstone, M., D. Reinecke, and J. Ozga. (2005). The auxins IAA and 4-Cl-IAA differentially modify gibberellin action via ethylene response in developing pea fruit. *J. Plant Growth Reg.* **24:214-225.**

Ozga, J., D. Reinecke, B. Ayele, P. Ngo, C. Nadeau, and A. Wickramarathna. (2009). Developmental and Hormonal Regulation of Gibberellin Biosynthesis and Catabolism in Pea Fruit. *Plant Physiol.* **150:**448-462.

Reinecke, D., J. Ozga, N. Ilić, V. Magnus, and B. Kojić-Prodić. (1999). Molecular properties of 4-substituted indole-3-acetic acids affecting pea pericarp elongation. *Plant Growth Reg.* **27**:39-48

Chapter 5

Appendix

5.1 Hormone Profiling

To allow the metabolite data collected during this study to be more widely useful to other researchers, the same metabolite abundance data presented in chapters 2 and 3 are repeated here in ng gDw^{-1} (Table 5.1; Table 5.2; Table 5.3). While measurements in ng gFw^{-1} more accurately reflect physiological concentrations and are not conflated by variance in water content, ng gDw^{-1} is sometimes used if accurate fresh weights are

unavailable. Additionally, to better reflect the differences in metabolite level between solid tissues and liquid endosperm, hormones are presented on total per seed basis (Table 5.4; Table 5.5).

Table 5.1: Abundance of several 13-hydroxylated (GAs 1, 8, 20, and 29) and non 13-hydroxylated (GA_9) gibberellins in embryo (A), embryo axes, and cotyledons (B) from 10 to 18 DAA. Most results are represented as mean of two independent samples ± standard error (n.d.= not detected, although relevant standard added at tissue homogenization was recovered), except all GAs in 10 DAA embryo and 18 DAA embryo axis, and GA9 in 12 DAA embryo, n=1. Data are presented in ng gDw^{-1}.

A	GA_9	GA_1	GA_8	GA_{20}	GA_{29}
Embryo 10 DAA	-	2.07	24.86	1033.81	92.45
Embryo 12 DAA	832.91	0.99 ± 0.07	15.30 ± 0.33	2849.04 ± 555.46	390.56 ± 17.08
Embryo 14 DAA	716.1 ± 126.36	0.74 ± 0.18	11.08 ± 0.91	662.01 ± 43.88	349.60 ± 15.83
Embryo 16 DAA	304.82 ± 32.37	1.06 ± 0.13	9.34 ± 0.18	1222.21 ± 43.92	343.57 ± 3.45
Embryo 18 DAA	7.18 ± 1.53	n.d.	3.25 ± 0.34	243.86 ± 0.46	206.87 ± 7.81

B	GA_9	GA_1	GA_8	GA_{20}	GA_{29}
Embryo Axis 18 DAA	4.49	3.97	44.96	4833.80	898.55
Cotyledon 18 DAA	38.03 ± 0.91	0.26 ± 0.26	4.44 ± 0.98	557.99 ± 126.34	706.21 ± 26.34

Table 5.2: Abundance of several 13-hydroxylated (GAs 1, 8, 20, and 29) and non 13-hydroxylated (GA_9) gibberellins in seed coats from 10 to 18 DAA. Results are represented as mean of two independent samples ± standard error (n.d.= not detected, although relevant standard added at tissue homogenization was recovered). Data are presented in ng gDw^{-1}.

	GA_9	GA_1	GA_8	GA_{20}	GA_{29}
Seed Coat 10 DAA	n.d.	8.51 ± 2.23	45.61 ± 3.07	27.33 ± 1.50	52.71 ± 0.07
Seed Coat 12DAA	n.d.	0.76 ± 0.02	14.22 ± 1.93	84.90 ± 11.43	633.79 ± 125.63
Seed Coat 14 DAA	n.d.	1.01 ± 0.18	5.52 ± 0.24	60.80 ± 9.06	600.38 ± 36.85
Seed Coat 16 DAA	3.73 ± 0.79	n.d.	5.69 ± 0.20	198.25 ± 22.05	536.32 ± 32.01
Seed Coat 18 DAA	n.d.	n.d.	5.32	119.63 ± 23.42	649.74 ± 39.21

Table 5.3: Abundance of ABA, IAA, and 4-Cl-IAA in embryos (A), embryo axes and cotyledons (B), and seed coats (C) from 10 to 18 DAA. Most results are represented as mean of two independent samples ± standard error (n.d.= not detected although internal standard added at tissue homogenization was recovered), except in several instance n=1, in which case data are presented without standard error. Results are expressed in ng gDw^{-1}.

A	ABA	IAA	4-Cl-IAA
Embryo 10 DAA	471.65	481.99	791.98
Embryo 12 DAA	1923.49 ± 15.03	210.32 ± 18.95	754.02
Embryo 14 DAA	1297.03 ± 63.49	107.91 ± 11.57	3622.34 ± 1478.71
Embryo 16 DAA	1520.50 ± 98.09	148.28 ± 29.26	2790.21
Embryo 18 DAA	1120.88 ± 7.87	40.81 ± 10.4	393.19 ± 172.93

B	ABA	IAA	4-Cl-IAA
Embryo Axis 18 DAA	4943.97	273.86	1019.34
Cotyledon 18 DAA	852.44 ± 58.74	29.00 ± 3.37	288.56 ± 19.54

C	ABA	IAA	4-Cl-IAA
Seed Coat 10 DAA	652.42 ± 82.61	298.85 ± 53.68	4507.49
Seed Coat 12 DAA	1276.69 ± 113.87	99.91 ± 5.86	2404.44
Seed Coat 14 DAA	828.70 ± 34.21	40.71 ± 5.25	618.34 ± 106.4
Seed Coat 16 DAA	1061.91 ± 113.66	47.39 ± 8.93	1393.87
Seed Coat 18 DAA	521.40 ± 80.26	24.87 ± 1.99	960.5

Table 5.4: Abundance of major GAs in embryos, seed coats, and endosperm from 10 to 18 DAA and embryo axes and cotyledons at 18 DAA. Most results are represented as mean ± standard error, n=2 (n.d.= not detected although internal standard added at tissue homogenization was recovered), except in several instance n=1, in which case data are presented without standard error. Results are expressed in pg per seed.

	GA_9	GA_1	GA_8	GA_{20}	GA_{29}
Embryo 10 DAA	-	1	15	612	55
Seed Coat 10 DAA	n.d.	85 ± 22	455 ± 31	273 ± 15	526 ± 1
Endosperm 10 DAA	n.d.	1 ± 0	7 ± 2	65 ± 11	13 ± 5
Embryo 12 DAA	4929	6 ± 0	91 ± 2	8308 ± 924	799 ± 214
Seed Coat 12 DAA	n.d.	15 ± 3	277 ± 38	1654 ± 223	12 349 ± 2448
Endosperm 12 DAA	134 ± 2	n.d.	9 ± 2	7174 ± 798	690 ± 185
Embryo 14 DAA	18 866 ± 3329	19 ± 5	292 ± 24	17 441 ± 1156	9210 ± 417
Seed Coat 14 DAA	n.d.	23 ± 4	126 ± 5	1385 ± 206	13 677 ± 839
Embryo 16 DAA	14 817 ± 1573	51 ± 6	454 ± 9	59 408 ± 2135	16 700 ± 167
Seed Coat 16 DAA	94 ± 20	n.d.	144 ± 5	5019 ± 558	13 579 ± 810
Embryo 18 DAA	655 ± 140	n.d.	296 ± 31	22 254 ± 42	18 879 ± 713
Cotyledons 18 DAA	2483 ± 81	33 ± 33	290 ± 66	36 496 ± 8568	46 083 ± 1313
Embryo Axis 18 DAA	21	5	55	5964	1109
Seed Coat 18 DAA	n.d.	n.d.	152	3425 ± 670	18 604 ± 1122

Table 5.5: Abundance of ABA, IAA, and 4-Cl-IAA in embryos, seed coats, and endosperm from 10 to 18 DAA and embryo axes and cotyledons at 18 DAA. Most results are represented as mean of two independent samples ± standard error (n.d.= not detected although internal standard added at tissue homogenization was recovered), except in several instance n=1, in which case data are presented without standard error. Results are expressed in pg per seed.

	ABA	IAA	4-Cl-IAA
Embryo 10 DAA	279	285	469
Seed Coat 10 DAA	6508 ± 824	2981 ± 536	45 774
Endosperm 10 DAA	145 ± 7	1699 ± 368	2827 ± 635
Embryo 12 DAA	2130 ± 99	1244 ± 112	4468
Seed Coat 12 DAA	24 876 ± 2219	1947 ± 114	47 238
Endosperm 12 DAA	1839 ± 86	9181 ± 415	8989
Embryo 14 DAA	34 170 ± 1673	2843 ± 305	94 841 ± 37 512
Seed Coat 14 DAA	18 878 ± 779	927 ± 119	14 070 ± 2328
Embryo 16 DAA	73 908 ± 4768	7207 ± 1422	130 604
Seed Coat 16 DAA	26 885 ± 2878	1200 ± 226	35 292
Embryo 18 DAA	102 290 ± 718	3724 ± 949	34 357 ± 12 313
Cotyledons 18 DAA	55611 ± 3344	1895 ± 240	18847 ± 1441
Embryo Axis 18 DAA	6100	338	1258
Seed Coat 18 DAA	14 929 ± 2298	712 ± 57	24 659

5.2 Pericarp GA Metabolism

5.2.1 Background

The spatial localization of *PsAFB6A* and *PsAFB2* transcripts in the regions of the pericarp, combined with their presumed roles in auxin signalling and the interactions between the auxin, GA, and ethylene pathways, suggest that transcript abundance of the

GA metabolism genes may be different in the various regions of the pericarp described in Chapter 3 (Figure 3.3). As both *PsAFB6A* and multiple GA biosynthesis genes are regulated by 4-Cl-IAA, the variable levels of *PsAFB6A* transcript abundance in the vascular sutures, pericarp wall, and funiculus raise the possibility that the GA metabolism genes are also expressed at different levels in these regions of the pericarp. To examine spatial differences in pericarp GA metabolism, transcript abundance of three GA biosynthesis (*PsGA3ox1*, *PsGA20ox1*, and *PsGA20ox2*) and two GA catabolism (*PsGA2ox1* and *PsGA2ox2*) genes was analyzed with qRT-PCR in 8 to 20 DAA funiculi, pericarp wall, and dorsal and ventral vascular sutures.

5.2.2 Results

In comparison to the main pericarp wall, each of the three vascular tissues had higher steady-state transcript abundance of *PsGA3ox1* (Figure 5.1B). *PsGA3ox1* mRNA is more abundant from 8 to 20 DAA in the ventral vascular trace (where seed attachment occurs) than in the dorsal trace. Finally, steady-state *PsGA3ox1* mRNA was several orders of magnitude greater in the funiculus than in any other pericarp tissues tested (Figure 5.1A). *PsGA3ox1* transcript abundance increased in the funiculus between 10 and 12 DAA and remained high until 20 DAA, whereas mRNA abundance in the other vascular tissues increased later, from 14 DAA on (Figure 5.1B).

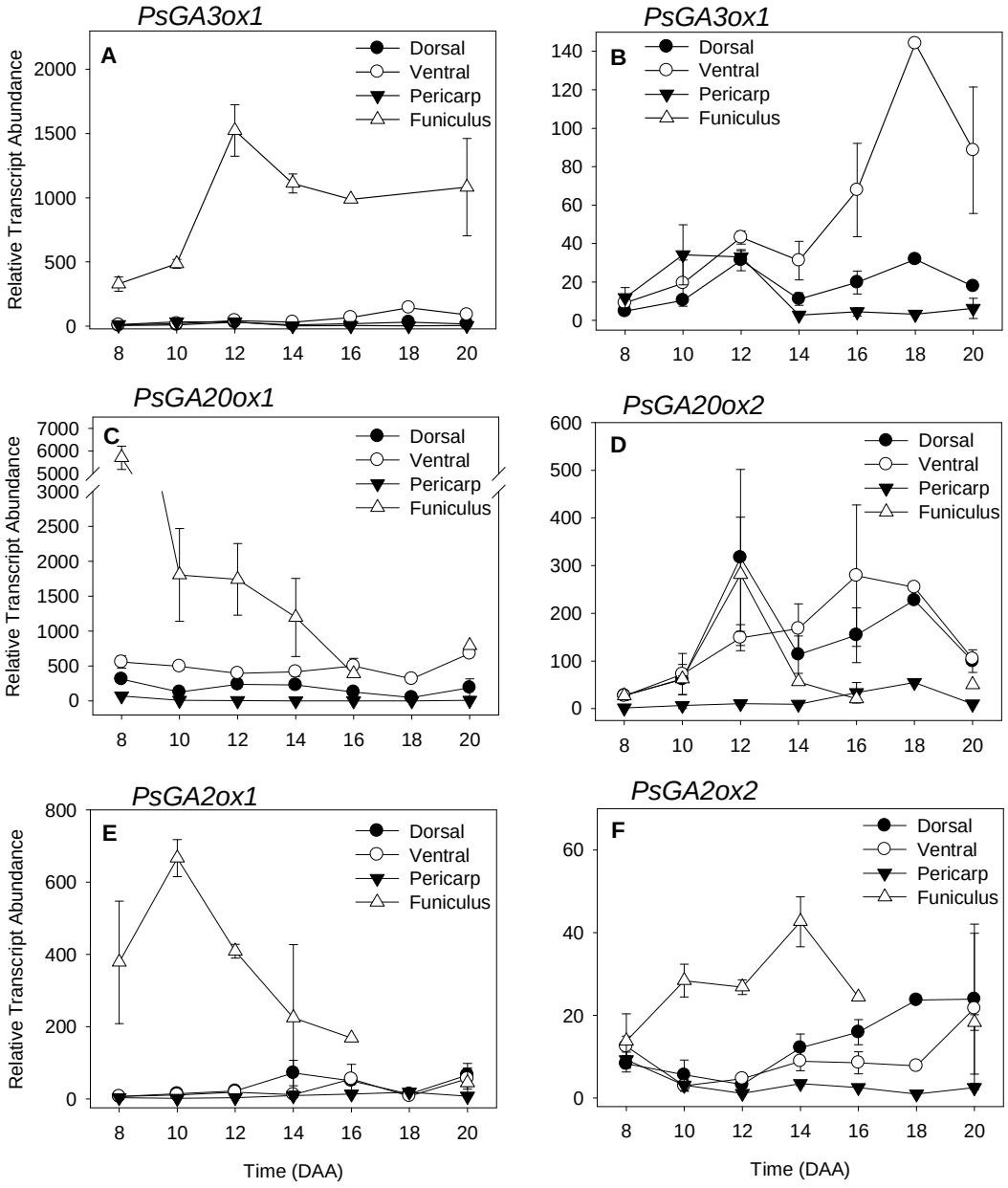

Figure 5.1: Transcript abundance of GA biosynthesis genes in fruit tissues across development. Data are expressed as mean ± standard error. Where standard error is too small, error bars may be obscured by symbols. Samples are representative of between 2 and 3 independent samples, except for all vascular tissues at 18 DAA and funiculus at 16 DAA, where n=1.

Much like *PsGA3ox1*, *PsGA20ox1* transcript abundance was greater in the funiculus and vascular tissues than in the pericarp body (Figure 5.1C). *PsGA20ox1* transcript was also present at greater levels in the ventral than in the dorsal vasculature, similar to *PsGA3ox1* transcript (Figure 5.1C). While steady-state *PsGA20ox2* transcript abundance was also greater in the vascular tissues of the pericarp than in the main pericarp body, mRNA levels were similar between the two traces and the funiculus (Figure 5.1D).

PsGA2ox1 mRNA was detected primarily in the funiculus, and no differences in steady-state transcript abundance were detected between the vascular traces and the main pericarp body (Figure 5.1E). Transcript abundance of *PsGA2ox2* is greater in the vascular traces than in the pericarp body, and from 14 DAA on abundance is higher in the dorsal than in the ventral vascular trace (Figure 5.1F). *PsGA2ox2* mRNA accumulates at very high levels in the funiculus from 10 on, and levels peak at 14 DAA before decreasing (Figure 5.1F).

The differential expression of the GA biosynthesis genes in the four regions of the pericarp demonstrate spatial regulation of GA metabolism within the pea fruit, and may be indicative of differential developmental or physiological processes.

5.3 Putative AFB Protein Sequences

5.3.1 Background

This appendix contains the putative translated gene products of both *PsAFB2* and *PsAFB6A*, presented as alignments with putative and confirmed members of their

respective sub-families of AFB proteins from other species of angio- and gymnosperms. Alignments were performed in ClustalW2 using NJ clustering and the BLOSUM distance matrix. Additionally, domain prediction with the SMART (Simple Modular Architecture Research Tool) program (Schultz *et al.*, 1998, Letunic *et al.*, 2005) was performed using the protein sequences from *PsAFB2*, *PsAFB6A*, and *AtTir1* (for reference).

5.3.2 Results

The structure of the putative gene products of *PsAFB2* and *PsAFB6A* follows that of other AFB proteins, with an F-box domain near the C-terminal and a series of leucine rich repeats towards the mid and N-terminal portions of the protein. Non-redundant domains with significant E-values for PSAFB2 and PSAFB6A are listed in Table 5.6. The F-box domain of PSAFB6A did not pass the threshold E-value under default settings, but is located between residues 7 and 55 (E-value=1.20e+00). It is included in Table 5.6 because of the high sequence similarity it shares to other AFB6 members. While this software identified corresponding numbers of LRR in PSAFB6A and ATTir1, it identified two additional LRRs in PSAFB2, which are expansions of an already identified LRR found in both other proteins.

Table 5.6: Predicted domains of PSAFB2 and PSAFB6A from SMART algorithm. LRR=leucine rich repeat. To confirm the validity of this approach, ATTIR1, for which experimental confirmation of these domains and crystal structures are available, was also analyzed.

PSAFB2				PSAFB6A				ATTIR1			
Domain	Start	End	E-value	Domain	Start	End	E-value	Domain	Start	End	E-value
F-box	4	45	6.97e-04	F-box	7	55	1.20e+00	F-box	9	50	7.18e-06
LRR	99	123	5.08e+02	LRR	107	131	2.99e+02	LRR	129	154	1.03e+02
LRR	124	149	8.67e+01	LRR	132	157	2.67e+01	LRR	155	192	4.38e+02
LRR	283	308	1.92e+02								
LRR	309	332	8.93e+01	LRR	316	339	7.71e+01	LRR	313	336	4.01e+02
LRR	333	364	6.06e+02								
LRR	365	389	3.47e+00	LRR	374	398	3.00e+01	LRR	371	395	8.09e-01
LRR	425	448	1.61e+02	LRR	434	457	4.27e+01	LRR	431	454	1.71e+02
LRR	474	499	5.57e+01	LRR	483	507	2.50e+02	LRR	480	504	2.91e+01

Alignment of AFB2/3 Proteins

```
                 ....|....| ....|....| ....|....| ....|....| ....|....|
                          10         20         30         40         50
PsAFB2           -------MNY FPDEVIEHVF DYVVSHSDRN SLSLVCKSWY RIEGFTRKRV
AtAFB2           -------MNY FPDEVIEHVF DFVTSHKDRN AISLVCKSWY KIERYSRQKV
AtAFB3           -------MNY FPDEVIEHVF DFVASHKDRN SISLVCKSWH KIERFSRKEV
PtrAFB2A         -------MNY FPDEVLEHIF DFVTSQRDRN SVSQVCKPWY KIESSSRQKV
PtrAFB2B         -------MNY FPDEVLEHIF DFVTSQRDRN SVSQVCKPWY KIESTSRQKV
MtAFB2           -------MNY FPDEVIEHVF DYVVSHSDRN SLSLVCKSWY RIERFTRQRV
GmAFB2A          ------MMNY FPDEVIEHIF DYVVSHSDRN ALSLVCKSWY RIERCTRQRV
GmAFB2B          ------MMNY FPDEVIEHIF DYVVSHSDRN ALSLVCKSWY RIERCTRQRV
MgAFB2A          MCLFRDMMSY FPEEVLEHVF DFLTSHRDRN AVSLVCKSWY SLERFSREKV
MgAFB2B          -------MNY IPEEVLEHVF DFITSHRDRN AVSLVCKSWY SVERFSRDKV
AqAFB2           -------MTY FPEEVLEYIF DFITTNQDRN SISLVCKSWF IVEKGSRKRV
OsAFB2A          -------MTY FPEEVVEHIF SFLPAQRDRN TVSLVCKVWY EIERLSRRGV
OsAFB2B          -------MVF FPEEVVEHIL GFLASHRDRN AVSLVCREWY RVERLSRRSV
SbiAFB2A         -------MTY FPEEVVEHIF SFLPSHSDRN TVSLVCKVWY EVERLSRRAV
SbiAFB2B         -------MAY FPEEVVEYIL GYVTSHRDRN AASLVCRVWY DIERRGRRSV
```

Alignment of AFB2/3 Proteins

```
                ....|....| ....|....| ....|....| ....|....| ....|....|
                         60         70         80         90        100
PsAFB2          FIGNCYSISP ERLVERFPDF KSLTLKGKPH FADFSLVPHG WGGFVYPWIE
AtAFB2          FIGNCYAINP ERLLRRFPCL KSLTLKGKPH FADFNLVPHE WGGFVLPWIE
AtAFB3          FIGNCYAINP ERLIRRFPCL KSLTLKGKPH FADFNLVPHE WGGFVHPWIE
PtrAFB2A        FVGNCYAISP QRVIERFPGL KSITLKGKPH FADFNLVPND WGGFVYPWIE
PtrAFB2B        FVGNCYAISP ERVIERFPGL KSITLKGKPH FADFNLVPHD WGGFVYPWIE
MtAFB2          FIGNCYSISP ERLVERFPDL KSLTLKGKPH FADFSLVPHG WGGFVYPWIE
GmAFB2A         FIGNCYSITP ERLIQRFPGL KSLTLKGKPH FADFSLVPYD WGGFVHPWIE
GmAFB2B         FIGNCYSITP ERLIQRFPGL KSLTLKGKPH FADFSLVPYD WGGFVHPWVE
MgAFB2A         FIGNCYAVNP ERLIARFPRV RSLTLKGKPH FADFNLVPHD WGGDVYPWIE
MgAFB2B         FIGNCYSISP ERLIARFPRL RSLTLKGKPH FADFNLVPHD WGGHVYPWID
AqAFB2          FIGNCYAITP ERLISRFPRV KALTLKGKPH FADFNLIPHD WGGFLLPWIE
OsAFB2A         FVGNCYAVRA GRVAARFPNV RALTVKGKPH FADFNLVPPD WGGYAGPWIE
OsAFB2B         LVRNCYAARP ERVHARFPGL RSLSVKGRPR F-----VPAG WGAAARPWVA
SbiAFB2A        FVGNCYAVRP ERVVLRFPNV KALTVKGKPH FADFNLVPPD WGGYAGPWIE
SbiAFB2B        LVSNCYAVHP ERVHMRFPNM RALSVKGKPH FADFNLVPAG WGASAEPWVD

                ....|....| ....|....| ....|....| ....|....| ....|....|
                        110        120        130        140        150
PsAFB2          ALAKSRVGLE ELRLKRMVVS DESLELLSRS FMNFKSLVLV SCEGFTTDGL
AtAFB2          ALARSRVGLE ELRLKRMVVT DESLELLSRS FVNFKSLVLV SCEGFTTDGL
AtAFB3          ALARSRVGLE ELRLKRMVVT DESLDLLSRS FANFKSLVLV SCEGFTTDGL
PtrAFB2A        AFARNSVGLE ELKLKRMIIS DECLELISRS FPNFKSLVLV SCEGFTADGL
PtrAFB2B        AFARNNMGLE ELKLKRMIIS DECLELISRS FANFKSLVLV SCEGFSTDGL
MtAFB2          ALAKNKVGLE ELRLKRMVVS DESLELLSRS FVNFKSLVLV SCEGFTTDGL
GmAFB2A         ALAKNKVGLE ELRLKRMVVS DESLELLSRS FTHFKSLVLV SCEGFSTDGL
GmAFB2B         ALAKSRVGLE ELRLKRMVVS DESLELLSRS FTHFKSLVLV SCEGFSTDGL
MgAFB2A         AMTKNGINLE ELRLKRMLVS DESLELLAKS FPNFKSLVLV SCEGFTTDGL
MgAFB2B         AMAKSGINLE ELRLKRMVVT DESLELLAKS FPTFRSLVLV SCEGFTTDGL
AqAFB2          AMAMSYPGLE ELRLKRMVVT DESLELLSRS FANFKSLVLV TCEGFTTDGL
OsAFB2A         AAARGCHGLE ELRMKRMVVS DESLELLARS FPRFRALVLI SCEGFSTDGL
OsAFB2B         ACVAACPGLE ELRLKRMVVT DGCLKLLACS FPNLKSLVLV GCQGFSTDGL
SbiAFB2A        AAARSCVGLE ELRMKRMVVS DENLELLARS FPRFKVLVLI SCEGFSTDGL
SbiAFB2B        ACARACPGLE ELRLKRMVVT DECLKLLSCS FTNFESLVLV CCEGFSTAGL

                ....|....| ....|....| ....|....| ....|....| ....|....|
                        160        170        180        190        200
PsAFB2          AAVAANCRSL RELDLQENEV EDHKGQWLSC FPENCTSLVA LNFACLKGEI
AtAFB2          ASIAANCRHL RDLDLQENEI DDHRGQWLSC FPDTCTTLVT LNFACLEGET
AtAFB3          ASIAANCRHL RELDLQENEI DDHRGQWLNC FPDSCTTLMS LNFACLKGET
PtrAFB2A        AAIASNCRFL RELDLQENDV EDHRGHWLSC FPDTCTSLVS LNFACLKGEV
PtrAFB2B        AAIASNCRFL RELDLQENDV EDHRGHWLSF FPDTCTSLVS LNFACLKGDV
MtAFB2          AAVAANCRSL RELDLQENEV EDHKGQWLSC FPESCTSLVS LNFACLKGDI
GmAFB2A         AALAANCRFL RELDLQENEV EDHKGQWLSC FPDNCTSLVS LNFACLKGEV
GmAFB2B         AAIAANCRFL RELDLQENEV EDHKGQWLSC FPDNCTSLVS LNFACLKGEV
MgAFB2A         AAIASNCRFL RELDLQENEV DDRKGHWLSC FPDSCTSLVS LNFACLKGEV
MgAFB2B         AAIASGCRFL RELDLQENEV DDRKGQWLSC FPDTCTSLVS LNFACLKGEV
AqAFB2          AAIAANCRVL RELVLYENDV EDCRGHWLSC FPENYTSLVS LDFACLKGEV
OsAFB2A         AAVASHCKLL RELDLQENEV EDRGPRWLSC FPDSCTSLVS LNFACIKGEV
OsAFB2B         ATVATNCRFM KELDLQESLV EDRDSRWLGC FPKPSTLLES LNFSCLTGEV
SbiAFB2A        AAVASHCKLL RELDLQENDV EDRGPRWLSF FPDSCTSLVS LNFACIKGEV
SbiAFB2B        ANIATNCRFL KELDLQESCV KHQGHQWINC FPKPSTSLEC LNFSCLTGEV
```

Alignment of AFB2/3 Proteins

```
                ....|....| ....|....| ....|....| ....|....| ....|....|
                        210        220        230        240        250
PsAFB2          NVGALERLVA RSPNLKTLRL NRSVPADALQ RILMRAPQIA DLGIGSFIHD
AtAFB2          NLVALERLVA RSPNLKSLKL NRAVPLDALA RLMACAPQIV DLGVGSYEND
AtAFB3          NVAALERLVA RSPNLKSLKL NRAVPLDALA RLMSCAPQLV DLGVGSYENE
PtrAFB2A        NVAALERLIA RSPNLRSLRL NHAVPLDVLQ KILIRAPHLV DLGVGSYVND
PtrAFB2B        NLAALERLVA RSPNLRSLRL NHAVPLDILQ KILMRAPHLV DLGVGSYVHD
MtAFB2          NLGALERLVS RSPNLKSLRL NRSVPVDALQ RILTRAPQLM DLGIGSFFHD
GmAFB2A         SLGALERLVA RSPYLKSLKL NRSVPFDALQ RIMMRAPQLS DLGIGSFVHD
GmAFB2B         SLGALERFVA RSPNLKSLKL NRSVPVDALQ RIMMRAPQLS DLGIGSLVHD
MgAFB2A         NVAALERLVA RCHNLRSLRV NHAVPLEALQ KILVKAPQIN DLGTGSFVHD
MgAFB2B         NVSALERLVG RCPNLTSLRL NHTVPLDALH KILARAPQLN DLGTGSFVHD
AqAFB2          NLASLEKLVA RCPNLKSLKL NRAVPLQTLH KILIRAPQLM DLGIGSLVHH
OsAFB2A         NAGSLERLVS RSPNLRSLRL NRSVSVDTLA KILLRTPNLE DLGTGNLTDD
OsAFB2B         NSPALEILVA RSPNLRSLRL NRSVPLDVLA RILCRRPRLV DLCTGSFVRG
SbiAFB2A        NSGALERLVA RSPNLRSLRL NRSVSVDTLS KILARTPNLE DLGTGNLTDE
SbiAFB2B        NAVALEELVA RSPNLKSLRL NPSVPIDVLP RILSHTPMLE DLGTGSFVLG

                ....|....| ....|....| ....|....| ....|....| ....|....|
                        260        270        280        290        300
PsAFB2          LNSEAYIKLK NTILRCRSIT SLSGFLEVAP FSLA-AVYPI CRN--LTSLN
AtAFB2          PDSESYLKLM AVIKKCTSLR SLSGFLEAAP HCLS-AFHPI CHN--LTSLN
AtAFB3          PDPESFAKLM TAIKKYTSLR SLSGFLEVAP LCLP-AFYPI CQN--LISLN
PtrAFB2A        PDSETYNKLV MAIQKCMSVK SLSGFLEVAP HCLS-AFHLI CPN--LTSLN
PtrAFB2B        PDSETYNKLV TALQKCKSVK SLSGFLEAAP QCLS-AFHLI CPN--LTSLN
MtAFB2          LNSDAYAMFK ATILKCKSIT SLSGFLEVAP FSLA-AIYPI CQN--LTSLN
GmAFB2A         PESEAYIKLK NTILKRKSIT SLSGFLEVAP HCLA-AIYPI CPN--LTSLN
GmAFB2B         PESEAYIKLK NTILKCKSIT SLSGFLEVAP HCLA-AIYPI CPN--LTSLN
MgAFB2A         PDSETSKKMK NTLENCKSVR SLSGFLDVNP HCLP-AVYPI CTD--LTSLN
MgAFB2B         PDSESCNKLK NVLRMCTSIR SLSGFLDVNG RSLP-SIYPI CTN--LTSLN
AqAFB2          RDPILYNHLR EVVRQCKSVR SLSGCFEVSL YFLS-PFYPV CKN--LTSLN
OsAFB2A         FQTESYFKLT SALEKCKMLR SLSGFWDASP VCLS-FIYPL CAQ--LTGLN
OsAFB2B         NIVGAYAGLF NSFQHCSLLK SLSGFWDATS LFIP-VIAPV CKN--LTCLN
SbiAFB2A        FQAESYARLT SALEKCKMLR SLSGFWDASP ICVP-YIYPL CHQ--LTGLN
SbiAFB2B        NNAGAYISLY RALGKCTLLK SLSGFWDAPG LYVRGMLLPI CRTRALTCLN

                ....|....| ....|....| ....|....| ....|....| ....|....|
                        310        320        330        340        350
PsAFB2          LSYAASIQGA ELIKLIRHCG KLQRLWIMDC IGDKGLVAVA TICKELQELR
AtAFB2          LSYAAEIHGS HLIKLIQHCK KLQRLWILDS IGDKGLEVVA STCKELQELR
AtAFB3          LSYAAEIQGN HLIKLIQLCK RLQRLWILDS IGDKGLAVVA ATCKELQELR
PtrAFB2A        LSYAPGIHGA ELIKLIRHCM KLQRLWILDC IGDQGLEVVA STCKDLQEIR
PtrAFB2B        LSYAPGIHGT ELIKLIRHCR KLQRLWILDC IGDEGLEVVA STCKHLQEIR
MtAFB2          LSYAAGILGI ELIKLIRHCG KLQRLWIMDR IGDLGLGVVA STCKELQELR
GmAFB2A         LSYAAGIQGS DLIKLIRHCV KLQRLLIMDC IGDKGLDVVA TSCKDLQELR
GmAFB2B         LSYAAGIQGS ALVKLIHHCV KLQRLWIMDC IGDKGLGVVA TTCKDLQELR
MgAFB2A         LSYAPGIYSN ELIKLICHCK KLERLWILDT IGDKGLGAVA STCKELQELR
MgAFB2B         LSYAPGIYSN ELIKLICHCK KLERLWILDT IGDKGLGVVA STCKELQELR
AqAFB2          LSYAPGIPGS DLIMLILKCP KLQRLWVVDS IGDKGLGVVA STCKELLELR
OsAFB2A         LSYAPTLDAS DLTKMISRCV KLQRLWVLDC ISDKGLQVVA SSCKDLQELR
OsAFB2B         LSSAPMVRSA YLIEFICQCK KLQQLWVLDH IGDEGLKIVA SSCIQLQELR
SbiAFB2A        LSYTPTLDYS DLTKMVSRCV KLQRLWVLDC ISDKGLQVVA SSCKDLQELR
SbiAFB2B        LSYAPLIQSD QLISIVRQCT RLHVLWVLDH IGDEGLKVLS YSCPDLQELR
```

Alignment of AFB2/3 Proteins

```
                ....|....| ....|....| ....|....| ....|....| ....|....|
                        360        370        380        390        400
PsAFB2          VFPSAPFG-- -NQAAVTEVG LVAISKGCPK LHSLLYFCHQ MTNAALITVA
AtAFB2          VFPSDLLG-- GGNTAVTEEG LVAISAGCPK LHSILYFCQQ MTNAALVTVA
AtAFB3          VFPSDVHGEE DNNASVTEVG LVAISAGCPK LHSILYFCKQ MTNAALIAVA
PtrAFB2A        VFPSDPHV-- -GNAAVTEVG LVALSSGCRK LHSILYFCQQ MTNVALITVA
PtrAFB2B        VFPSDPFV-- -GNAAVTEVG LVALSSGCRN LHSILYFCQQ MTNAALITVA
MtAFB2          VFPSAPFG-- -NQAAVTEKG LVAISMGCPK LHSLLYFCHQ MTNAALIAVA
GmAFB2A         VFPSVPFG-- -NPAAVTEKG LVAISMGCPK LHSLLYFCHQ MTNAALITVA
GmAFB2B         VFPSVPFG-- -DPAAVTEKG LVAISMGCPK LHSLLYFCHQ MTNAALITVA
MgAFB2A         VFPSDLYGA- DNAAAVTEEG LVSISAGCPK LNSLLYFCQQ MTNAALITVA
MgAFB2B         VFPSDI---- ---AAVTEEG LVAISAGCPK LNSLLYFCQQ MTNAALITVA
AqAFB2          VFPSVYGA-- -EHASVTEEG LVAVSLGCPK LHSVLYFCHQ MTNAALIAVA
OsAFB2A         VFPSDFYVA- -GYSAVTEEG LVAVSLGCPK LNSLLYFCHQ MTNAALVTVA
OsAFB2B         VFPANANAR- -AST-VTEEG LVAISAGCNK LQSVLYFCQR MTNSALITVA
SbiAFB2A        VFPSDFYVA- -GASAVTEEG LVAISSGCPK LSSLLYFCHQ MTNEALITVA
SbiAFB2B        VYPSDPNAA- -ARTSVTEEG LAAISF-CRK LECVLFFCDR MTNTALITIA


                ....|....| ....|....| ....|....| ....|....| ....|....|
                        410        420        430        440        450
PsAFB2          KNCPNFIRFR LCILDATKPD SDTMQPLDEG FGAIVQSCKR LRRLSLSGQL
AtAFB2          KNCPNFIRFR LCILEPNKPD HVTSQPLDEG FGAIVKACKS LRRLSLSGLL
AtAFB3          KNCPNFIRFR LCILEPHKPD HITFQSLDEG FGAIVQACKG LRRLSVSGLL
PtrAFB2A        KNCPNFTRFR LCILDPTKPD AVTNQPLDEG FGAIVHSCKG LRRLSMTGLL
PtrAFB2B        KNCPNFTRFR LCILDPTKPD ADTNQPLDEG FGAIVHSCKG LRRLSMSGLL
MtAFB2          KNCPNFIRFR LCILDATKPD PDTMQPLDEG FGAIVQSCKR LRRLSLSGQL
GmAFB2A         KNCPNFIRFR LCILDATKPD PDTMQPLDEG FGAIVQSCRR LRRLSLSGQL
GmAFB2B         KNCPNFIRFR LCILDATKPD PDTMQPLDEG FGAIVQSCRR LRRLSLSGKL
MgAFB2A         KNCPNFIRFR LCTLNPVIPD AVTNLPLDEG FGAIVQSCKG LKRLSVSGRL
MgAFB2B         KNCPNFIRFR LCTLNPTIPD AATNLPLDEG FGAIVQSCKG LKRLSVSGLL
AqAFB2          KSCPNFTRFR LCILDPRKPD PATLQPLDEG FGAIVQSCKS LKRLSLSGHL
OsAFB2A         KNCPNFTRFR LCILEPGKPD VVTSQPLDEG FGAIVRECKG LQRLSISGLL
OsAFB2B         KNCPRFTSFR LCVLDPGSAD AVTGQPLDEG YGAIVQSCKG LRRLCLSGLL
SbiAFB2A        KNCPNFIRFR LCILEPKKPD AMTGQPLDEG FGAIVRECKG LRRLSMSGLL
SbiAFB2B        KYCPLLTSFR LCILEPRSAD AVTGQPLDEG FGAIVQSCKG LRRFAMSGLL


                ....|....| ....|....| ....|....| ....|....| ....|....|
                        460        470        480        490        500
PsAFB2          TDQVFLYIGM YAEQLEMLSI AFAGESDKGM LYVLNGCKKL RKLEIRDCPF
AtAFB2          TDQVFLYIGM YANQLEMLSI AFAGDTDKGM LYVLNGCKKM KKLEIRDSPF
AtAFB3          TDQVFLYIGM YAEQLEMLSI AFAGDTDKGM LYVLNGCKKM RKLEIRDSPF
PtrAFB2A        TDKVFLYIGM YAEQLEMLSI AFAGDTDKGM QYLLNGCKKL RKLEIRDCPF
PtrAFB2B        TDQVFLYIGM YAEQLEMLSI AFAGDTDKGM QYLLNGCKKL RKLEIRDCPF
MtAFB2          TDQVFLYIGM YAEQLEMLSI AFAGESDKGM LYVLNGCKKI RKLEIRDCPF
GmAFB2A         TDQVFLYIGM YAEKLEMLSI AFAGESDKGM LYVLNGCKKL RKLEIRDCPF
GmAFB2B         TDQVFLYIGM YAEKLEMLSI AFAGDGDKGM LYVLNGCKKL RKLEIRDCPF
MgAFB2A         TDQVFLYIGM YAEQLEMLSI AFAGDSDKGM LYVLNGCKKL KKLEIRDSPF
MgAFB2B         TDQVFLYIGM YGEHLEMLSI AFAGNSDKGM LYVLNGCKKL KKLEIRDSPF
AqAFB2          TDRVFLYIGM YAEQLEMLSI AFAGESDKGM LYVLNGCKNL RKLEIRDSPF
OsAFB2A         TDKVFMYIGK YAKQLEMLSI AFAGDSDKGM MHVMNGCKNL RKLEIRDSPF
OsAFB2B         TDTVFLYIGM YAERLEMLSV AFAGDTDDGM TYVLNGCKNL KKLEIRDSPF
SbiAFB2A        TDRVFMYIGK YAKYLEMLSI AFAGDSDKGM MDVMNGCKNL RKLEIRDSPF
SbiAFB2B        TDSVFLYIGM YAEKLEMLSV AFAGDTDDGM VYVLNGCKNL KKLEIRDSPF
```

Alignment of AFB2/3 Proteins

```
                ....|....| ....|....| ....|....| ....|....| ....|....|
                        510        520        530        540        550
PsAFB2          GDTALLTDVG KYETMRSLWM SSCEVTVGAC KTLAKKMPSL NVEIFN-ESE
AtAFB2          GDTALLADVS KYETMRSLWM SSCEVTLSGC KRLAEKAPWL NVEIIN-END
AtAFB3          GNAALLADVG RYETMRSLWM SSCEVTLGGC KRLAQNSPRL NVEIIN-ENE
PtrAFB2A        GNAALLMDVG KYETMRSLWM SSCEVTLGGC KSLAKKMPRL NVEIIN-END
PtrAFB2B        GNAALLMDVG KYETMRSLWM SSCDITLGGC KSLAKKMPRL NVEIIN-ESD
MtAFB2          GDTALLTDIG KYETMRSLWM SSCEVTVEAC KTLAKKMPRL NVEIFS-ESE
GmAFB2A         GNVALLTDVG KYETMRSLWM SSCEVTVGAC KLLAKKMPRL NVEIFN-ENE
GmAFB2B         GDMALLTDVG KYETMRSLWM SSCEVTVGAC KLLAKKMPRL NVEIFN-ENE
MgAFB2A         GNAALLSDMG KYETMRSLWM SSCEVTYGAC KTLAEKMPTL NVEIIN-EGE
MgAFB2B         GDVALLADVG KYETMRSLWM SSCEVTFGGC KTVAQKMPRL NVEIINNEGG
AqAFB2          GNGALLEDMG KYETMRSLWM SSCDVTLGGC KTLAKKMPRL NLEIIN---D
OsAFB2A         GDAALLGNFA RYETMRSLWM SSCNVTLKGC QVLASKMPML NVEVIN-ERD
OsAFB2B         GDSALLAGMH QYEAMRSLWL SSCNVTLGGC KSLAASMANL NIEVMNRA-A
SbiAFB2A        GDVALLGNVA KYETMRSLWM SSCDVTLKGC QVLASKMPML NVEIMN-ELD
SbiAFB2B        GDAALLAGAH RYESMRSLWM SSCEITLGAC KTLAAAMPNI NVEVISEAGA


                ....|....| ....|....| ....|....| ....|....| ....|....|
                        560        570        580        590        600
PsAFB2          Q--------- ---------- --ADCYVEDG QRVEKMYLYR SVAGKREDAP
AtAFB2          NNR------- ---------- -MEENGHEGR QKVDKLYLYR TVVGTRMDAP
AtAFB3          NNG------- ---------- -MEQNEEDER EKVDKLYLYR TVVGTRKDAP
PtrAFB2A        Q--------- ---------- --MDASADDR QKVEKMFLYR TLAGRREDAP
PtrAFB2B        Q--------- ---------- --MDITADDG QKVEKMFLYR TLAGRRKDAP
MtAFB2          Q--------- ---------- --ADCYVEDG QRVEKMYLYR TVAGKREDAP
GmAFB2A         Q--------- ---------- --EDCSLEDG QKVEKMYLYR TLAGKRKDAP
GmAFB2B         Q--------- ---------- --EDCSLEDG QKVEKMYLYR TLAGKRKDAP
MgAFB2A         DQV------- ---------- -EASSSPDAR HRVEKMYLYR TLVGPRRDAP
MgAFB2B         EPM------- ---------- -DDDDDVDG- KKVEKMYLYR TLVGPRRDAP
AqAFB2          K--------- ---------- --MEEYIDDS QKVEKMYLYR TLDGPRKDAP
OsAFB2A         GSN------- ---------- -EMEENHGDL PKVEKLYVYR TTAGARDDAP
OsAFB2B         SIN------- ---------- -EADN-ANDA KKVKKLYIYR TVAGPRGDAP
SbiAFB2A        GSSEMEENHT DISKVDKLHV SEMEENHTDL SKVDKLYVYR TTAGARDDAP
SbiAFB2B        SVG------- ---------- -ATDDGISNA RKVDKLYLYR TIAGPRSDTP
```

Alignment of AFB2/3 Proteins

```
            ....|.

PsAFB2      DYVWTL
AtAFB2      PFVWIL
AtAFB3      PYVRIL
PtrAFB2A    EFVWTL
PtrAFB2B    EFVWTL
MtAFB2      DYVWTL
GmAFB2A     EYVWTL
GmAFB2B     EYVWTL
MgAFB2A     DFVWTL
MgAFB2B     EFVWTL
AqAFB2      DFVWNL
OsAFB2A     NFVKIL
OsAFB2B     EFISTF
SbiAFB2A    NFVKIL
SbiAFB2B    GFVSIL
```

Figure 5.2: Putative PSAFB2 Protein aligned with AFB2/3 homologues from other species. Ps=*Pisum sativum*, At=*Arabidopsis thaliana*, Ptr=*Populus trichocarpa*, Mt=*Medicago truncatula*, Gm=*Glycine max*, Mg=*Mimulus guttatus*, Aq=*Aquilegia*, Os=*Oryza sativa*, Sbi=*Sorghum bicolor*. F-box is underlined and in bold, while predicted leucine rich repeats are underlined and italicized.

While the structural features of the AFB group of F-box proteins are very highly conserved, the C-terminals of members of the AFB6 clade are somewhat variable in length (Figure 5.3). The major structural features of the AFB proteins are retained.

Alignment of AFB6 Proteins

```
            ....|....| ....|....| ....|....| ....|....| ....|....|
                     10         20         30         40         50
PsAFB6A     ---------- ----MEPQTM NPSSV----- -------FPD EVLERILSMV
PtrAFB6A    ---------- ----MKREFL DSTR------ ----SSPFPD EVLERVLSLL
PtrAFB6B    --------MD SNPKMRKEFL DSTR------ ----SSLFPD EVLERVLSLL
MtAFB6A     MNMVECKRKK ESQGEKNNNM DSNSD----- -------FPD EVLERVLGMM
MtAFB6B     ---------- ----MEECKR EK-------- ---------D EVLKQVLGTV
MgAFB6A     --------MD PDTKKCKESK PHSSNSN--G SKCSHLKFPD EALEKVLSFI
MgAFB6B     --------MD HPSEDSPSSS DKSLGP---- TNHPQLPFPD EVLEKVLSFV
StuAFB6     ------MEMN PSLKKPRESV DLSNSS---- -ELTQSAFPD EVLEKVLSLV
LsaAFB6     ------MDLN QKRTKTVDRV DPVDPAAVSP ESTPVYPFPD EVLEPVLSLI
HanAFB6     ------MDLN QKRTRTVDRV DSVDPDLVSP ESTPMCPFPD EVLEPVLSLI
PtaAFB6     ---------- ----MMKKRG DS-------- ----SSTFPD EVLEHVLLFV
```

Alignment of AFB6 Proteins

```
          ....|....| ....|....| ....|....| ....|....| ....|....|
                    60         70         80         90        100
PsAFB6    KSRKDKSSVS LVCKDWFDAE RWSRKNVFIG NCYSVTPEIL TQRFPNVRSV
PtrAFB6A  KSHKDRSAVS LVCKDWYNAE SWSRTHVFIG NCYSVSPEIV ARRFPIIKSV
PtrAFB6B  KSHKDRSAVS LVCKDWYNAE SWSRTHVFIG NCYSVSPEIV ARRFPRIKSV
MtAFB6A   KSRKDRSSVS LVCKEWYNAE RWSRRNVFIG NCYAVSPEIL TRRFPNIRSV
MtAFB6B   KSRKDRNSAS LVCKQWYNAE RLSRRNVFIG NCYSVTPEIL TRRFPNIRSI
MgAFB6A   DSHKDRNTVS LVCKEWYNAE RWTRSNLFIG NCYSVSPEIV SRRFPRIKSV
MgAFB6B   NSHKDRSSVS LVRKDWYNAE RWTRSKLFIG NCYSVSPEIV ARRFPRIKSV
StuAFB6   QSHKDRNSAS LVCKDWYNAE RWTRTKLFIG NCYSVTPEIV ARRFPKIKSV
LsaAFB6   NSHKDRSSVS LVCKDWYNAE RWSRRHVFIG NCYSVSPEIV AGRFPQIRSV
HanAFB6   NSHKDRSSVS LVCKDWYNAE RWSRRHVFIG NCYSVSPEIV VGRFPKIRSV
PtaAFB6   VSIKDRSAVS LVCKAWYRAE AWSRRKVFIG NCYSVSPEIL VRRFPKITGI

          ....|....| ....|....| ....|....| ....|....| ....|....|
                   110        120        130        140        150
PsAFB6    TLKGKPRFSD FNLVPANWGA DIHPWLVVFA EKYPFLEELR LKRMVVTDES
PtrAFB6A  TLKGKPRFSD FNLVPENWGA DVHPWLVVFA TKYPFLEELR LKRMAVSDES
PtrAFB6B  TLKGKPRFSD FNLVPENWGA DVHPWFVVFA AKYPFLEELR LKRMAVSDES
MtAFB6A   TMKGKPRFSD FNLVPANWGA DIHSWLVVFA DKYPFLEELR LKRMAVSDES
MtAFB6B   TLKGKPRFSD FNLVPENWGA DIHSWLVVFA EKYPFLEELR LKRMVVTDES
MgAFB6A   RIKGKPRFSD FNMLPRDWGA NVHAWLVMFA EVYPFLEELR LKRMTVNDES
MgAFB6B   TLKGKPRFSD FNMLPRDWGA NVHPWLVMFA KVYPFLEELR LKRMTVTDES
StuAFB6   TLKGKPRFSD FNLVPENWGA DIQAWLDVFA KVYPFLEELR LKRMAVSDES
LsaAFB6   TLKGKPRFSD FNLVPEDWGA DVHPWLSVLA KAYPFLEELR LKRMAVSDES
HanAFB6   TLKGKPRFSD FNLVPEDWGA DVYPWLSVLA KAYPFLEELR LKRMAVSDES
PtaAFB6   TLKGKPRFSD FNLVPPHWGA DIHPWLLVIR GAYPWLRELR LKRMIVTDES

          ....|....| ....|....| ....|....| ....|....| ....|....|
                   160        170        180        190        200
PsAFB6    LEFLAFSFPN FKALSLLSCD GFSTDGLAAV ATNCKNLTEL DIQENGIEDK
PtrAFB6A  LEFLAVNFPN FKVLSLLSCD GFSTDGLAAI ATHCKSLTQL DIQENGIDDK
PtrAFB6B  LEFLALNFPN FKVLSLLSCD GFSTDGLAAI ATHCKNLTQL DVQENGIDDK
MtAFB6A   LEFLAFSFPN FKALSLLSCD GFSTDGLAAV ATNCKNLTEL DIQENGVDDK
MtAFB6B   LEFLAFSFHN FKALSLLSCE GFSTDGLAAV AANCKNLTEL DIQENDIDDK
MgAFB6A   LELLAKSFTG FKALSLLSCD GFTDDGLKFV ATHCRNLTEL DIQDSVAVDV
MgAFB6B   LELLAKSFSG FKALSLSSCD GFTENGLKAL ASHCRNLTEL DIQDSISEDV
StuAFB6   LEFLAKSFLG FKALSLLSCD GFSTDGISSI AAHCKNLTEL DIQENGMDDI
LsaAFB6   LEFLATNFPE FKALSLLSCD GFSTDGLKAI ATHCRNLTEL DIQENGIDDL
HanAFB6   LEFLAMNFPE FKALSLLSCD GFSTDGLKAI ATHCRNLAEL DIQENGIDDL
PtaAFB6   LELIARSFSD FRALSLTTCE GFSTDGLAVI ATHCRNLQEL DLQESEVDDR

          ....|....| ....|....| ....|....| ....|....| ....|....|
                   210        220        230        240        250
PsAFB6    SGNWLSCFPE SFTSLEVLNF ANLTNEVNID ALEKLVGRCK -SLKTLKVNK
PtrAFB6A  SGGWLSCFPE NFTSLEVLNF ANLNTDVNFD ALERLVSRCK -SLKVLKVNK
PtrAFB6B  SGNWLSCFPE NFTSLEVLNF ANLNTDVNFD ALERLVSRCK -SLKVLKANK
MtAFB6A   SGNWLSCFPE SFTSLEILNF ANLSNDVNFD ALEKLVARCN -SLKTLKVNK
MtAFB6B   SGDWLSCFPE SFTSLEVLNF ANLNNDVNID ALEKLVGRCK -SLKTLKVNK
MgAFB6A   GGDWLTCFPE NFSSLEILNF ASLNSEVNFE SLEKLVNRCK NTLRVLKVNE
MgAFB6B   GGGWLSSFPE NFSSLEVLNF ASLNSDISFD DLERLVSRCK -SLRVLKVNE
StuAFB6   CGSWLSCFPD DFTSLEVLNF ACMNTEISKD ALERLVGRCK -SLRVLKVNK
LsaAFB6   GGDWLSCFPE TLTSLEVLNF ASLNSEVDYN ALEKLVTRCK -SLRVLKVNR
HanAFB6   GGDWLSCFPE TLTTLQVLNF ASLNSEVSFS DLEKLVTRCK -SLRVLKVNR
PtaAFB6   GGYWLSCFPE SCVSLVSLNF ACLQSEVNFD ALQRLVARCI -SLRSLKLNK
```

Alignment of AFB6 Proteins

```
            ....|....| ....|....| ....|....| ....|....| ....|....|
                    260        270        280        290        300
PsAFB6      SVTLEQLKKL LVRAPQLCEL GSGSFS-QEL TSQQYAELET AFKNCKSLHT
PtrAFB6A    SISLEHLQRL LVCAPQLTEL GTGSFT-PEL TTRQYAELES AFNQCKNLHT
PtrAFB6B    SISLEHLQRL LVCAPQLTEL GTGSFM-PEL TARQYAELGS SFNQLKNLNT
MtAFB6A     SVTLEQLQRL LVRAPQLCEL GTGSFS-QEL TGQQYSELER AFNNCRSLHT
MtAFB6B     SVTLEQFQRL LVLAPQLCEL GSGSFS-QDL TCQQYLELES AFKNCKSLHT
MgAFB6A     SITLDQLQRL LVHAPNLVEL GTGSFM-QEL TPRQYEDVGS AFSNCGKLRV
MgAFB6B     TISLDQLQRL LVHAPLLTEL GTGSFM-QEL TPRQYEEVET AFSNCKNLEA
StuAFB6     NVTLPQLQRL LVRAPQLMEL GTGCFLPDQL TSRQYAELES AFSNCKHLHS
LsaAFB6     NISLDQLQRL LLRAPQLTEL GTGTFM-QDL VTRSVSELEG SFGNCKNLLT
HanAFB6     TINLDQLQKL LLRAPQLTEL GTGTFT-QDL VTRPVADLEA TFGSCKNLLT
PtaAFB6     TLSLEQLKRL LVIAPQLMEL GTGSFF-QEF SRQQFADLGK AFNSCKELRT

            ....|....| ....|....| ....|....| ....|....| ....|....|
                    310        320        330        340        350
PsAFB6      LSGLWVASAR YL----QVLY PACANLTFLN FSYAPLDSED LTKILVHCPN
PtrAFB6A    LSGLWEATAL YL----PVLY PVCSNLTFLN LSYTFLQSLE LASLLRQCPR
PtrAFB6B    LSGLWEATAP YL----PVLY PACTNLTFLN LSYAFLQSIE LASLLCQCPR
MtAFB6A     LSGLWVASAQ YH----QVLY PVCTNLTFLN FSYAPLDSEG LSKLLVRCPN
MtAFB6B     LSGLWVASAS AQYIQLQVLY SACTNLTFLN FSYALVDSED LTDLLVHCPN
MgAFB6A     LSGLWDATDL HF----SVLY GACARLTFLN FSEAVLQSGE LAKLLAHCPN
MgAFB6B     LSGLWDANSL YL----PLLY GACAGLTFLN LSDAPLQSGD FANLLVHCPN
StuAFB6     LSGFWEANRR YL----PSLY AACARLTFLN LSYEAIRSGE FSKLLAHCPN
LsaAFB6     ISGLWDTTTL FL----PVIY PACAKLTFLN LSYATLRSVE LAELLTHCKS
HanAFB6     ISGLWDTNSL YL----PVIY PACASLTFLN LSCAALRSFE LAMLLIHCKS
PtaAFB6     LSGMWEVAPL YL----PALY SVCSNLTFLN LSYANIRSLE LACLVFNCHH

            ....|....| ....|....| ....|....| ....|....| ....|....|
                    360        370        380        390        400
PsAFB6      LRRLWVVDTV EDKGLEAVGS NCPLLEELRV FPADPFDEEA EGGVTESGFV
PtrAFB6A    LRRLWVLDTV GDKGLEAVGS NCPLLEELRV FPADPFDEEI IHGVTEAGFV
PtrAFB6B    LRRLWVLDTV GDKGLEAVGS NCPLLEELRV FPADPFDEEV IHGVTEAGFL
MtAFB6A     LRRLWVLDTV EDKGLEAVGS YCPLLEELRV FPGDPFEEGA AHGVTESGFI
MtAFB6B     LRRLWVVDTV EDKGLEAVGS YCPLLEELRV FPADPFDEGV VHGVTESGFI
MgAFB6A     LRRLWVIDTV QDKGLEAVGS SCPLLEELRV FPLDPYDLDH QHGVTEQGLL
MgAFB6B     LRRLWVIDTV EDKGLEAVGS SCPLLEELRV FPADPYDRHH RDGVSESGFL
StuAFB6     LRRLWVLDTV KDKGLEAVGT SCPLLEELRV FPADPFEEDM DHGVTESGFV
LsaAFB6     LKRLWVLDTV GDSGLEAVGS CCPLLEELRV FPADPFDQE- VAGVTESGFV
HanAFB6     LRRLWVLDTV GDMGLEAVGS WCPLLEELRV FPADPFEQEN VAGVTESGFV
PtaAFB6     LRRLWVLDTV GDKGLETVSS SCKDLRELRV FPMDPFGQD- RVGVTENGIL

            ....|....| ....|....| ....|....| ....|....| ....|....|
                    410        420        430        440        450
PsAFB6      AVSEGCRKLH YVLYFCRQMT NAAVATVVQN CPDFTHFRLC IMNPGQQDYL
PtrAFB6A    AVSYGCRRLH YVLYFCRQMT NAAVATIVQN CPDFTHFRLC IMNPGQPDYL
PtrAFB6B    AVSYGCRRLH YVLYFCRQMT NAAVATIVQN CPDFTHFRLC IMNPGQPDYL
MtAFB6A     AVSEGCRKLH YVLYFCRQMT NAAVATVVEN CPDFTHFRLC IMTPGQPDYQ
MtAFB6B     AVSEGCRKLH YILYFCHQMT NDAVATVVQN CPDFTHFRLC IMTPNQPDYL
MgAFB6A     AVSLGCPKLH YLLYFCRRMT NAAVIAAVKN CPNFTHFRLC IMNPGQPDHL
MgAFB6B     AVSHGCPKLH YVLYFCRRMT NAAVITIVKN CPDFTHFRLC IMTPGQPDHL
StuAFB6     AVSAGCPKLQ YVLYFCRQMT NAAVATIVRN CPNFTHFRLC IMNPGQPDYL
LsaAFB6     SVSRGCPKLH YVLYFCHQMT NAAVATIARN CPGFTHFRLC IMNPGQPDYL
HanAFB6     AVSRGCPKLH YVLYFCHQMT NAAVATVVQN CPGFTHFRLC IMNLGQPDYV
PtaAFB6     AISEGCHNLS YVLYFCRQMT NATIIAVAQN RPKLTHFRLC IMYPCQPDHL
```

Alignment of AFB6 Proteins

```
            ....|....| ....|....| ....|....| ....|....| ....|....|
                    460        470        480        490        500
PsAFB6      TDEPMDEAFG EVVKNCTKLQ RLAVSGYLTD LTFEYIGKYA KNLETLSVAF
PtrAFB6A    TNEPMDEAFG AVVRTCTKLQ RLSVSGLLTD LTFEYIGQYA KNLETLSVAF
PtrAFB6B    TNEPMDEAFG AVVRTCTKLQ RLSVSGLLTD LTFEYIGQYA KNLETLSVAF
MtAFB6A     TGEPMDEAFG AVVKTCTKLQ RLAVSGSLTD LTFEYIGKYA KNLETLSVAF
MtAFB6B     TNEPMDEAFG AVVKTCTKLQ RLSVSGYLTD LAFEYIGKYA KNLETLSVAF
MgAFB6A     TKSPMDAAFA AVVKTCPKLR RLSVSGLLTD KTFESIGEYA KNLETLSVAF
MgAFB6B     TNEPMDEAFG AVAKTCTKLK RLSVSGLLTD VSFEYIGKYA KNLETLSVAF
StuAFB6     TNEPMDEAFG AVVKTCKKLQ RLSVSGLLTD LTFEYIGKYA KNLETLSVAF
LsaAFB6     TNEPMDEAFG AVVKTCPNLQ RLAVSGRLTD LMFEYIGKYA KNLETLSVAF
HanAFB6     TNEPMDEAFG AVVKTCPNLQ RLAVSGLLTD LTFEYIGKYA KNLEILSVAF
PtaAFB6     TDEPMDEDFG AIVKNCKNLQ RLAVSSLLTD KAFEYIGLYA KNLETLSVAF

            ....|....| ....|....| ....|....| ....|....| ....|....|
                    510        520        530        540        550
PsAFB6      AGSSDWGMEC VLVGCPKLRK LEIRDSPFGN AALLAGLEKY ESMRSLWMSS
PtrAFB6A    AGSSDRGMQC VLEGCPKLRK LEIRDCPFGN AALLSGLEKY ESMRSLWMSA
PtrAFB6B    AGSSDRGMQC MLEGCPKLRK LEIRDCPFGN AALLSGLEKY ESMRSLWMSA
MtAFB6A     AGSSDWAMQC VLVGCPKLRK LEIRDSPFGN AALLSGFDKY ESMRSLWMSD
MtAFB6B     AGSSDLGMQC VLAGCPKLKK LEIRDCPFGD AALLSGLEKY ESMRSLWMSD
MgAFB6A     AGSSDKAMVC VLRGCPKLRK LEIRDCPFGN AALLSGVEKY EMMRSLWMSA
MgAFB6B     AGSSDWGMQS VLEGCPKLRK LEIRDCPFGN TALLSGKLKY ETMRSLWMSA
StuAFB6     AGSSDWGMQC VLDGCSKLRK LEIRDSPFGN AALLSGMGKY ESMRCLWMSA
LsaAFB6     AGSSDLGLKY VLGGCPKLRK LEIRDCPFGN AALLSGLTKY ESMRSLWMSA
HanAFB6     AGSSDLGLKY VLGGCPRLRK LEIRDCPFGN AALLSGLTKY ESMRSLWMSA
PtaAFB6     AGSSDLGMEC VLRGCPKLRK LEIRDSPFGN AALLSGLEQY ESMRSLWMSS


            ....|....| ....|....| ....|....| ....|....| ....|....|
                    560        570        580        590        600
PsAFB6      CRLMMNGCRF LAGEKPRLNV EVMQEEGGD- DSRAEKLYVY RSVAGPRRDA
PtrAFB6A    CNVTMNGCRL LAREMPRLNV EVMKEDGSD- DSQADKVYVY RSVAGPRRDA
PtrAFB6B    CNVTMNGCRV LAREMPRLNV EVMKEDGSD- DSQADKVYVY RSVVGPRRDA
MtAFB6A     CKVTMNGCRL LAQERPRLNV EVMQEEGGD- DSQAGKLYVY RSVAGPRRDA
MtAFB6B     CQVTMNGCRL LAKEKPRLNV EVIKEEGSG- DSQAEKVYVY RSVAGPRRDA
MgAFB6A     CDVTMKGCRM LAREMPRLNV EVIEDEGSDD GAKAGKVYVY RTVAGPRRDA
MgAFB6B     CNVTMKGCGI LAREMPRLNV EVINDEGSD- GSQADKVYVY RTVAGPRRDA
StuAFB6     CRVTMNGCRI LAQERPRLNV EVIKDEHSD- -DYADKLYVY RSVAGPRKDA
LsaAFB6     CNLTMNGCRV LAKKMPRLNV EVMKDEDSE- DSQAHKVYVY RTVAGPRRDA
HanAFB6     CNLTMNGCRV LAKEMPRLNV EVMKDEDSE- DSQAHKVYIY RTVAGPRRDA
PtaAFB6     CKVTMSGCRY LAQNKPRLNV EIIKENDED- DNDADKLYVY RTIAGPRRDA
```

Alignment of AFB6 Proteins

```
           ....|....|
                   610
PsAFB6A    PPFVLTL---
PtrAFB6A   PPCVLTLSGL
PtrAFB6B   PPCVLTLSGL
MtAFB6A    PPFVLTL---
MtAFB6B    PLFVLTL---
MgAFB6A    PPFVLTL---
MgAFB6B    PGFVLTL---
StuAFB6    PPFVVTL---
LsaAFB6    PPFVLTL---
HanAFB6    PPFVLTL---
PtaAFB6    PNFVLTL---
```

Figure 5.3: Putative PSAFB6A Protein aligned with AFB6 homologues from other species. Ps=*Pisum sativum*, Pta=*Pinus taeda*, Han=*Helianthus*, Lsa=*Lactuca sativa*, Stu=*Solanum tuberosum*, Mg=*Mimulus guttatus*. Mt=Medicago truncatula, Ptr=*Populus trichocarpa*. F-box is underlined and in bold, while predicted leucine rich repeats are underlined and italicized.

5.4 *PsAFB6A* Cloning

While the full-length coding region of *PsAFB2* was cloned from multiple tissue sources, all attempts to isolate the putative coding region of *PsAFB6A* were unsuccessful. To facilitate future research, this appendix describes, in brief, reaction conditions already utilized in cloning attempts. Tissue sources, RNA isolation, and cDNA generation protocols are described in Chapter 3.

Attempts were made with multiple primer sets (primers 1 and 2, 3 and 4, or 7 and 8 at 25µM final concentration; Table 5.7) to amplify the complete *PsAFB6A* coding sequence from four cDNA pools (final concentration 15 ng μL^{-1}) generated from first-strand synthesis with oligo-dT. Using constant dNTP levels (0.5 µM final concentration), both $MgCl_2$ levels (1.25, 1.75, 2.25, 2.5, 2.75, 3, and 3.125 µM final concentration) and

annealing temperature (55, 52.5, 52, 51, 50, and 48 °C) were varied. Primer concentration was maintained at 2.5 µM each primer (final concentration). In addition to standard PCR protocols (30 to 35 cycles), touchdown PCR (15, 20, or 30 cycles followed by standard PCR for 12, 15, or 20 cycles at a fixed annealing temperature) was attempted.

Using the 5'-RACE cDNA pools (generated with template switching, not RLM-RACE protocols), attempts were made to amplify the complete sequence from the 3' end of the gene and primers specific to the sequence added in RACE. These attempts utilized the three primers from PsAFB6A 5' RACE (A, B, and C in Figure 3.5; Table 3.3) and the AFB6 3' Primer (primer 5; Table 5.7). Reaction conditions were as mentioned above, and both standard and touchdown PCR were performed using each of the three 5' primers individually as well as combinations of the short and long primers (A and B in Figure 3.5; Table 3.3). Nested PCR was also carried out on diluted product of the initial PCR reactions with either the short or long primers (A or B in Figure 3.5; Table 3.3) by a second round of amplification with the Nested Race Primer (C in Figure 3.5; Table 3.3).

A similar strategy was employed using the 3'-RACE cDNA pools. These attempts used the three primers from PsAFB6A 3' RACE (A, B, and C in Figure 3.5; Table 3.3) and the AFB6:5'UTR-I Primer (primer 6; Table 5.7). Reaction conditions were as mentioned above, but dNTP levels were tested at both 0.5 and 0.3 µM. Both standard and touchdown PCR were performed using each of the three 3' primers individually as well as combinations of the short and long primers (A and B in Figure 3.5; Table 3.3). Nested PCR was also carried out on the products of PCR reactions with either the short or long primers (A or B in Figure 3.5; Table 3.3) by a second round of amplification with the Nested Race Primer (C in Figure 3.5; Table 3.3).

Transcript profiling experiments revealed high levels of *PsAFB6A* mRNA in emasculated pericarps (Figure 3.11). To maximize the levels of *PsAFB6A* cDNA in the PCR templates, cDNA synthesis from an oligo(dT) primer was carried out as described in Chapter 3 on RNA isolated from 3 DAA pericarps which were emasculated at -2 DAA. PCR was attempted with two sets of primers (primers 7 and 8 or 9 and 10; Table 5.7) with the conditions described above, but additionally with primer concentrations of either 2.5 or 1.25 µM, and $MgCl_2$ concentrations of 1 mM were also tested. In some cases, reactions products were diluted and subjected to a second round of PCR under similar conditions.

Table 5.7: Primers used in cloning attempts of the full-length putative coding region of *PsAFB6A.*

Primer	Sequence	Number
MtAFB6A 5’	5’-ATG AAC ATG GTA GAG TGT AAG AGA AAG AA	1
MtAFB6A 3’	5’-TCA GAG AGT GAG AAC AAA TGG AGG	2
MtAFB6B 5’	5’-ATG GAG GAG TGT AAG AGA GAG AAA GA	3
MtAFB6B 3’	5’-TCA GCT TCG GAC AGC CA	4
AFB6 3’ Primer	5’-TAT AAC TTT AAA TCT CAT TTA TTT CCA TGA ACT T	5
AFB6:5’UTR-I	5’-CGA ATT CGC CCT TAA GCA CTC GT	6
AFB63’-II	5’-CTA ATA GCA CTC ACT ATA GGG CAA GCA GTC G	7
AFB65’-II	5’-ATG GAA CCA CAA ACC ATG AAT CCC AGT TC	8
PsAFB6A-F3	5’-ATG GAA CCA CAA ACC ATG AAT CCC AG	9
PsAFB6A-R3	5’-TCA GAG AGT GAG AAC AAA AGG AGG TG	10

5.5 AFB qRT-PCR Specificity

Table 5.8 contains results of searches of the qRT-PCR amplicons (including validation primer sets) of *PsAFB2* sequentially against the non-redundant nucleotide (Table 5.8) database using the BLASTN 2.2.21 program (Zhang *et al*., 2000). Searches using the same protocol with *PsAFB6A* returned no hits. Additionally, the *PsAFB2* amplicon could not be aligned to the nucleotide sequence of *PsAFB6A* using default settings, and vice versa.

Table 5.8: Results of search of nr/nt library using the PsAFB2 qRT-PCR amplicon as query. Default settings of the BLASTN 2.2.21 program were used.

Accession	Description	Total score	E value
AC133780.33	Medicago truncatula clone mth2-27f3, complete sequence	228	7e-57
AK286220.1	Glycine max cDNA, clone: GMFL01-24-D14	152	4e-34

5.6 Literature Cited

Letunic, I., R. Copley, B. Pils, S. Pinkert, J. Schultz, and P. Bork. (2005). SMART 5: domains in the context of genomes and networks. *Nuc. Acid Res.* **34**: D257-D260

Schultz, J., F. Milpetz, P. Bork, and C. Ponting. (1998). SMART, a simple modular architecture research tool: Identification of signalling domains. *Proc. Nat. Acad. Sci. USA* **95**:5857-5864

Zhang, Z., S. Schwartz, L.s Wagner, and W. Miller. (2000). A greedy algorithm for aligning DNA sequences. *J. Comput. Biol.* **7**:203-214.